GROUND-MOTION SELECTION FOR SCENARIO RUPTURES USING THE GENERALIZED CONDITIONAL INTENSITY MEASURE (GCIM) APPROACH AND ITS APPLICATION FOR SEVERAL MAJOR EARTHQUAKE SCENARIOS IN NEW ZEALAND

Karim Tarbali & Brendon A. Bradley

Research Report 2014-03

Department of Civil and Natural Resources Engineering

University of Canterbury

New Zealand

4 June 2014

ISSN: 1172-9511

Abstract

Generalized conditional intensity measure (GCIM) method is extended to ground motion selection for scenario ruptures. Using different rupture scenarios and site conditions, various aspects of the GCIM methodology are scrutinized, including: (i) implementation of different weight vectors and the composition of the ***IM*** vector; (ii) quantifying the importance of replicate selections for different number of desired ground motions; and (iii) the effect of considering bounds on the implicit causal parameters of the prospective ground motions.

Using the extended methodology, representative ground motion ensembles for several major earthquake scenarios in New Zealand are developed. Cases considered include representative ground motions for the occurrence of Alpine, Hope, and Porters Pass earthquakes in Christchurch city, and the occurrence of Wellington, Wairarapa, and Ohariu fault ruptures in Wellington city. Challenges in the development of ground motion ensembles for subduction zone earthquakes are also highlighted. The selected scenario-based ground motion sets can be used to complement ground motions which are often selected in conjunction with probabilistic seismic hazard analysis, in order to understand the performance of structures for the question "what if this fault ruptures?"

Table of Contents

List of figures

List of tables

Chapter 1: Ground-motion Selection for Scenario Ruptures Using the Generalized Conditional Intensity Measure (GCIM) Approach

1 Abstract

In this chapter, the generalized conditional intensity measure (GCIM) method is extended to ground motion selection for scenario ruptures. The selection algorithm is based on generating random realizations of the considered intensity measure (IM) distributions for a specific rupture scenario and then finding the prospective ground motions which best fit the realizations using an optimal amplitude scale factor. Using different rupture scenarios and site conditions, various aspects of the GCIM methodology are scrutinized, including: (i) implementation of different weight vectors and the composition of the ***IM*** vector; (ii) quantifying the importance of replicate selections for different number of desired ground motions; and (iii) the effect of considering bounds on the implicit causal parameters of the prospective ground motions. It is demonstrated that considering only spectral acceleration ordinates in the selection process, as is common in many conventional selection procedures, may result in motions with a biased representation for duration and cumulative ground motion effects. In contrast, considering IMs other than spectral acceleration ordinates can be achieved using the GCIM methodology, resulting in motions with an appropriate representation for different aspects of the seismic hazard. The positive effect of conducting replicate selections to select a suite of motions with a precise representation for the distribution of the considered IMs is demonstrated and a minimum number of replicates for different desired number of motions are presented. Although not a requirement in the GCIM-based ground motion selection, it is demonstrated that the application of 'wide' causal parameters bounds can be efficient removing unrealistic ground motions prior to the core ground motion selection steps to improve computational efficiency and causal parameters goodness of fit.

2 Introduction

Nonlinear response history analysis requires a ground motion time series as an input. One of the general approaches to acquire the input ground motion time series is to select appropriate as-recorded ground motions from previously recorded seismic events. Selecting a suite of ground motions for the purpose of conducting seismic response analysis can be based on the results from either scenario seismic hazard analysis (scenario SHA) or probabilistic seismic hazard analysis (PSHA) (Bommer 2002).

Methods have been proposed to select ground motions based on the intensity of motion predicted by scenario SHA or PSHA (e.g., McGuire 1995, Shome et al. 1998, Bommer and Acevedo 2004, Kottke and Rathje 2008, Baker 2010, Jayaram et al. 2011, Wang 2011). A review of the existing methods reveals that majority of them are principally based on matching the (pseudo) acceleration response spectrum of the selected ground motions to a target spectrum. This target spectrum is obtained from either scenario SHA, PSHA, or a seismic design code (see Katsanos et al. (2010) for a more detailed review). In addition to the predicted intensity of motion, in order to select ground motions with an appropriate representation of the dominant scenario ruptures, implicit causal parameters of ground motions (e.g., magnitude, source-to-site distance) as well as the site condition of the recorded motions are also considered in conventional methods (Katsanos et al. 2010). Another important aspect in ground motion selection is to consider variability in the characteristics of ground motions due to uncertain nature of seismic events. A few of the existing methodologies address this issue in terms of variability in spectral acceleration ordinates of ground motions (e.g., Kottke and Rathje 2008, Jayaram et al. 2011, Wang 2011).

It is important to note that the severity of ground motions is not dependent solely upon spectral accelerations, but is a general function of the amplitude, frequency content, cumulative effects, and duration of the ground motion. In addition, there are uncertainties associated with the calculated seismic hazard and the predicted severity of ground motions for a given site, which needs to be addressed in ground motions selection process. In order to properly represent the effect of seismic hazard on engineering systems via selected ground motions, a comprehensive ground motion selection methodology is required to consider all of the factors that affect the severity of a ground motion and also take into account the variability in these factors due to ground motion uncertainty.

The generalized conditional intensity measure (GCIM) approach (Bradley 2010a) provides a holistic framework to select ground motions considering the distribution of various intensity measures (IMs) to evaluate the appropriateness of a selected suite of ground motions. Application of the GCIM method to select ground motions based on the results of PSHA has been demonstrated by Bradley (2012a), however, an extension of this method has not previously been presented for scenario SHA, and it is therefore examined here. This chapter first provides an overview of the GCIM methodology for ground motion selection with scenario SHA, followed by several examples to illustrate the salient features of the procedure, including: (i) implementation of different weight vectors and the composition of the ***IM*** vector; (ii) quantifying the importance of replicate selections for different number of desired ground motions; and (iii) the effect of considering bounds on the implicit causal parameters of the prospective ground motions.

3 GCIM-based ground motion selection for scenario seismic hazard analysis (scenario SHA)

The GCIM method (Bradley 2010a) provides the distribution of a vector of ground motion IMs, ***IM***, consistent with the results of the seismic hazard analysis. It is considered that this general IM vector (which may contain, e.g., spectral acceleration ordinates, peak ground velocity, Arias intensity, and significant duration, among others) can adequately represent ground motion severity for the engineering systems considered. The steps towards conducting GCIM-based ground motion selection for scenario SHA are explained in the following sections.

3.1 Constructing the distribution of the IMs

Selection of ground motions for seismic response analysis requires a 'target', based on which the appropriateness of the selected ground motions is measured. In the GCIM approach, the multivariate distribution of the considered IMs is used as the target. Although not essential (Bradley 2010a), the lognormal multivariate distribution is considered here for the joint distribution of ***IM*** based on its observed appropriateness in previous applications (e.g., Baker and Jayaram 2008, Bradley 2011a, 2011b, 2011c, 2012b, 2012c, 2014). Based on this consideration, the marginal distribution of each IM_i in ***IM*** can be expressed as:

$$f_{IM_i|Rup} \sim LN(\mu_{lnIM_i|Rup}, \sigma^2_{lnIM_i|Rup}) \tag{1}$$

where $f_{IM_i|Rup}$ is the probability density function of IM_i, given the scenario rupture Rup; $X \sim LN(\,)$ is shorthand notation for X having a lognormal distribution; and $\mu_{lnIM_i|Rup}$ and $\sigma^2_{lnIM_i|Rup}$ are the mean and variance of $lnIM_i$, respectively. The necessary parameters to construct the marginal distribution of $IM_i$with respect to a specific scenario (i.e., $\mu_{lnIM_i|Rup}$ and $\sigma^2_{lnIM_i|Rup}$) can be obtained from empirical ground motion prediction equations (e.g., Boore and Atkinson 2008). In order to construct the multivariate distribution of the considered IMs, empirical correlation equations, (i.e., Baker and Jayaram 2008, Bradley 2011a, 2011b, 2011c, 2012b, 2012c, 2014), are used to construct the correlation matrix (i.e., $\boldsymbol{\rho}_{ln\boldsymbol{IM}|Rup}(i,j) = \rho_{ij}$, where ρ_{ij} is the correlation coefficient between $lnIM_i$ and $lnIM_j$ for the given rupture, Rup. The methodology adopted here to select ground motions is similar in concept to the method proposed by Wang (2011), however, the GCIM-based approach considers the multivariate distribution of a general vector of IMs as the target model in contrast to considering only spectral acceleration ordinates as in Wang (2011), and also allows for non-uniform weighting of the different intensity measures (as discusses in the next section).

3.2 Ground motion selection

3.2.1 Generating random realizations for the IMs

In order to account for the inherent variability of the IM values for a given scenario rupture it is necessary to select ground motions with an explicit representation of this variability. The most computationally efficient means to select ground motions that capture this variability is to generate random realizations of the considered IMs based on the multivariate GCIM distribution, and then select ground motions that most closely match the generated random realizations (Jayaram et al. 2011, Wang 2011, Bradley 2012a)

In order to generate random realizations for the considered IMs, a vector of uncorrelated random numbers with standard normal distribution is first generated ($\boldsymbol{u}^{nsim}$). Using the calculated correlation matrix, $\boldsymbol{\rho}_{ln\boldsymbol{IM}|Rup}$, the uncorrelated random numbers ($\boldsymbol{u}^{nsim}$) are converted to a vector of correlated random numbers, as illustrated in Equation (2):

$$\boldsymbol{v}^{nsim} = \boldsymbol{L}.\boldsymbol{u}^{nsim} \tag{2}$$

where $\boldsymbol{L}$ is from the Cholesky decomposition of the correlation matrix (i.e., $\boldsymbol{\rho}_{ln\boldsymbol{IM}|Rup} = \boldsymbol{L}\boldsymbol{L}^T$) and $\boldsymbol{v}^{\mathrm{nsim}}$ is the resulting vector of correlated random numbers with a standard normal

distribution. Subsequently, random realizations of the considered IMs are calculated using Equation (3):

$$lnIM_i^{nsim} = \mu_{lnIM_i|Rup} + \sigma_{lnIM_i|Rup}\, v_i^{nsim} \tag{3}$$

where $\sigma_{lnIM_i|Rup}$ is the square root of the variance (i.e., standard deviation) of $lnIM_i$ and v_i^{nsim} is the i^{th} element of v^{nsim}. The various values of IM_i^{nsim} for all i represent the $nsim^{\text{th}}$ realization of the IM vector, IM^{nsim}.

3.2.2 Finding an appropriate ground motion for nsimth realization

For each realization of the IM vector, $\boldsymbol{IM}^{nsim}$, a specific ground motion can be selected from a set of prospective motions, e.g., from the NGA database (Chiou et al. 2008), based on the specific motion which has the minimum mismatch to the generated random realization. Following Bradley (2012a), the mismatch of a prospective ground motion before applying any amplitude scale factor is calculated using Equation (4):

$$r^{m,nsim} = \sum_{i=1}^{N_{IM_i}} w_i \left[\frac{lnIM_i^{nsim} - lnIM_i^m}{\sigma_{lnIM_i|Rup}}\right]^2 \tag{4}$$

where IM_i^{nsim} is the i^{th} IM value of the $nsim^{\text{th}}$ random realization; IM_i^m is the i^{th} IM value of the m^{th} prospective ground motion; $\sigma_{lnIM_i|Rup}$ is the standard deviation of $lnIM_i$; w_i is the weight-vector component emphasizing the importance of IM_i, as discussed further in Bradley (2012a); and r_m^{nsim} is the calculated residual of the m^{th} prospective ground motion with respect to $nsim^{\text{th}}$ random realization.

It is important to highlight that, unlike the PSHA-based ground motion selection case, there is no uniquely defined amplitude scale factor for each ground motion (Bradley 2010a). Therefore, in order to rank the appropriateness of a prospective ground motion in the database, and identify the most suitable ground motion for $nsim^{\text{th}}$ realization, the calculated residual for each prospective ground motion is minimized with respect to the applied amplitude scale factor (*SF*), as presented in Equation (5):

$$r_{min}^{m,nsim} = \min_{SF}\left(\sum_{i=1}^{N_{IM_i}} w_i \left[\frac{lnIM_i^{nsim} - ln(SF^{\alpha} IM_i^m)}{\sigma_{lnIM_i|Rup}}\right]^2\right) \tag{5}$$

where SF is the amplitude scale factor; α is an integer describing how the IM value scales with SF (e.g., $\alpha = 1$ for spectral acceleration; $\alpha = 2$ for Airas Intensity; and $\alpha = 0$ for

significant duration) (Bradley 2012a). The $r_{min}^{m,nsim}$ value for the m^{th} prospective ground motion is used to rank it among all of the prospective ground motions in the database. The ground motion with the smallest $r_{min}^{m,nsim}$ value among all prospective motions is then selected as the ground motion for the $nsim^{th}$ realization. It is also noted that the minimization problem to be solved in Equation (5) is straightforward using standard single variable optimization routines because $r^{m,nsim}$ is a smooth function of SF.

3.2.3 Conducting Replicate Selections

Since ground motions are selected based on the random realization of the considered IMs using the above procedure, performing the selection process successive times may result in different selected ground motions. By repeating the selection process several times, the 'best' replicate can be obtained by comparing the distribution of the IMs from the selected sets with the predicted GCIM distribution for the scenario rupture (Bradley 2013a). This comparison is made on basis of calculating an overall residual, R, for a given selected set of ground motions, presented in Equation (6):

$$R = \sum_{i=1}^{N_{IM}} w_i (D_{IM_i})^2 \tag{6}$$

where D_{IM_i} is the Kolmogorov-Smirnov (KS) test statistic which is the maximum difference between the empirical distribution of IM_i (i.e., from the selected ground motions) and the corresponding target (theoretical) distribution calculated by the GCIM approach (i.e., Equation (1)). As indicated by Equation (6), the calculated overall residual, R, consists of the mismatch between the empirical and theoretical distributions of all of the IMs (i.e., D_{IM_i}), considering their relative importance dictated by the weight-vector component (i.e., w_i). Therefore, R is used to identify the best set of ground motions among the selected sets from the various replicates. It is expected that when a small number of ground motions is desired, the effect of replicate selection will be important (as one small set of realizations may not well represent the target distribution), with a decreasing importance as the desired number of ground motions increases. The process of conducting replicate selections along with the other steps in a GCIM-based ground-motion selection process is illustrated in Figure 1.

3.2.4 Summary of the scenario-based GCIM ground motion selection procedure

In order to summarize the required steps to select ground motions based on the GCIM methodology for scenario SHA, and depict the role of ground motion selection in a seismic

performance assessment framework, Figure 1 presents a flow chart illustrating the ground motion selection steps along with the necessary calculations before and after the selection. As seen in this flow chart, ground motion selection provides the key link between seismic hazard analysis and seismic response analysis. Therefore, it is important to note that any bias introduced at the ground motions selection stage may lead to bias in the obtained responses of the system and consequently decisions regarding the performance of the system.

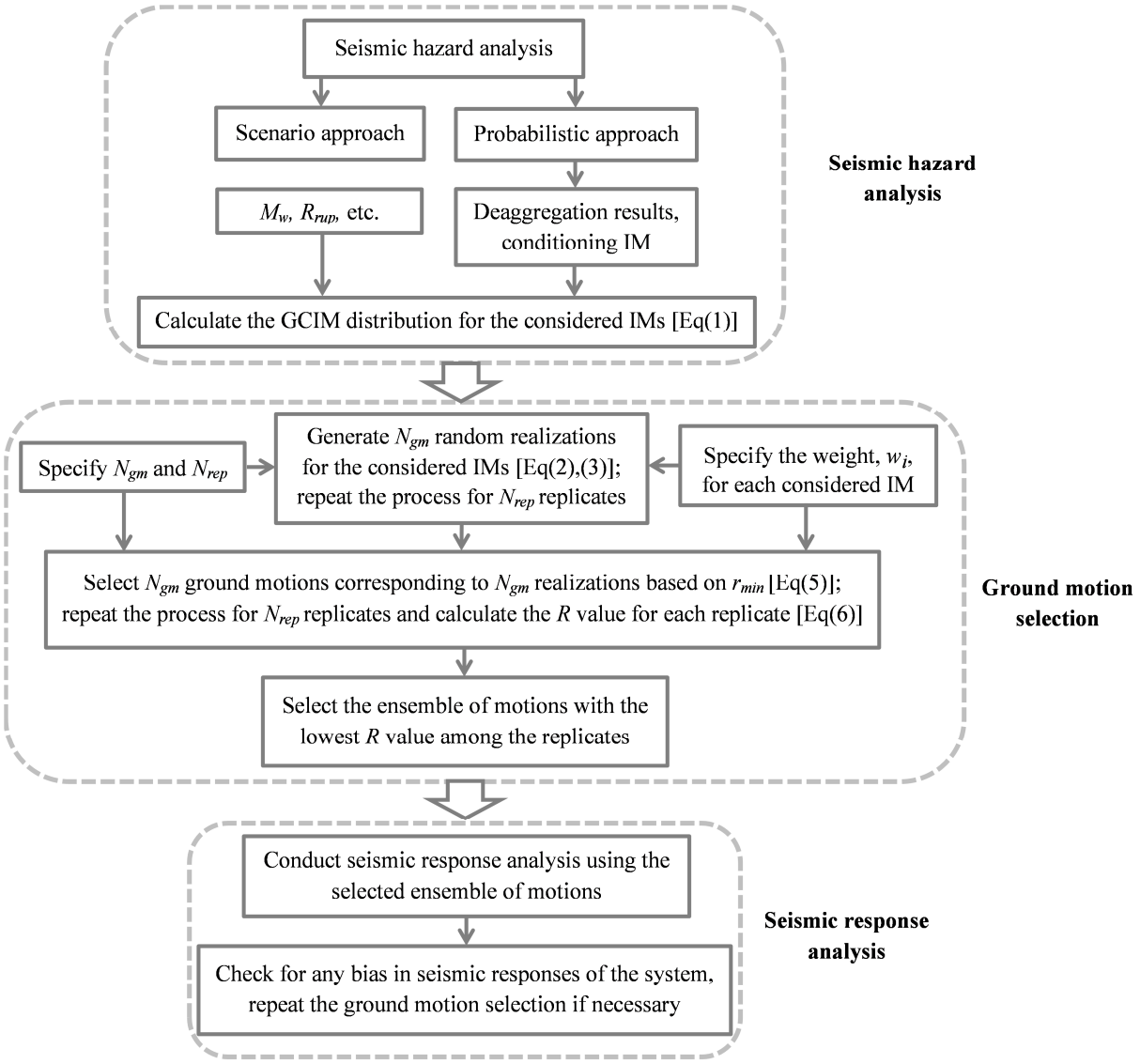

Figure 1: Ground motion selection based on the GCIM methodology in a seismic performance assessment framework

4 Application of the GCIM methodology for scenario SHA-based ground motion selection

In this section, ground motion selection applications using the GCIM methodology is presented. Different rupture scenarios and site conditions are considered and particular

attention is given to the possible external inputs required by the user to facilitate the ground motion selection. The specific issues covered in this section are:

i. Using different weight vectors, w_i, and their corresponding effects on the characteristics of selected ensemble of ground motions.
ii. Quantifying the importance of replicate selection for different numbers of desired ground motions.
iii. Effects of considering bounds on the implicit causal parameters (i.e., magnitude, source-to-site distance, site condition) of the prospective ground motions.

The considered rupture scenarios and the site conditions are presented in Table 1. As seen in this table, rupture scenarios with moderate and large magnitudes (M_w6.5 and 7.5) are considered, as well as small and moderate source-to-site distances (10km and 40km). Since the empirical ground motion prediction equations are not well-constrained for ruptures with extremely large magnitudes (8~9 M_w), these scenarios are not considered here. Soil conditions considered represent soft and stiff soil, and soft rock conditions (V_{s30}= 200, 400, 600 m/s). A strike-slip mechanism is used as the only focal mechanism for the considered scenario ruptures, because the average effect of focal mechanism are well captured simply through amplitude scaling of ground motions.

Table 1: Characteristics of the considered scenario ruptures and site conditions

Scenario	Magnitude, M_w	Source-to-site distance, R_{rup} (km)	Fault type	Site condition, V_{s30} (m/s)
M7.5R10V200	7.5	10	Strike Slip	200
M7.5R10V400	7.5	10	Strike Slip	400
M7.5R10V600	7.5	10	Strike Slip	600
M7.5R40V200	7.5	40	Strike Slip	200
M7.5R40V400	7.5	40	Strike Slip	400
M7.5R40V400	7.5	40	Strike Slip	600
M6.5R10V200	6.5	10	Strike Slip	200
M6.5R10V400	6.5	10	Strike Slip	400
M6.5R10V600	6.5	10	Strike Slip	600
M6.5R40V200	6.5	40	Strike Slip	200
M6.5R40V400	6.5	40	Strike Slip	400
M6.5R40V600	6.5	40	Strike Slip	600

A range of IMs are considered in this study in order to adequately represent ground motion amplitude, frequency content, duration, and cumulative effects. Specifically, these IMs include spectral acceleration for 18 vibration periods (T=0.05, 0.075, 0.1, 0.15, 0.2, 0.25, 0.3, 0.4, 0.5, 0.75, 1.0, 1.5, 2.0, 3.0, 4.0, 5.0, 7.5, and 10.0 s); peak ground acceleration (PGA); peak ground velocity (PGV); acceleration spectrum intensity (ASI); spectrum intensity (SI); displacement spectrum intensity (DSI); cumulative absolute velocity (CAV); arias intensity (AI); and 5-75% and 5-95% significant durations (D_{s575} and D_{s595}, respectively). Empirical ground motion prediction equations (GMPEs) to obtain the marginal distribution of these IMs are presented in Table 2. Also, presented in Table 3 are the empirical correlation equations and the corresponding values between the considered IMs based on Baker and Jayaram (2008) and Bradley (2011a, 2011b, 2011c, 2012b, 2012c, 2014).

Table 2: GMPEs to obtain the marginal distribution of the considered IMs

IM	SA, PGA, PGV	ASI	SI	DSI
GMPE	Boore and Atkinson (2008)	Bradley (2010b)	Bradley et al. (2009)	Bradley (2011a)
IM	CAV	AI	D_{s575}	D_{s595}
GMPE	Campbell and Bozorgnia (2010)	Campbell and Bozorgnia (2012)	Bommer et al. (2009).	Bommer et al. (2009).

Table 3: Empirical correlation equations and values between the considered IMs

IM	SA	PGA	PGV	ASI	SI	DSI	CAV	D_{s575}	D_{s595}	AI
SA	BJ08*	B11(b)*	B12(b)*	B11(b)*	B11(b)*	B11(a)*	B12(c)*	B11(c)*	B11(c)*	B14(a)*
PGA	-	1.0	0.73	0.93	0.60	0.40	0.70	-0.41	-0.44	0.83
PGV	-	-	1.0	0.73	0.89	0.80	0.69	-0.21	-0.26	0.73
ASI	-	-	-	1.0	0.64	0.37	0.70	-0.41	-0.37	0.81
SI	-	-	-	-	1.0	0.78	0.68	-0.13	-0.08	0.68
DSI	-	-	-	-	-	1.0	0.57	0.07	0.16	0.51
CAV	-	-	Symmetric		-	-	1.0	0.08	0.12	0.89
D_{s575}	-	-	-	-	-	-	-	1.0	0.84	-0.19
D_{s595}	-	-	-	-	-	-	-	-	1.0	-0.20
AI	-	-	-	-	-	-	-	-	-	1.0

*Equations are functions of vibration period: BJ08=Baker and Jayaram (2008); B11(b)=(Bradley 2011b); B12(b)=(Bradley 2012b); B11(a)=(Bradley 2011a); B12(c)=(Bradley 2012c); B11(c)=(Bradley 2011c); B14(a)=(Bradley 2014);

4.1 Effect of the weight vector on the characteristics of selected ensemble of motions

Different aspects of a ground motion affect the seismic response of different engineering systems, and even different seismic response metrics within the same system (Bradley et al. 2010). Therefore, prior to selecting ground motions, it is important to identify the type of engineering system and seismic response metrics considered for seismic performance assessment, so that the selection process can aim to place emphasis on those intensity measures important to determine the characteristic response of the system. For instance, empirical evidence suggests that the peak inter-story drift of a building structure is strongly affected by spectral acceleration ordinates of the applied motion for periods near the first several vibration modes of the structure (e.g., Shome et al. 1998, Tothong and Cornell 2007). In contrast, for example, the response of geotechnical structures with liquefaction-susceptible soils and the collapse capacity of building structures can be considerably affected by duration and cumulative effects of ground motions (Bradley 2010a, Bradley et al. 2013, Villaverde 2007). This problem-specific issue has been addressed in the GCIM-based ground motion selection methodology by using a weight vector in the selection algorithm (Bradley 2012a), to weight these different ground motion aspects in record selection. In order to consider different aspects of a ground motion (i.e., intensity, frequency content, duration, and cumulative effect) the selection procedure should be based on representativeness of multiple intensity measures for the considered rupture scenarios.

The effect of the weight vector is illustrated by presenting the results for the selection of 20 motions (i.e., $N_{gm} = 20$) by conducting 10 replicate selections (i.e., $N_{rep} = 10$). $N_{rep} = 10$ is shown subsequently to be more than sufficient to give stable results for $N_{gm} = 20$. Table 4 presents the weight vectors examined in this study to scrutinize the corresponding effects on the characteristics of selected ensembles of ground motions. Weight vector case 1 represents the conventional approach to select ground motions based only on SA ordinates. Case 2 represents a selection mainly based on SA ordinates with some consideration allocated to significant duration of motion. Case 3, 4, and 5 represent the consideration of CAV and AI (as well as SA ordinates) as metrics to account for cumulative effects of ground motions in lieu of duration. Case 6 represents a selection based on significant duration and cumulative effects (i.e., CAV and AI) as well as SA ordinates. Finally, case 7 represents a selection based on ASI, SI, and DSI in lieu of SA ordinates given that ASI, SI, and DSI represents the amplitude of the ground motion in short, moderate, and long vibration periods.

Because of the large number of permutations resulting from the consideration of the numerous values of the above variables, a complete presentation of all of the permutation results is not attempted. Rather, illustrative figures and summary statistics are used to convey the key features of the obtained results.

Table 4: Weight vectors considered for the ground motion selections

Case	SA	D_{s575}	D_{s595}	AI	CAV	ASI	SI	DSI
1	1.0[1]	-	-	-	-	-	-	-
2	0.7[1]	0.15	0.15	-	-	-	-	
3	0.7[1]	-	-	0.3	-	-	-	-
4	0.7[1]	-	-	-	0.3	-	-	-
5	0.7[1]	-	-	0.15	0.15	-	-	-
6	0.6[1]	0.10	0.10	0.10	0.10	-	-	-
7	-	-	-	-	-	0.33	0.33	0.33

[1]Evenly distributed to 18 *SA* ordinates, e.g., for case 1 each SA ordinates has a weight of $w_i = 1/18$

4.1.1 Selection based only on spectral acceleration ordinates

Spectral acceleration ordinates have been conventionally used as a metric to represent the amplitude of ground motions via the response of a simplified substitute single-degree-of-freedom system. As a result, acceleration response spectral ordinates are considered in the majority of ground motion selection procedures as the target to select ground motions (e.g., Jayaram et al. 2011, Wang 2011, ASCE/SEI7-10 2010, NIST 2011, NZS1170.5 2004). In order to investigate the characteristics of the motions selected based only on SA ordinates, GCIM-based ground motion selection is conducted for the considered rupture scenarios and site conditions, considering only SA ordinates in the weight vector (i.e., case 1).

Figure 2a presents the 16th, 50th, and 84th percentiles of the target (i.e., GCIM) distribution for SA ordinates of the M6.5R10V400 rupture scenario (i.e., $M_w = 6.5$, $R_{rup} = 10\ km$, , $V_{s30} = 400\ m/s$) and the acceleration response spectrum of the individual motions selected using weight vector case 1. The 16th, 50th, and 84th percentiles of SA ordinates of the selected motions are also presented in this figure. It can be seen that the selected motions properly address the variability in SA ordinates of the target (i.e., GCIM) distribution for the whole range of vibration periods, as intended by the adopted weight vector. An appropriate representativeness of the selected motions can be seen by the conformity of the 16th-, 50th-, and 84th-percentiles of the selected motions to the 16th, 50th, and 84th percentiles of the GCIM distribution.

Despite the conformity of the selected motions to the target distribution of SA ordinates, the selected motions may have a biased representation for other important IMs. As depicted in Figure 2b, as an example, the 5-95% significant duration, D_{s595}, of the selected motions based only on SA ordinates (i.e., weight vector case 1) have a bias in representing the predicted distribution of D_{s595} for the considered rupture scenario, as indicated by the empirical distribution lying outside the Kolmogorov-Smirnov (KS) test bounds for $\alpha = 5\%$ significance level (Ang and Tang 1975). It is important to note that having a biased distribution for certain IMs will cause a bias in the obtained seismic responses of the system, if such responses are affected by these biased IMs (Bradley 2010a, 2012a).

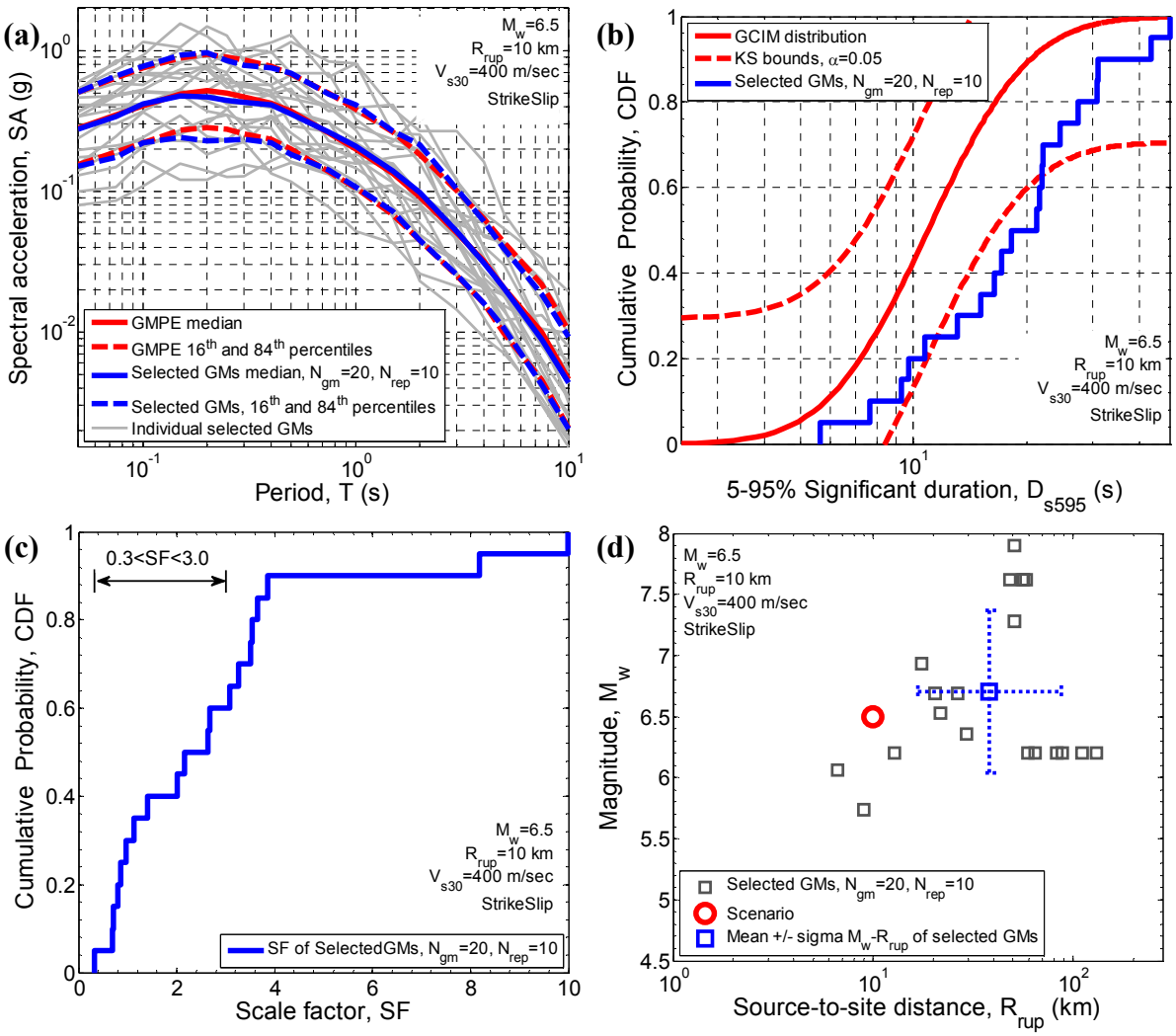

Figure 2: Properties of selected motions based only on SA ordinates (i.e., weight vector case 1) for the M6.5R10V400 rupture scenario: (a) SA ordinates; (b) cumulative distribution of Ds595; (c) cumulative distribution of the amplitude scale factors; and (d) $M_w - R_{rup}$ distribution

While ground motion selection using the GCIM method does not make explicit use of the amplitude scale factors or other implicit causal parameters such as magnitude, source-to-

site distance, and site condition, examining the distributions of these parameters for the selected motions is often a good independent check of the quality of the obtained results (Bradley 2012a). Figure 2c presents the cumulative distribution of the amplitude scale factors of the selected motions for the considered scenario. As seen in this figure, approximately 70% of the selected ground motions have an amplitude scale factor in the range of 0.3-3.0. Similar ranges are often recommended as scaling limits in seismic design standards (ASCE/SEI7-10 2010, NZS1170.5 2004).

Figure 2d illustrates the magnitude and source-to-site distance distribution of the motions selected based only on SA ordinates with respect to the target rupture scenario. As seen in this figure, the mean magnitude of the selected motions is fairly close to the magnitude of the target scenario, however, the selected motions have mostly greater R_{rup} values when compared to the small R_{rup} of the rupture scenario. The slightly larger magnitude, and larger source-to-site distance are the likely reason for the biased distribution of D_{s595} shown in Figure 2b, given that D_{s595} increases with M_w and R_{rup} (Bommer et al. 2009).

The $M_w - R_{rup}$ distribution of selected motions is also obviously a function of the seismic rupture scenario considered in addition to the weight vector adopted. For example, in contrast to Figure 2d (with $M_w = 6.5, \quad R_{rup} = 10\,km, \; V_{s30} = 400\,m/s$), Figure 3a illustrates the $M_w - R_{rup}$ distribution of the selected motions for the M7.5R10V400 rupture scenario (i.e., $M_w = 7.5, \; R_{rup} = 10\,km, V_{s30} = 400\,m/s$), using weight vector case 1 (i.e., SA only). In this case it can be seen that the average magnitude of the selected motions is less than that for the rupture scenario, principally as a result of the paucity of the recorded motions during events with large magnitudes (and the use of a weight vector with non-zero values only for SA ordinates). As presented in Figure 3b, in contrast to the results presented in Figure 2c, amplitude scale factors of the selected motions for the M7.5R10V400 rupture scenario are mostly larger compared to those for the M6.5R10V400 rupture scenario. This is due to the fact that the database of strong ground motions is not well-constrained for motions from large magnitude scenarios, therefore, large amplitude scaling factors are required to scale the available motions to match the intensity of motion predicted for those scenarios.

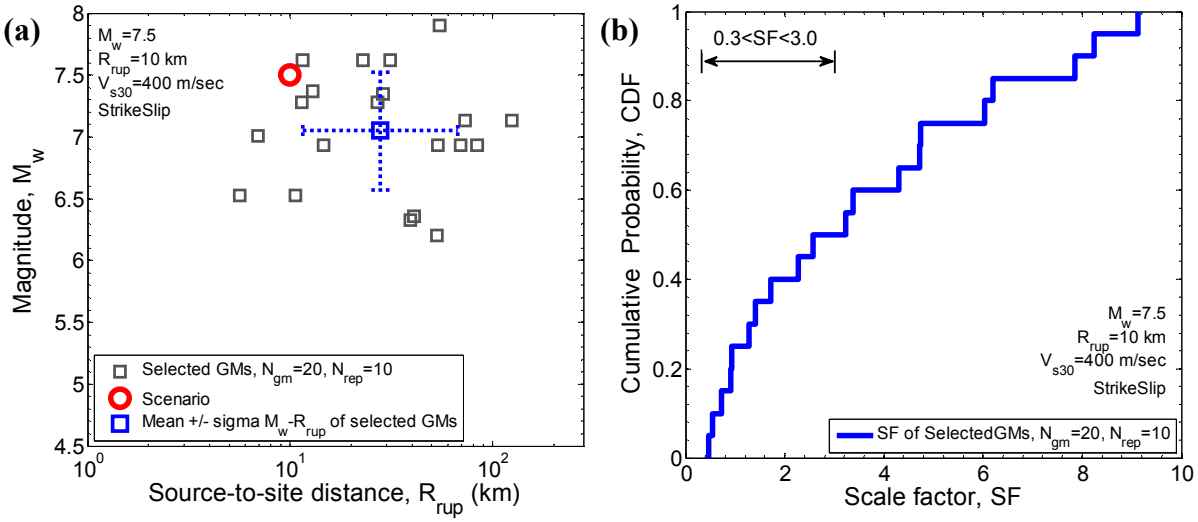

Figure 3: (a) $M_w - R_{rup}$ distribution; and (b) amplitude scale factors of selected ground motions for the M7.5R10V400 rupture scenario using weight vector case 1 (i.e., SA only)

Figure 4b-c presents the shear wave velocity versus source-to-site distance (i.e., $V_{s30} - R_{rup}$) distribution of the selected motions for the scenarios with $M_w = 6.5$, $R_{rup} = 10\ km$ and V_{s30} =200, 400, and 600 m/s soil conditions. As seen in this figure, the selected motions do not have an appropriate representation for V_{s30} of a soft soil (i.e., $V_{s30} = 200$) and soft rock (i.e., $V_{s30} = 600$), as much as they have for a stiff soil (i.e., $V_{s30} = 400$). This is again likely a result of the larger portion of ground motions recorded on stiff soils in empirical ground motion databases than records on soft soils and soft rock. Similar results have been obtained using other weight vectors for the considered rupture scenarios presented in Table 1.

Further discussion on the representativeness of the selected motions for these and other implicit causal parameters is elaborated on further when bounds are applied on the implicit causal parameters of prospective ground motions in section 4.3.

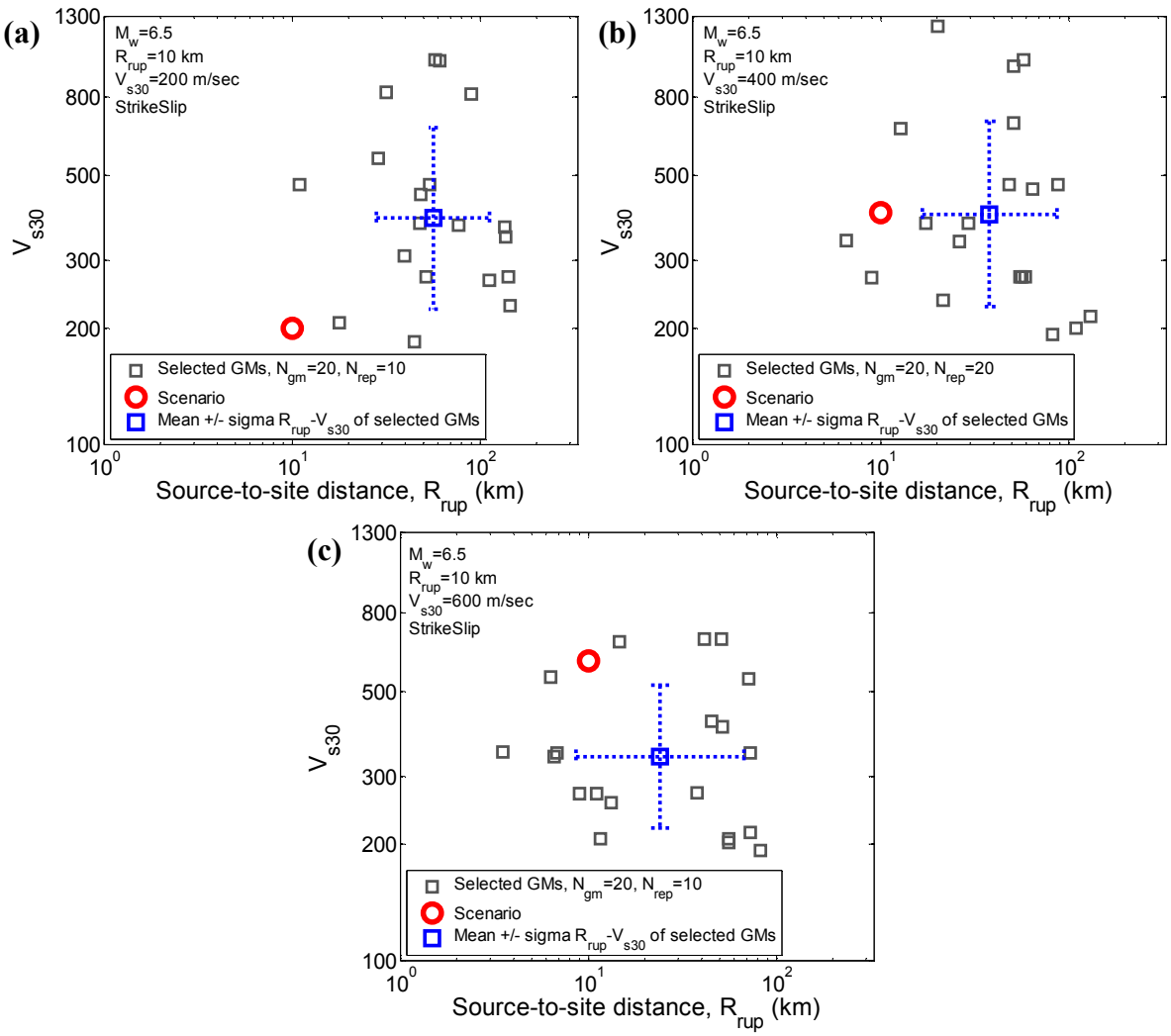

Figure 4: $M_w - R_{rup}$ distribution of selected motions using weight vector case 1 (i.e., SA only) for the M6.5R10 rupture scenario with: (a) $V_{s30} = 200$; (b) $V_{s30} = 400$; and (c) $V_{s30} = 600$ soil conditions

4.1.2 Selection based on SA ordinates and significant duration

As depicted in Figure 2b, selecting ground motions based only on SA ordinates may result in motions with an inadequate representation for significant duration, a result of the fact that SA ordinates only explicitly consider the amplitude and frequency content of a ground motion. Although there are many definitions to represent duration of ground motions (Bommer and Martinez-Pereira 1999), significant duration is chosen here as the duration-metric for reasons discussed in Bradley (2011c).

In order to explicitly examine the influence of considering significant duration on the characteristics of the selected ground motions, a second weight vector case was considered (i.e., case 2) which prescribes a total of 70% weight across the SA ordinates and 30% weight to significant duration-based metrics (i.e., D_{s575} and D_{s595}). The reason for allocating 30% of

the total weight on D_{s575} and D_{s595} is based on the numerous selections conducted in this study, indicating that using a total weight of less than 60% on SA ordinates results in motions with a poor representation for the target distribution of SA ordinates.

Figure 5a-c presents the cumulative distribution of 5-75% and 5-95% significant duration IMs of the ground motions selected for the M6.5R10V400 scenario using weight vector case 2 (i.e., SA, D_{s575}, and D_{s595}). As seen in this figure, the selected motions have an unbiased representation for D_{s575} and D_{s595}, along with an appropriate representation for the median, 16^{th}, and 84^{th} percentiles of the SA ordinates presented in Figure 5c. Figure 5d illustrates the magnitude and source-to-site distance distribution of the selected motions using weight vector case 2 (i.e., SA, D_{s575}, and D_{s595}). It can be seen that source-to-site distance of the selected motions are closer to the target scenario in comparison with the results presented in Figure 2d (i.e., the mean-standard deviation of R_{rup} now encompass the R_{rup} value of the rupture scenario). Since, as mentioned previously, significant duration of a ground motion is correlated with magnitude and source-to-site distance of the rupture scenario (Bommer et al. 2009), then enforcing ground motion selection to consider significant duration is seen to have a positive effect on the proper representation of the scenario source-to-site distance.

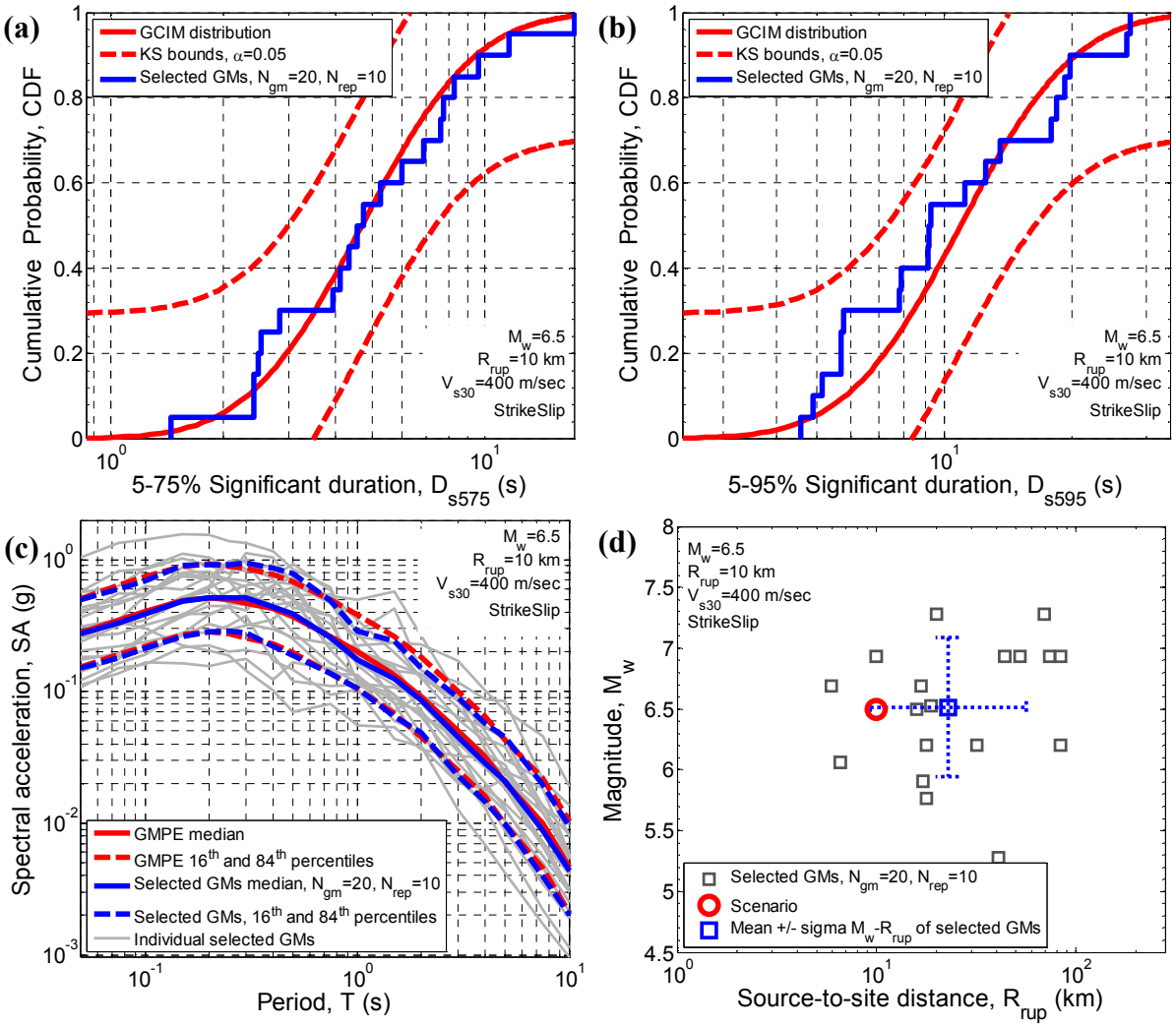

Figure 5: Properties of selected motions using weight vector case 2 (i.e., SA, D_{s575}, and D_{s595}) for the M6.5R10V400 rupture scenario: (a) cumulative distribution of D_{s575}; (b) cumulative distribution of D_{s595}; (c) SA ordinates; and (d) $M_w - R_{rup}$ distribution

4.1.3 Including cumulative effects in ground motion selection

Considering ground motion cumulative effects is an important issue for seismic response analysis of systems susceptible to these effects. Arias intensity (AI) and cumulative absolute velocity (CAV) are commonly used in research and practice to consider the cumulative effects of ground motions (Campbell and Bozorgnia 2010, 2012). Each of these IMs represents slightly different cumulative aspects of a ground motion. Bradley (2014) illustrates that AI is principally correlated with the high frequency content of a ground motion, whereas CAV is principally correlated with the moderate-to-low frequency content. As a result, depending on the problem considered, ground motion selection based on only one of these IMs may not appropriately represent the important cumulative aspects of the ground motions for the system considered. This issue is elaborated on in this section.

Before considering cumulative effects in ground motion selection, it is worthwhile observing the distribution of AI and CAV in selected ground motions when they are not explicitly considered in the weight vector. Figure 6 presents the cumulative distribution of AI and CAV for the M6.5R40V200 scenario using weight vector case 1 (i.e., SA only). As seen in this figure, both distributions of AI and CAV are biased with respect to the target distribution.

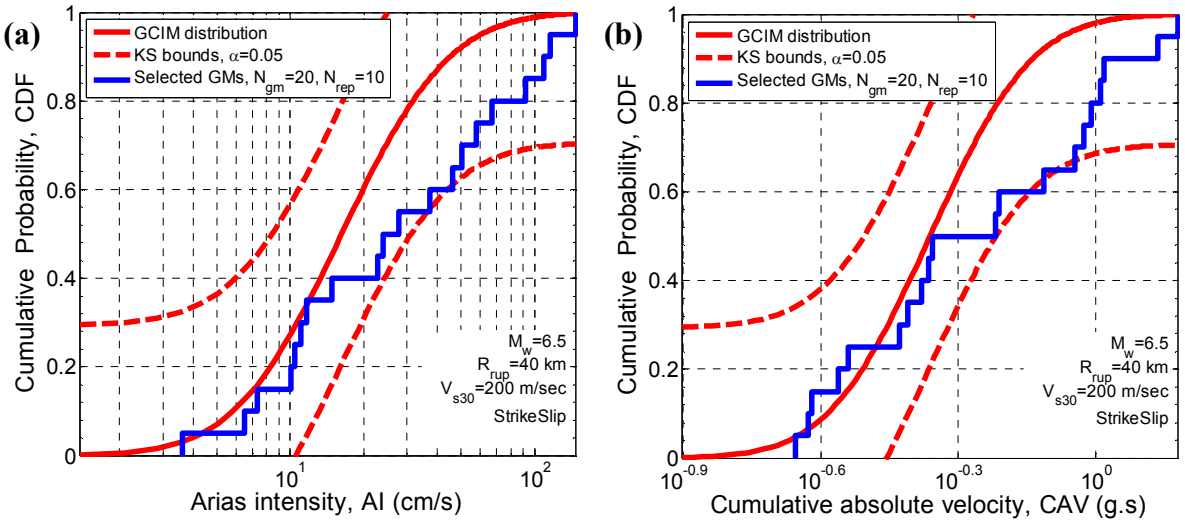

Figure 6: Cumulative distribution of: (a) AI; and (b) CAV for the M6.5R40V200 rupture scenario using weight vector case 1 (i.e., SA only)

Figure 7 presents the cumulative distribution of AI and CAV for the M6.5R10V200 scenario when weight vector case 2 (i.e., SA, D_{s575}, and D_{s595}) is used for selecting ground motions. As seen in Figure 7, considering both significant duration IMs (i.e., D_{s575}, D_{s595}) and SA ordinates does not result in an unbiased representation of AI and CAV for the M6.5R10V200 rupture scenario, as the empirical distribution of AI and CAV for this scenario are intersecting with the KS bounds at 5% significance level. It should be noted that, as presented in Table 3, the correlation between significant duration IMs and cumulative effects of ground motions (i.e., AI and CAV) is relatively small (having negative correlation with AI). Therefore it is not unexpected that considering the significant duration IMs in the weight vector (i.e., case 2) does not assist in achieving a proper representation for AI and CAV.

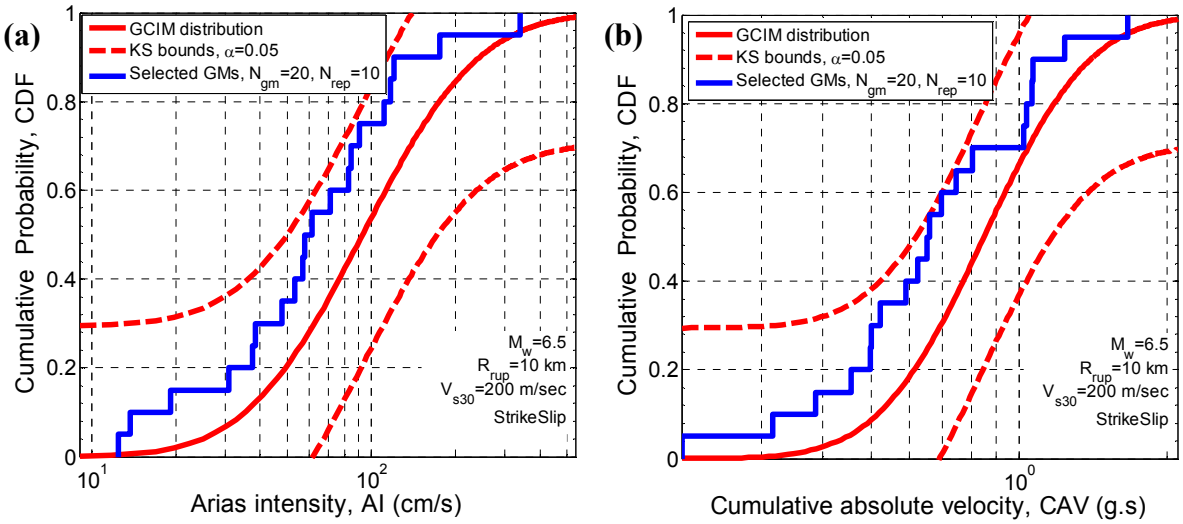

Figure 7: Cumulative distribution of: (a) AI; and (b) CAV for the M6.5R10V200 rupture scenario using weight vector case 2 (i.e., SA, D_{s575}, and D_{s595})

The results presented in Figure 6 and Figure 7 indicate the inadequacy of considering only SA, or SA and significant duration IMs, to capture the cumulative effects of ground motions. Therefore it is necessary to consider these effects by assigning non-zero weights to them in the weight vector, rather than relying on SA and duration to enforce an appropriate representation for them. In this regard, weight vector cases 3, 4, and 5 (see Table 4) are used to investigate incorporating cumulative ground motion effects in the selection process. Specifically, in weight vector cases 3 and 4, only AI or CAV are considered in addition to SA ordinates, while in weight vector case 5 both AI and CAV are considered in addition to SA ordinates. In all three weight vector cases, similar to weight vector case 2 (i.e., SA, D_{s575}, and D_{s595}), a 70% weight is given to SA ordinates and 30% weight to the cumulative intensity measures (as presented in Table 4).

Figure 8 presents the cumulative distribution of AI and CAV for the M6.5R10V400 scenario when the cumulative effects are considered by placing a weight only on AI and SA ordinates (i.e., weight vector case 3). It can be seen in Figure 8 that the AI distribution of the selected motions is consistent with the target distribution, however, the selected motions have a bias in representing CAV for the considered scenario at the 5% significance level. It should be noted, though not shown, that these selected motions have an appropriate representation for the distribution of SA ordinates, but a biased representation for D_{s575}, and D_{s595}.

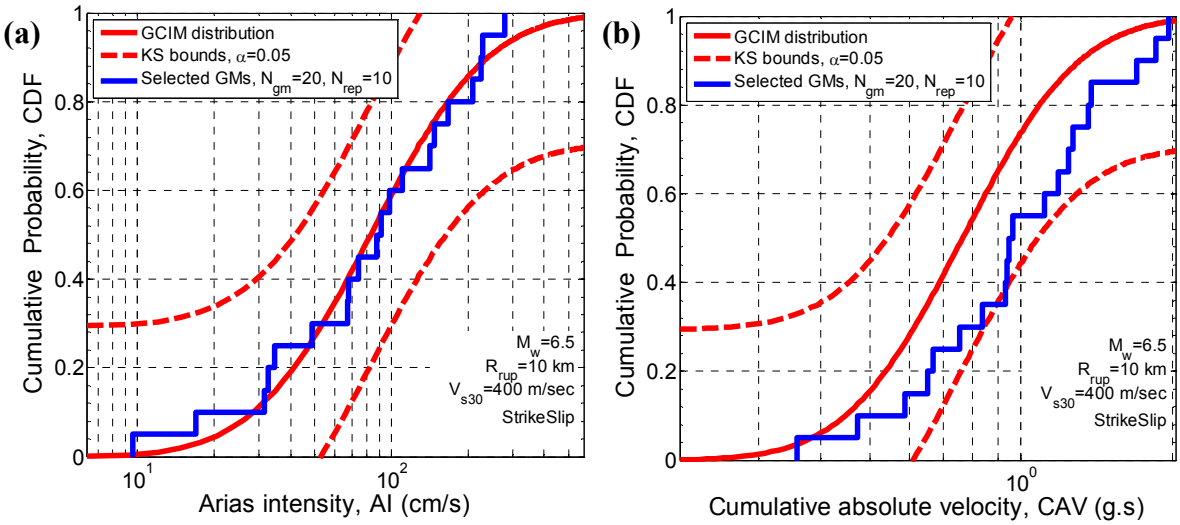

Figure 8: Properties of selected motions using weight vector case 3 (i.e., SA and AI) for the M6.5R10V400 rupture scenario: cumulative distribution of (a) AI; and (b) CAV

In contrast to the results presented in Figure 8, Figure 9 presents the cumulative distribution of AI and CAV when the weight is only placed on CAV and SA ordinates (i.e., weight vector case 4). As seen in this figure, there is a proper representation for CAV (as expected), and also there is an unbiased distribution of AI. The reason for having an unbiased representation of the AI distribution for most of the considered scenarios and site conditions in Table 1 when CAV and SA ordinates are considered in the weight vector (i.e., weight vector case 4) can be related to the strong correlation of AI with the short-period SA ordinates of the ground motion (Bradley 2014), which are relatively well covered by the implemented weight vector here (i.e., 18 SA ordinates). Although not shown here, the selected motions provide an appropriate representation for the SA ordinates, but a biased representation for significant duration IMs exists, illustrating that the observed bias in AI and CAV when only SA and D_{s575}/ D_{s595} are considered in the weight vector is also reciprocated with bias in D_{s575}/ D_{s595} when only SA and CAV or AI are considered in the weight vector (discussed in the subsequent paragraph).

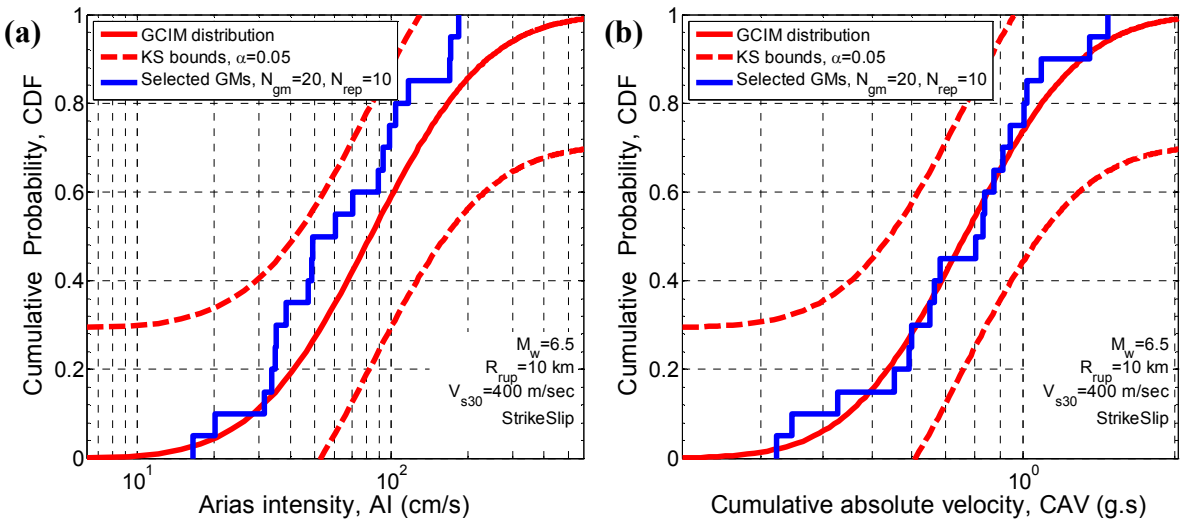

Figure 9: Properties of selected motions using weight vector case 4 (i.e., SA and CAV) for the M6.5R10V400 rupture scenario: cumulative distribution of (a) AI; and (b) CAV

Given the fact that considering AI or CAV in ground motion selection does not necessarily imply that the distribution of the other intensity measure will be well represented in the selected ground motions, it is beneficial to consider the effect of including both of AI and CAV in the selection process with equal weights (i.e., weight vector case 5 in Table 4). Figure 10a-b illustrates AI and CAV distributions of the selected motions compared with the corresponding target distributions, for which it can be seen that the selected motions provide a good representation. Figure 10c also illustrates the appropriate representation of the selected motions for SA ordinates. However, as shown in Figure 10d, the selected motions have a biased representation for the 5-95% significant duration of the considered rupture scenario. Although not presented here, distribution of the 5-75% significant duration is also biased.

Based on the obtained results it can be seen that having an appropriate representation for the cumulative effects of ground motions for a scenario rupture does not necessarily guarantee an appropriate representation for significant duration IMs of the motions as well. This is consistent with the results of Bradley (2011c) and (2014) who found a near-zero correlation between the residual of significant duration IMs (i.e., D_{s575} or D_{s595}) and AI and CAV; and the results of Bommer et al. (2006) who found a relatively weak correlation between durations and equivalent number of cycles (a cumulative IM).

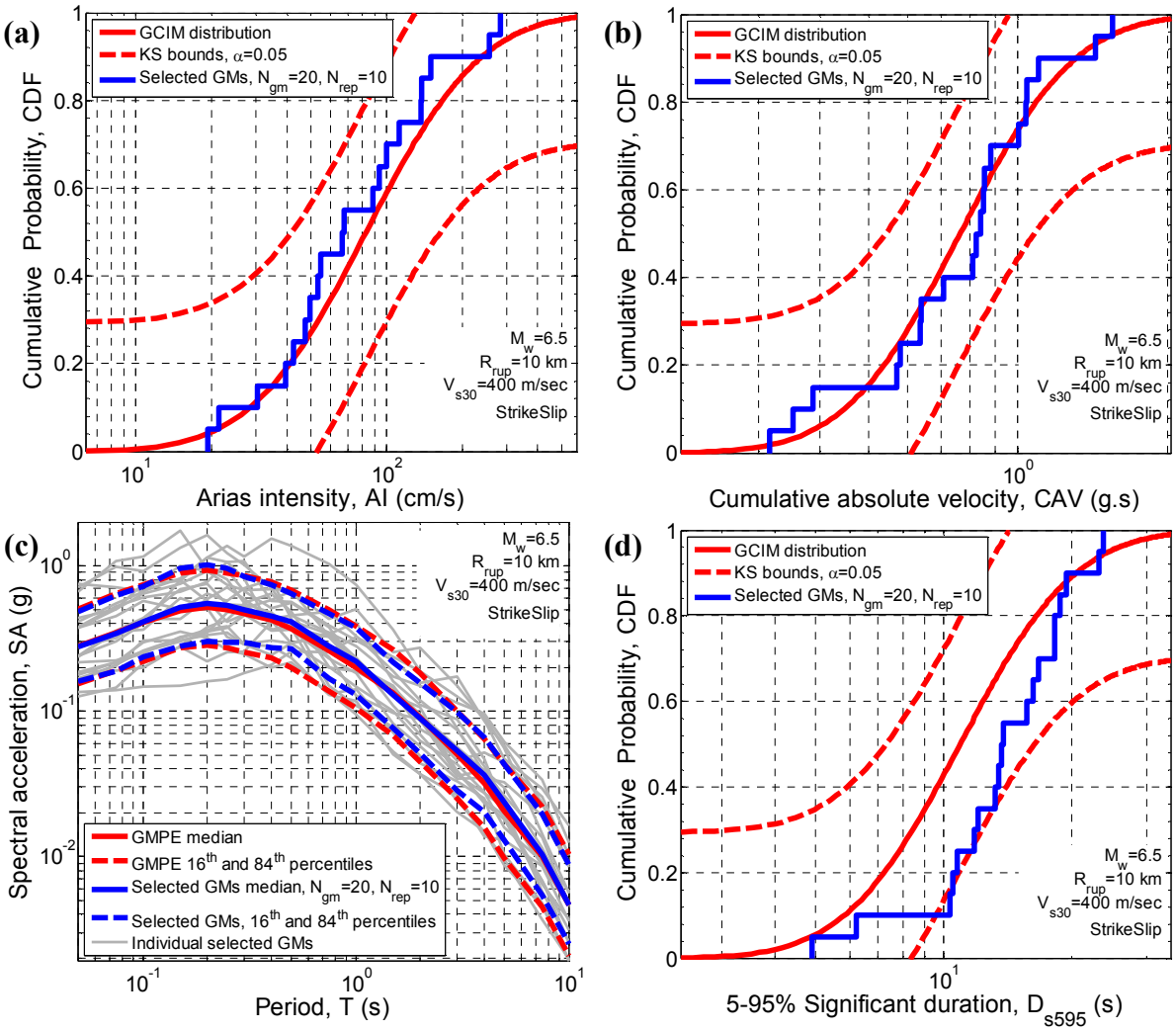

Figure 10: Properties of selected motions using weight vector case 5 (i.e., SA, AI, and CAV) for M6.5R10V400 rupture scenario: (a) cumulative distribution of AI; (b) cumulative distribution of CAV; (c) SA ordinates; and (d) cumulative distribution of D_{s595}

It is worth mentioning that depending on the rupture scenario characteristics and the site condition, having a biased representation for D_{s595} does not necessarily imply a biased representation for D_{s575}. This is due to the fact that the 5-75% and 5-95% significant duration IMs do not have a perfect correlation (i.e., $\rho(D_{s575}, D_{s595})$ =0.843, as presented in Table 3.

4.1.4 Including both cumulative and duration effects in ground motion selection

Based on the presented results so far, it is evident that neglecting certain aspects of the ground motion for a rupture scenario (e.g., duration or cumulative effects) will most likely result in ground motions with a biased representation for the IMs representing those aspects. For instance, as elaborated, capturing the cumulative effects of the ground motion does not necessarily result in capturing the duration effect of the motion and vice versa. This is due to the fact that the cumulative effects of ground motions (presented in this study by AI and

CAV) are proxy representatives for the total energy content of the motion and not the duration of motion, whereas, significant duration IMs (i.e., D_{s595} and D_{s575}) represents the arrival time between certain thresholds of the total energy of the motion and not the amount of the energy itself. Therefore, the distinction between the cumulative effects (i.e., energy content) and the significant duration of the motion should be noted in the selection process. In order to conduct response history analysis of systems susceptible to the cumulative and duration effects, such as geotechnical structures with liquefaction-susceptible soils or structural systems (i.e., buildings and bridges) with strength and stiffness degrading behaviour, it is therefore prudent to consider both significant duration and cumulative effects (as well as SA ordinates) in the selection process, because the damage in these types of structures is dependent upon amplitude of the applied motion, as well as the total input energy and duration of the strong phase of the motion (Bradley 2010a, Bradley et al. 2013, Villaverde 2007, Bommer et al. 2006).

Based on the abovementioned issues, ground motion selection is conducted using weight vector case 6, in which cumulative and duration effects are both considered with SA ordinates in the weight vector. Figure 11a illustrates the conformity of the 16^{th}, 50^{th}, and 84^{th} percentiles of the distribution of SA ordinates to the target distribution for the selected ground motions. Also, Figure 11b-d illustrate the appropriate representation of the selected motions to the target distribution of the D_{s595}, AI, and CAV, respectively. Although not presented in this figure, the selected motions have also an appropriate representation for D_{s575}.

It is important to note in the various results presented so far that considering IMs other than SA ordinates does not have an obvious detrimental effect on representativeness of the selected motions for the distribution of SA ordinates themselves. As noted previously, this is observed by the authors to be the results of assigning 60-70% weight to the SA ordinates, and the use of a total weight less than 60% for SA ordinates will result in a degraded representation of the SA ordinate distribution of the selected motions.

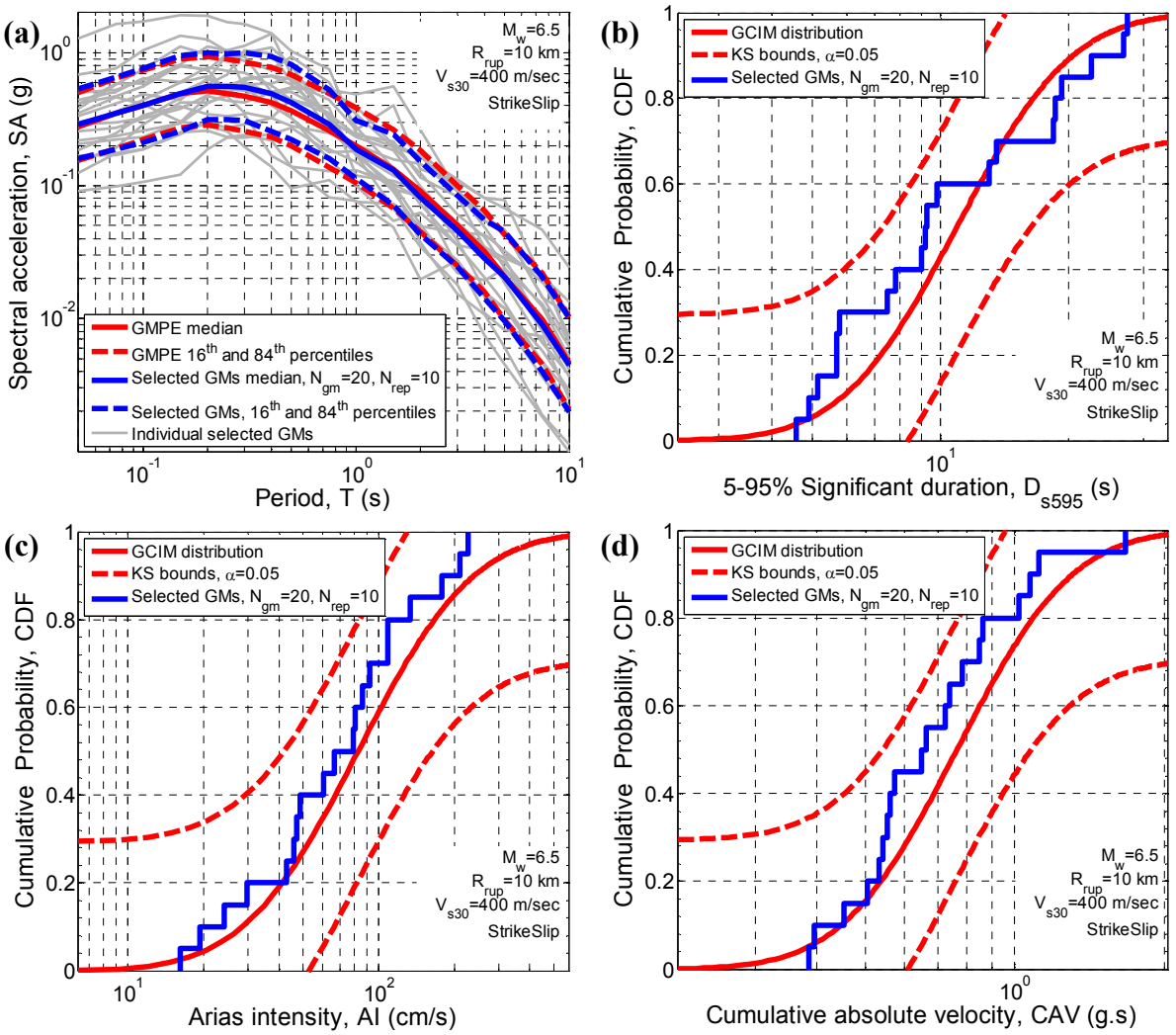

Figure 11: Properties of selected motions using weight vector case 6 (i.e., SA, AI, CAV, D_{s595}, and D_{s575}) for the M6.5R10V400 rupture scenario: (a) SA ordinates; cumulative distribution of (b) D_{s595}; (c) AI; and (d) CAV

4.1.5 Representation of the selected motions based on SA ordinates for other spectral intensities (i.e., ASI, SI, DSI)

Acceleration spectrum intensity (ASI), spectrum intensity (SI), and displacement spectrum intensity (DSI) are IMs calculated based on integration of the spectral ordinates over short (i.e., T=0.1s-0.5), medium (i.e., T=0.1-2.5), and long (i.e., T=2.0-5.0) vibration periods, respectively (Bradley 2011a, 2010b, Bradley et al. 2009). Therefore, motions selected based on an appropriate representation for the distribution of SA ordinates (i.e., weight vector case 1) may have a proper representation for ASI, SI, and DSI, without explicitly considering them in the weight vector. Figure 12 illustrates the cumulative distribution of ASI, SI, and DSI of the selected motions using weight vector case 1 (i.e., SA only) for the M6.5R10V400 scenario (i.e., the same selection case as considered in Figure 2),

as an example among the other considered rupture scenarios and site conditions. As seen in this figure, the selected motions have a proper representation for the predicted distribution of ASI, SI, and DSI, which is intuitively consistent with the proper representation of the selected motions for the whole range of the scenario spectrum illustrated in Figure 2a. This indicates that placing weights on these IMs in addition to those on SA ordinates would result in duplication.

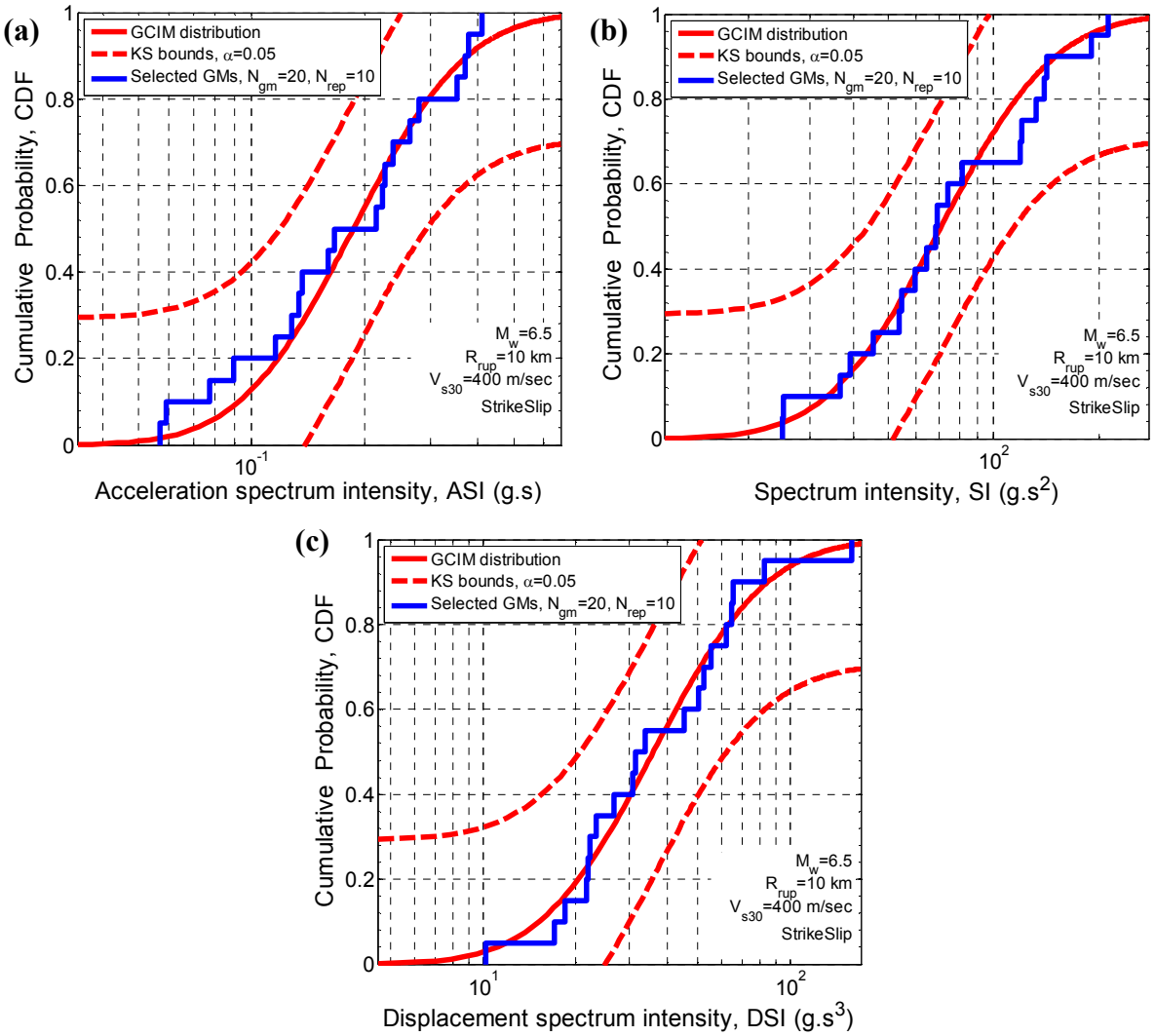

Figure 12: Cumulative distribution of ASI, SI, and DSI of selected motions using weight vector case 1 (i.e., SA only) for M6.5R10V400 rupture scenario

It is also worthwhile examining the characteristics of the motions selected based only on ASI, SI, and DSI without considering SA ordinates to see if the results of Figure 12 hold in the reverse sense. For this purpose, weight vector case 7 is used, in which an equal weight of 0.33 is given to each of ASI, SI, and DSI (see Table 4) for the purpose of ground motion selection. Figure 13 illustrates the median, 16th, and 84th percentiles of SA ordinates of the

selected motions for the M7.5R40V400 and M6.5R10 V400 scenarios. As seen in this figure, and based on the obtained results for other scenarios and site conditions, the selected motions have an appropriate representation for SA ordinates mostly at 0.2-3.5 period range, because this period range is well represented in the implemented weight vector via ASI, SI, and DSI. For the vibration periods out of this range, the median, 16th, and 84th percentile spectra of the selected motions may exhibit moderate to large deviations from the target GCIM distribution.

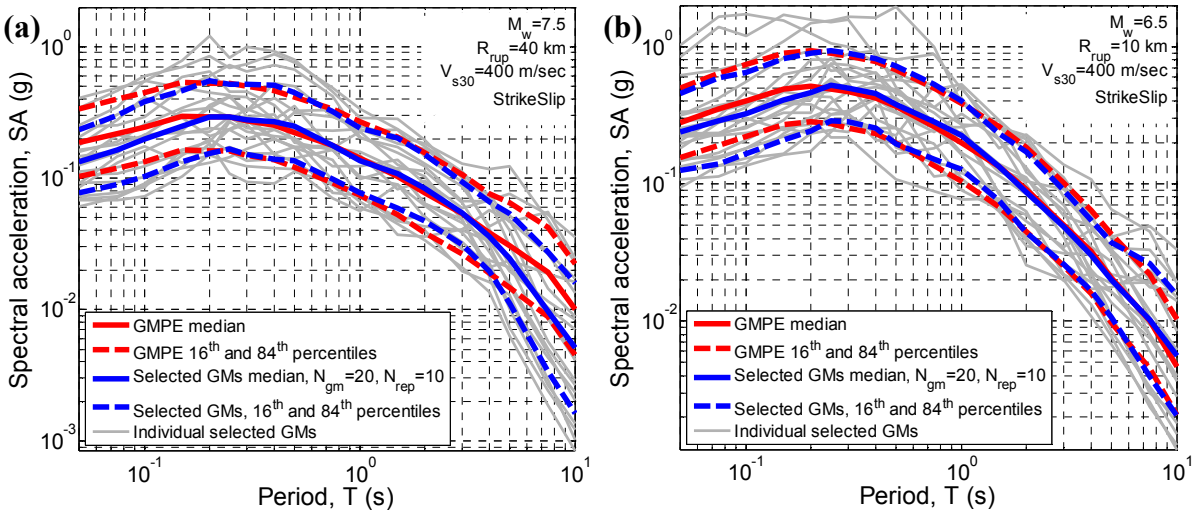

Figure 13: Median, 16th, and 84th percentiles of SA ordinates of selected motions using weight vector case 7 (i.e., ASI, SI, and DSI) for: (a) M7.5R40V400; and (b) M6.5R10V400 rupture scenarios

4.1.6 Discussion: Appropriate weight vectors for generic problems

It is evident that considering only SA ordinates, as it is common in many conventional ground motions selection procedures, will result in misrepresentation of the cumulative and duration effects of ground motions. Since considering these cumulative and duration effects does not impose any burden on the ground motion selection process it is recommended to include them in the selection procedure.

As investigated and discussed by Bradley (2011c), (2012c), and (2014), the residuals of duration and cumulative intensity measures have a relatively low correlation with each other, e.g., $\rho(D_{s595}, CAV) = 0.122$ and $\rho(D_{s595}, AI) = -0.2$, therefore considering only one of these aspects (e.g., D_{s575}, D_{s595}) in the ground motion selection does not imply a satisfactory representation for the others (e.g., AI, CAV). The low correlation between the duration and cumulative IMs indicates that these IMs provide non-redundant information useful for characterizing the severity of ground motions. In contrast, some IMs provide largely

redundant information (e.g., ASI, SI, DSI and SA ordinates over certain period ranges) and therefore their joint consideration is largely ineffective.

When using a total weight of 60-70% for all SA ordinates, the consideration of cumulative and duration-related IMs does not result in any appreciable reduction in the conformity of the distribution of SA ordinates of the selected ground motions to the target distribution. Thus, there is no obvious negative to the consideration of the cumulative and duration-related intensity measures. It should be noted here that this is for 60-70% weight given to SA ordinates. If a lower total weight is used, then the consideration of these other IMs is likely to result in a degraded representation of SA ordinates. The reason for having a large portion of the total weight on SA ordinates, compared to other IMs, is due to the fact that SA ordinates represent the amplitude and frequency content of the ground motion and are therefore of primary importance. In order for cumulative- and duration-related responses to become important, a ground motion's amplitude and frequency content must first be large enough to induce nonlinear response.

4.2 Effect of conducting replicate selections on ground motion selection

4.2.1 Number of replicate selections

In addition to the choice of weight vector discussed in the previous section, another important aspect of the GCIM-based ground motion selection is to conduct replicate selections to obtain an ensemble of motions with the 'best' representation for the considered scenario rupture (i.e., Equation (6)). The need for replicate selection is a result of the fact that random realization of the GCIM distributions are used in the selection process, meaning that each replicate may result in a different ground motion ensemble. The number of the replicate selections (i.e., N_{rep}) to reach to a stable result is dependent upon the number of the selected motions (i.e., N_{gm}), which is investigated here by selecting N_{gm} =10, 20, and 50 motions for 12 considered scenarios and site conditions outlined previously in Table 1. Table 5 presents the number of replicate selections considered for each corresponding number of selected motions. Because the amount of computation in the GCIM-based ground motion selection procedure is directly proportional to the number of replicates considered, identifying a minimum value of N_{rep} which produces stable results is desirable.

Table 5: Number of replicates (N_{rep}) considered corresponding to the number of selected motions (N_{gm})

N_{gm}	Numbers of replicates (N_{rep})					
10	1	3	5	10	20	50
20	1	3	5	10	20	
50	1	3	5			

As mentioned before, for a given number of desired motions, the ensemble with the lowest overall residual (i.e., R value) is chosen as the 'best' ensemble among the selected sets of motions, as illustrated in Figure 1. This process is repeated here for the different $N_{gm} - N_{rep}$ combinations in Table 5. In order to reach a conclusion about the required number of N_{rep} to obtain a stable result, the R value of the best set of motions from each replicate is compared with values obtained from the other replicates. Figure 14 presents the results from this process, as an example, for the motions selected using weight vector case 1 (i.e., SA only) for the stiff soil site condition cases. As seen in this figure, by conducting more than one replicate selection, the overall residual (i.e., R value) of the ensembles with the best representation for N_{gm} =10 and 20 selected motions decreases considerably compared to the R value for one replicate (i.e., $N_{rep} = 1$). For the replicate selections larger than N_{rep} =3, R tends to gradually decrease with some fluctuations due to the random nature of the sampling, which is more accentuated for N_{gm} =10. For ensembles with N_{gm} =50 motions, as illustrated in Figure 14c, the effect of conducting replicate selections is not as significant as it is for N_{gm} =10 or 20 motions, because a large number of selected motions are more likely to properly represent the target distribution of the IMs (i.e., the random simulations are a better representation of the probabilistic distribution). Whereas the representativeness of a smaller number of motions can be relatively weak, which is also implied by the smaller R values of the ensembles with $N_{gm} = 50$ in comparison to R values for the ensembles with $N_{gm} = 10$ and 20. However, due to the fact that the selection process in the GCIM method is based on random realizations for the considered IMs, conducting replicate selections is recommended even if the number of the selected motions is large.

Overall, conducting several replicate selections has generally a positive effect on obtaining a set of motions with a smaller overall residual, compared to using one replicate. As mentioned before, conducting an excessive number of replicate selections can result in unnecessary computational burden, therefore it is useful to identify an acceptable minimum number of replicate selections based on the number of the desired motions (N_{gm}). Based on

the obtained results for different considered scenarios, soil conditions, and weight vectors, conducting N_{rep} =10, 5, and 3 replicate selections are recommended to select N_{gm} =10, 20, and 50 motions, respectively.

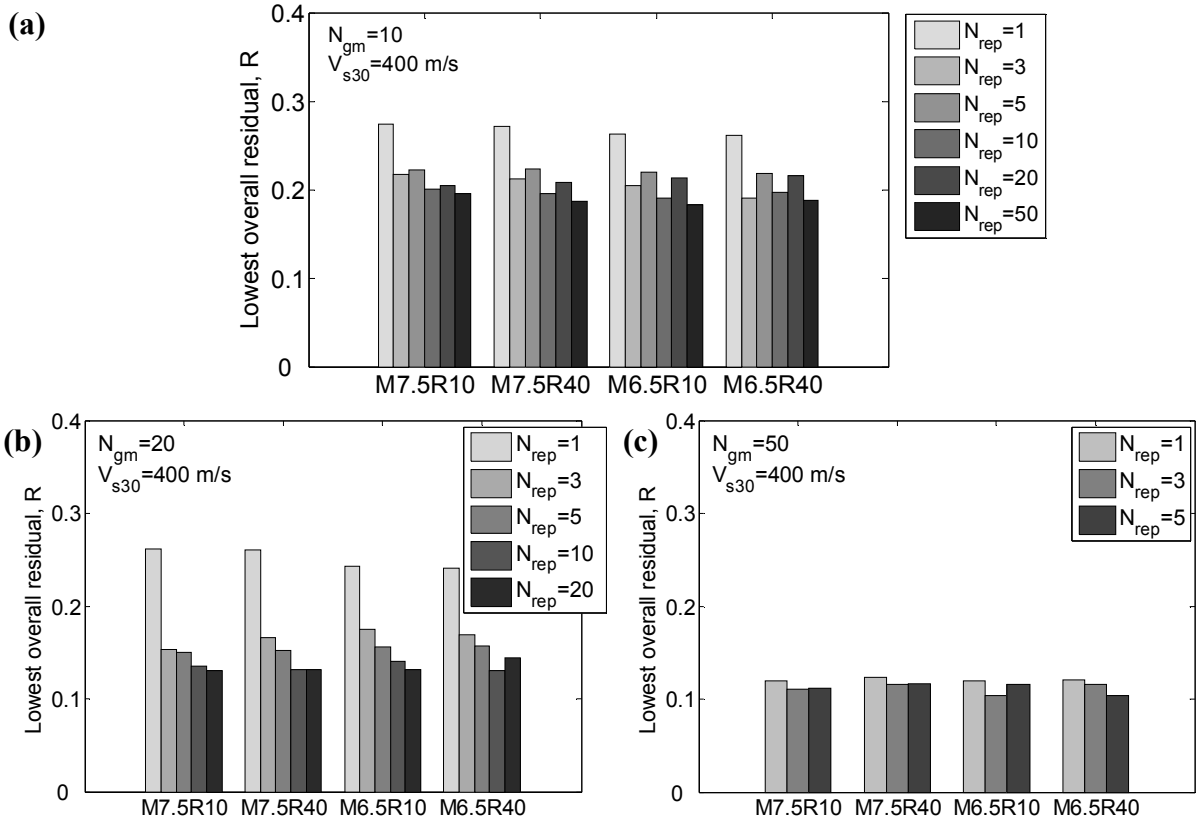

Figure 14: The lowest *R* value for different number of replicate selections, considering the selection based on the weight vector case 1 (i.e., SA only): (a) $N_{gm} = 10$; (b) $N_{gm} = 20$; (c) $N_{gm} = 50$

4.2.2 Replicate selections and representativeness of selected motions for the considered IMs

In order to investigate the effect of conducting replicate selections on the representativeness of the selected motions for the target distribution of the considered IMs, Figure 15a-c presents the median, 16th, and 84th percentiles of SA ordinates of the ensemble of motions with the best and worst representation (i.e., the ensembles with lowest and highest *R* values, respectively) when 10, 20, and 50 motions are selected for the M6.5R10V400 scenario using weight vector case 1 (i.e., SA only). As seen in this figure, by conducting replicate selections, considerable improvement can be achieved (especially when the number of selected motions is small, as seen in Figure 15a), in contrast to selecting motions using only one replicate in which the result might be similar to the set of motions

with the worst representation (i.e., the set with the highest R value). Although not presented here, the positive effect of conducting replicate selections holds true when other considered weight vectors are used for the selection.

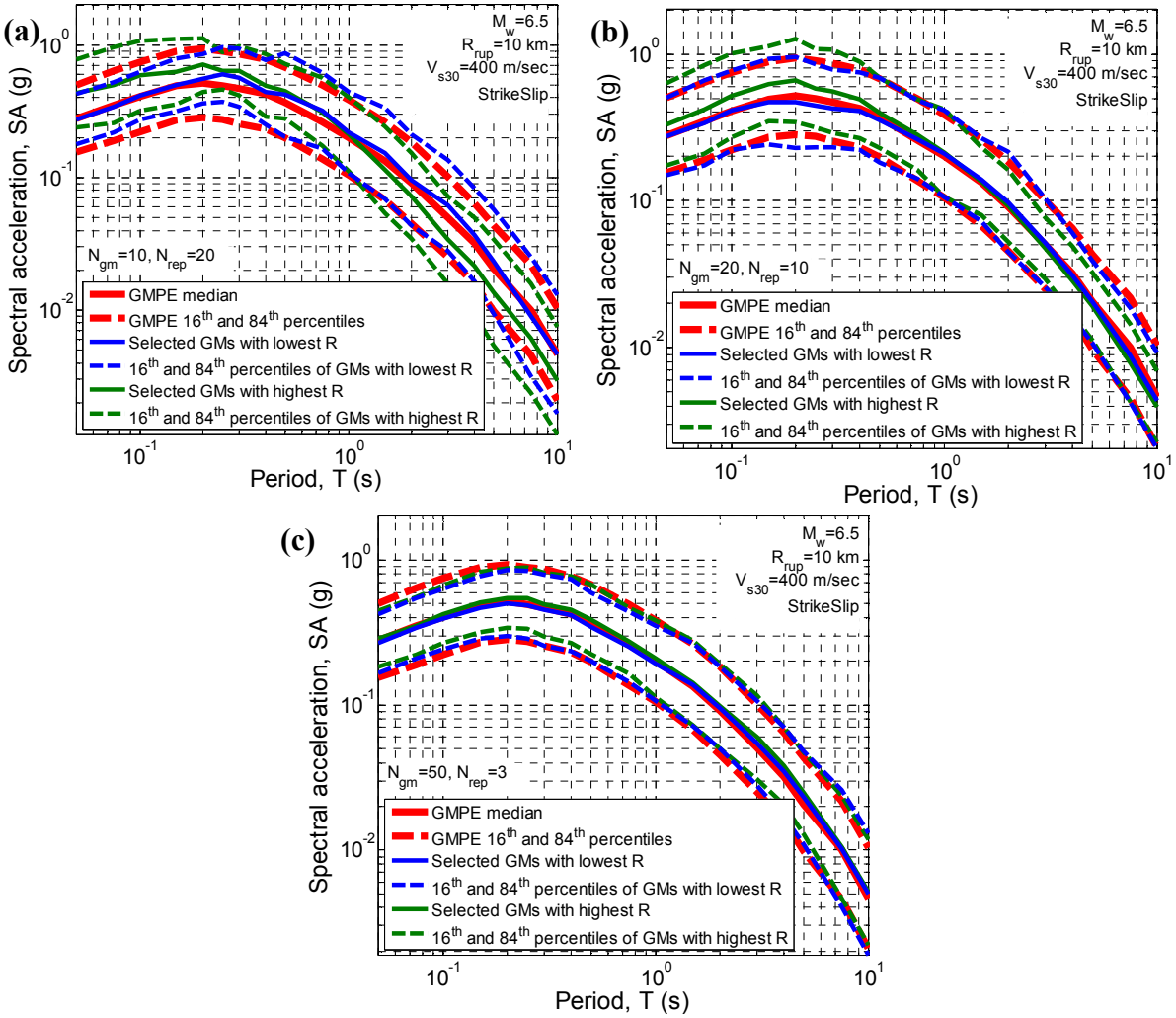

Figure 15: Median, 16th, and 84th percentiles of SA ordinates of selected motions using weight vector case 1 (i.e., SA only) for the M6.5R10V400 rupture scenario with: (a) $N_{gm} = 10$; (b) $N_{gm} = 20$; (c) $N_{gm} = 50$

In order to quantify the results in Figure 15 in a summative manner, Figure 16 presents the KS test statistic, D_{max}, which is the maximum difference between the empirical distribution of the considered IMs and the corresponding target (i.e., GCIM) distribution, for SA ordinates of the selected 10, 20, and 50 motions. D_{max} values for the ensembles with the best and worst representation are illustrated in this figure along with the scatter of D_{max} values for all of the replicate selections.

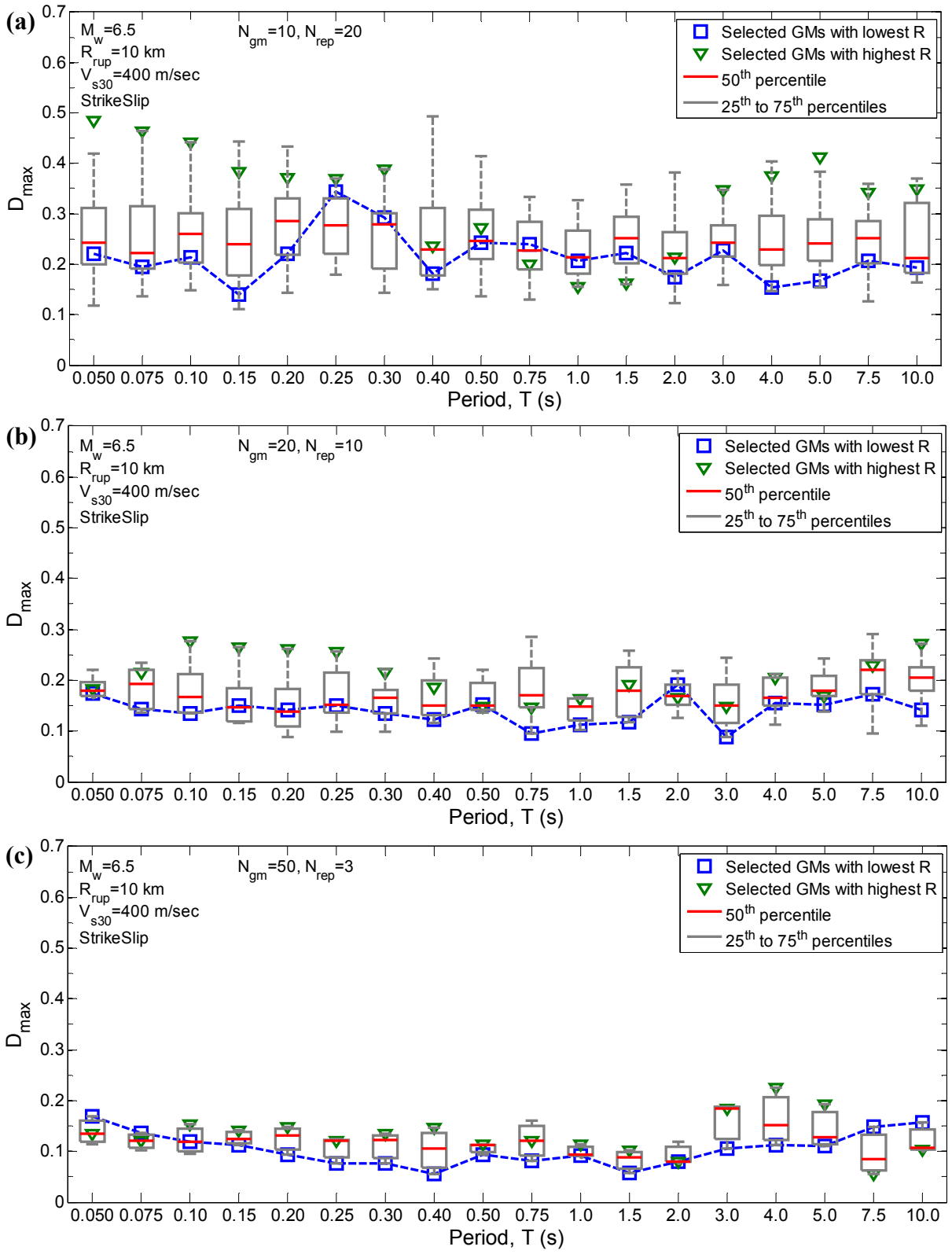

Figure 16: D_{max} value of SA ordinates of selected motions using weight vector case 1 (i.e., SA only) for the M6.5R10V400 rupture scenario with: (a) $N_{gm} = 10$; (b) $N_{gm} = 20$; (c) $N_{gm} = 50$;

As illustrated in this figure, although the D_{max} value for all of the IMs of the best ensemble may not be the minimum value for all vibration periods, by conducting replicate

selections, the IMs considered in the weight vector (i.e., SA ordinates in this case) tend to collectively have smaller D_{max} values for the best set of motions (depicted in the blue line in Figure 16). It is also important to note that the minimum values and also variability in the D_{max} values tends to decrease as the number of the selected motions increases. This indicates that for a small number of motions (e.g., $N_{gm} = 10$), conducting replicate selections is more crucial than is for a larger number of motions. This was also depicted in Figure 14 using the overall residual (i.e., R) value.

Figure 17a presents the D_{max} values of IMs other than SA ordinates (i.e., PGA, PGV, ASI, SI, DSI, AI, CAV, D_{s595}, and D_{s575}) for the selected motions based on weight vector case 1 (i.e., SA only) for the M6.5R10V400 rupture scenario. As seen in this figure, although none of these IMs are considered explicitly in the weight vector, the variability in the D_{max} values for CAV, D_{s575}, and D_{s595} is the greatest of those depicted. The variation can be seen to be related to the extent that these IMs correlate with those IMs contained within the weight vector. Since only SA ordinates are considered in the case 1 weight vector, then those IMs which correlate strongly with some of these SA ordinates (i.e., PGA, PGV, ASI, SI, DSI, and AI) will have relatively low variability and low D_{max} values. In contrast, those IMs which have little correlation with SA ordinates (i.e., CAV, D_{s775}, and D_{s595}) will have relatively high variability and high D_{max} values. This indicates the weak representation of motions selected using weight vector case 1 (i.e., SA only) for these IMs, as discussed before. These results also illustrate the reason why the considered weight vector case 3 (i.e. SA ordinates and AI) resulted in a biased distribution of CAV, but that weight vector case 4 (i.e., SA ordinates and CAV) did not result in a biased distribution of AI – because the distribution of AI of selected motions can be relatively well captured via the use of several short period SA ordinates because of the strong correlation (Bradley 2014).

Figure 17b presents the D_{max} values of PGA, PGV, ASI, SI, DSI, AI, CAV, D_{s595}, and D_{s575} of selected motions for the M6.5R10V400 scenario based on weight vector case 6 (i.e., considering weights on SA, AI, CAV, D_{s595}, and D_{s575}). By comparing the variation of the D_{max} values for CAV, D_{s575}, and D_{s595} with those presented in Figure 17a, it can be seen that the variation in the D_{max} values is considerably decreased for CAV, D_{s595}, and D_{s575}, indicating that in order to obtain ensemble of motions with a proper representation for duration (characterized by D_{s595}, and D_{s575}) and cumulative effects (characterized partially by CAV), these IMs should be explicitly considered in the weight vector. As seen in this figure, variation in the D_{max} values for AI of the selected motions is increased due to a negative

correlation between duration IMs and the AI (i.e., $\rho(D_{s595}, AI)$ = -0.2, $\rho(D_{s575}, AI)$ = -0.19). However, since AI is explicitly considered in the implemented weight vector, the D_{max} value of AI for the ensemble with the best representation has not been increased compared to the result presented in Figure 17a where only SA ordinates were included in the weight vector. It is important to note that the negative correlation of AI with D_{s595} and D_{s575} implies the necessity of including AI in the weight vector when D_{s595} and D_{s575} are considered in the selection, so that the negative correlation between these IMs is balanced.

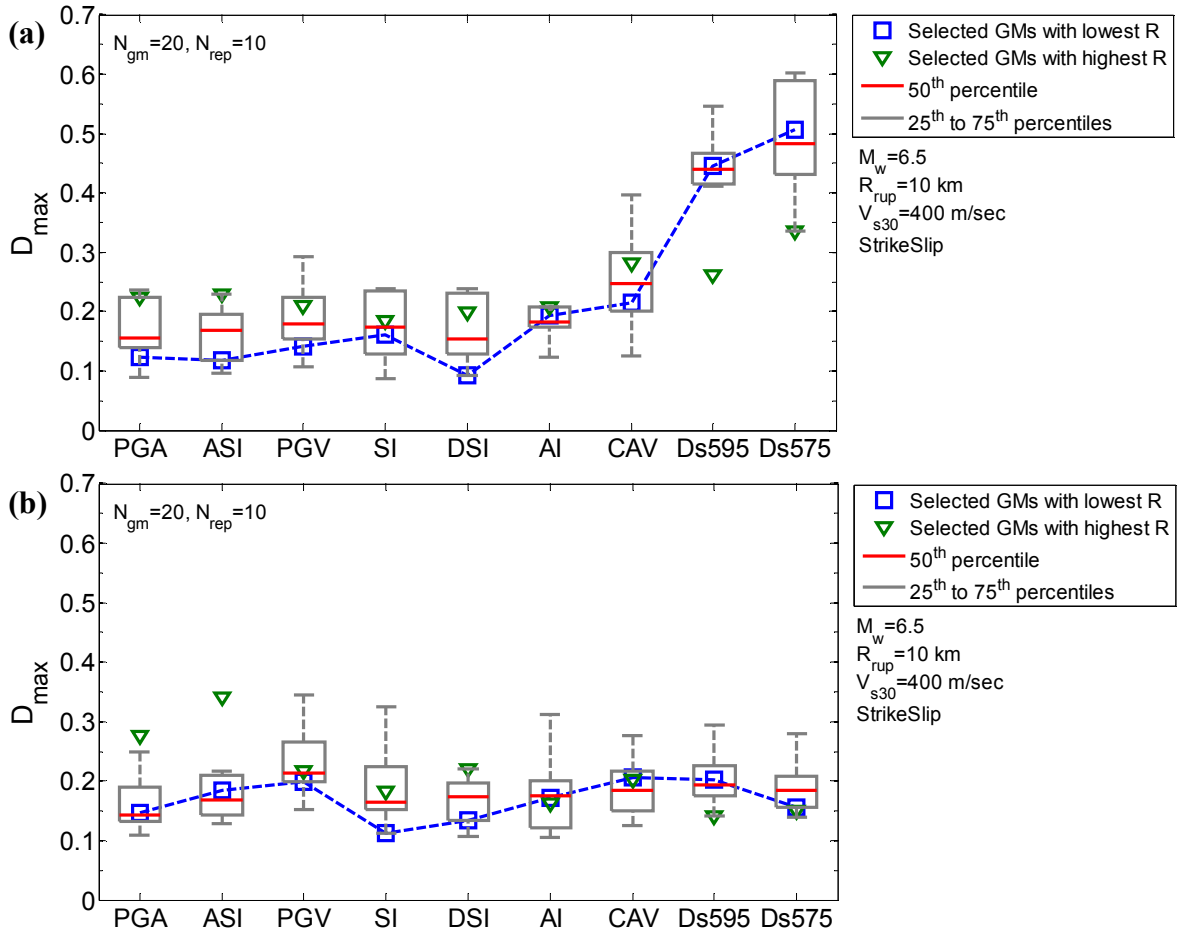

Figure 17: D_{max} value of PGA, PGV, ASI, SI, DSI, AI, CAV, Ds595, and Ds575 of selected 20 motions for the M6.5R10V400 rupture scenario using weight vector: (a) case 1 (i.e., SA only); and (b) case 6 (i.e., SA, AI, CAV, Ds595, and Ds575)

It is insightful to investigate the changes in the variation of the D_{max} values for SA ordinates, when weight vector case 6 (i.e., weights on SA, AI, CAV, D_{s595}, and D_{s575}) is implemented for the selection as compared to those in weight vector case 1 (i.e., weights only on SA ordinates). Figure 18 illustrates the D_{max} values for SA ordinates for weight vector case 6. Comparing Figure 18 and Figure 16b it can be seen that the variation of the D_{max} values for SA ordinates increases due to the smaller weight on SA ordinates, however, the

absolute values of these D_{max} values is still relatively small (recall that the distribution of the SA ordinates still conforms to the target distribution as shown in Figure 11a). The increase in the D_{max} values of SA ordinates for vibration periods around 0.5 for best ensemble of motions is also depicted in Figure 11a as the slight deviation of the 16th, 50th, and 84th percentiles of SA ordinates distributions form the target distribution. This particular observation is due to the fact that compromises have to be made to collectively have a proper representation for all of the considered IMs in the weight vector, especially when the considered IMs reflect different characteristics of the ground motion with a different correlation among them.

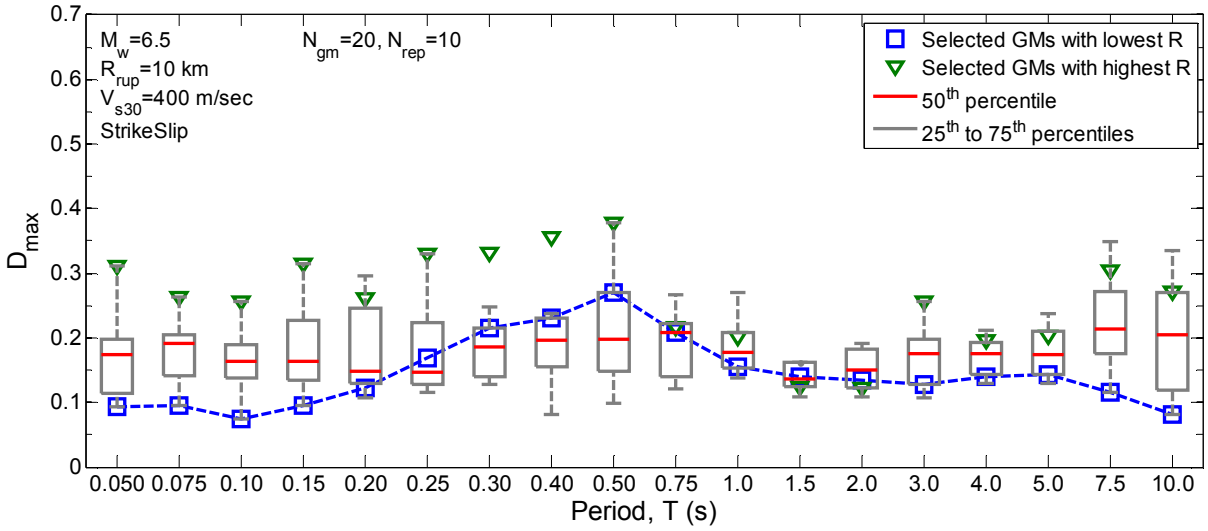

Figure 18: D_{max} value of SA ordinates of selected motions for $N_{gm} = 20$ using weight vector case 6 (i.e., SA, AI, CAV, D_{s595}, and D_{s575}) for the M6.5R10V400 scenario rupture

In order to investigate the effect of replicate selections on representation of the IMs which are not included in the weight vector, Figure 19 presents the cumulative distribution of 5-95% significant duration and CAV of the selected ensemble of motions using weight vector case 1 (i.e., SA weight only) with the best and worst representation for the M6.5R10V400 and M6.5R10V200 rupture scenarios, respectively. These IMs are not considered in the implemented weight vector for the presented results (i.e., weight vector case 1). As seen in this figure, the ensemble with the worst representation (i.e., highest *R* value) has an unbiased distribution at the 5% significance level, while, the ensemble with the best representation (i.e., lowest *R* value) has a biased distribution. This is due to the fact that replicate selections aim to minimize the *R* value with respect to the IMs considered in the weight vector, hence, the representation of IMs not considered in the weight vector will not directly improved by conducting replicate selections.

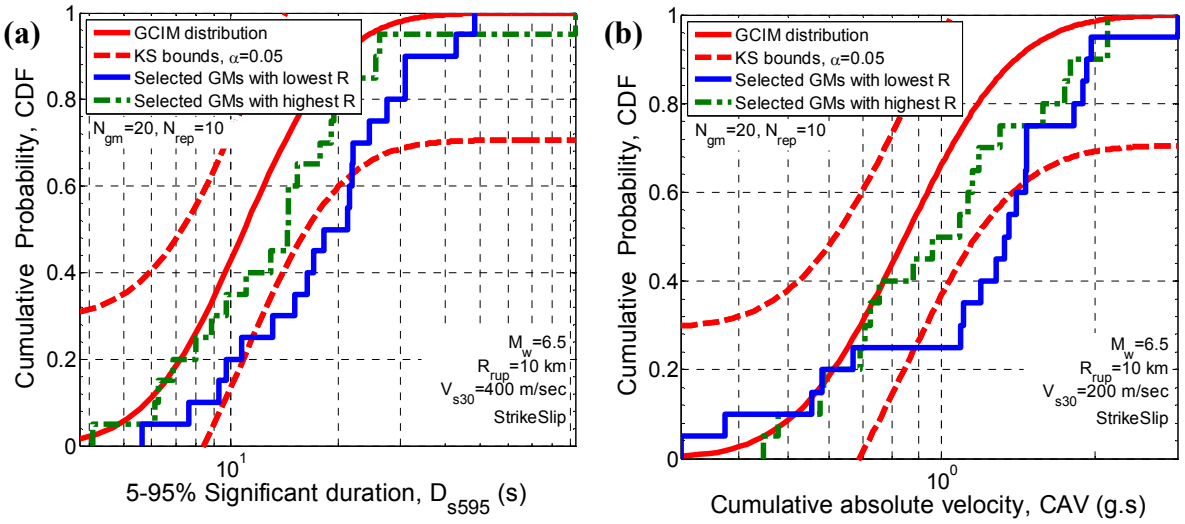

Figure 19: Illustration of the effect of replicate selection on the empirical distributions for intensity measures not considered in weight vector: (a) D_{s595} for the M6.5R10V400; and (b) CAV for the M6.5R10V200 rupture scenarios using weight vector case 1 (i.e., SA only)

4.2.3 Replicate selections and representativeness of selected motions for the implicit causal parameters

Figure 20 presents the $M_w - R_{rup}$ distribution of the selected motions with the best and worst representation using weight vector case 6 (i.e., SA, AI, CAV, D_{s575}, and D_{s595}). As seen in this figure and based on the general trend of the results, the representativeness of the implicit causal parameters of the selected motions does not notably change by conducting replicate selections. This is due to the fact that the replicate selections relies on the overall residual (i.e., R value) of the selected ensemble of motions, which is governed by the assigned weight values on the explicit IMs of ground motion and not the implicit causal parameters.

It is important to note that there is a trade-off when selecting motions with an appropriate representation for the explicitly predicted IMs; implicit causal parameters such as magnitude-distance distribution; and amplitude scale factors. While ideally the selected motions would have the appropriate representation of implicit causal parameters and amplitude scale factors near 1.0, an emphasis in ground motion selection should be placed on the appropriateness of the explicit intensity measures of the ground motion rather than the implicit causal parameters, as elaborated upon by Bradley (2012a).

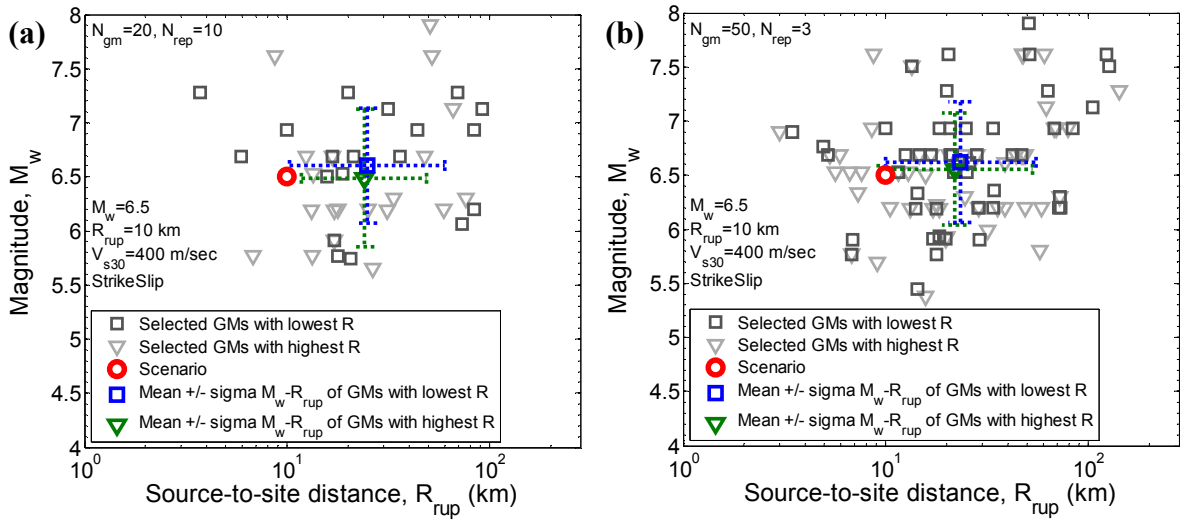

Figure 20: $M_w - R_{rup}$ distribution of selected motions for the M6.5R10V400 rupture scenario using weight vector case 6 (i.e., SA, AI, CAV, D_{s575}, D_{s595}): (a) 20; and (b) 50 motions

4.2.4 Number of the selected motions and their representativeness for the target distribution of IMs

Since, in the GCIM-based selection, motions are selected to represent the predicted distribution of the considered IMs, it is obvious that a large number of selected motions can have a better representativeness compared to a suite with a relatively smaller number of motions. Figure 21 compares the representativeness of SA ordinates and 5-95% significant duration of two suites with 10 and 50 motions selected for the M6.5R10V200 scenario using weight vector case 6 (i.e., SA, AI, CAV, D_{s575}, and D_{s595}). By selecting a larger number of motions, deviation in the distribution of the considered IMs with respect to the target distribution tends to decrease. It is important to note that, having a proper representation for an IM is dependent upon the weight of that IM in the implemented weight vector in the first place, rather than the number of the selected motions, however, for a given weight vector, using a large number of motions, on average, results in a better representation.

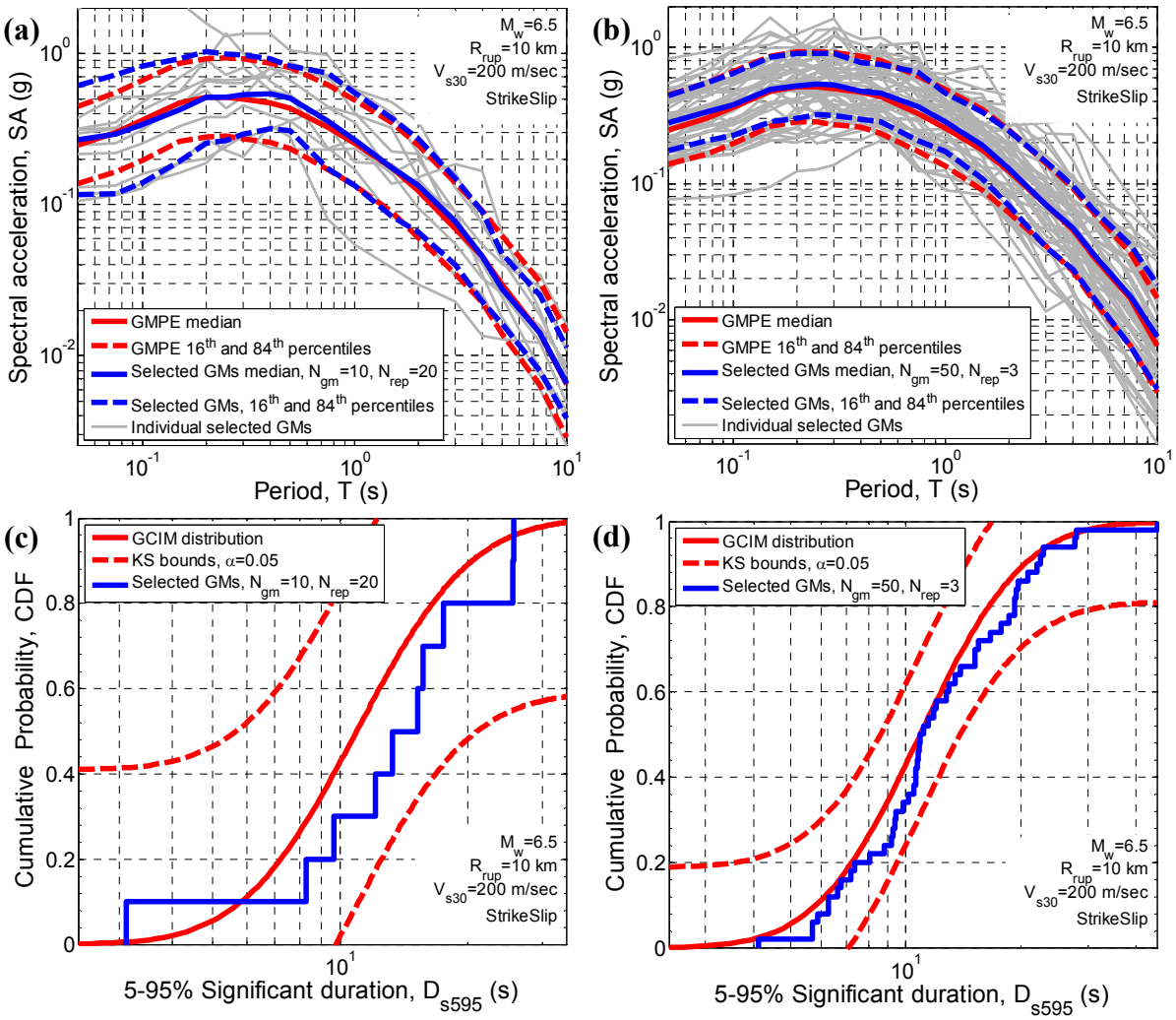

Figure 21: Properties of selected motions using weight vector case 6 (i.e., SA, AI, CAV, D_{s595}, and D_{s575}) for the M6.5R10V200 rupture scenario: (a)-(b) SA ordinates; (b)-(c) cumulative distribution of D_{s595}

4.3 Considering bounds on implicit causal parameters of the prospective ground motions

Consideration of bounds on implicit causal parameters such as magnitude, source-to-site distance, site condition, etc., is often used in many conventional ground motion selection procedures in order to account for various aspects of the seismic hazard which are not captured in the selection process when only SA ordinates are considered (see Katsanos et al. 2010 for some examples). As noted by Bradley (2012a), there are several limitations associated with the conventional use of such bounds on implicit causal parameters. The GCIM-based ground motion selection does not require bounds on implicit causal parameters and has been successfully used without such bounds for seismic performance assessment purposes (Bradley 2012d). However, as empirical ground motion databases continue to

increase, the use of causal parameter bounds can assist in efficiently removing unreasonable ground motions from consideration and ensure that the ground motion selection remains computationally efficient. It is important to note that having very tight bounds on implicit causal parameters may restrict the number of the prospective ground motions, depending on the characteristics of the considered rupture scenario. This is due to the fact that the available database of strong ground motions is not large for some ranges of causal parameters. Therefore, the consideration of bounds on the causal parameters of the prospective ground motions should aim to exclude those motions that have drastically different characteristics compared to the considered scenario, rather than unreasonably narrowing the database to a very small number of motions.

Table 6 illustrates the bounds implemented in this study on the considered implicit causal parameters with the above points in mind. As presented in this table, prospective ground motions are limited to those motions one order of magnitude greater and smaller than the corresponding rupture scenario magnitude. Source-to-site distances of the prospective motions for the scenarios considered in this study are bounded to distances between 0 and two times the scenario rupture value. V_{s30} values of the prospective motions are limited to V_{s30} values representative of approximately one site class either side of the considered site condition, according to the NEHRP site classification (NEHRP 2003).

Table 6: Bounds on the implicit causal parameters of the prospective motions

Causal parameters		Lower limit	Upper limit
Magnitude, M_w	6.5	5.5	7.5
	7.5	6.5	8.5
Site condition*, V_{s30}	200	-	600
	400	200	800
	600	400	-
Source-to-site distance, R_{rup}	10	0	20
	40	0	80

* Note: $V_{s30} = 600, 400, 200$ corresponds approximately to NEHRP site class A/B, C, and D/E, respectively

Table 7 presents the number of the available ground motions in the database after applying bounds on the implicit causal parameters. The total number of the motions in the original NGA database considered is 3225 (Chiou et al. 2008). As presented in this table, the

M7.5R10V200 and M6.5R40V400 scenarios have respectively the smallest and largest number of motions amongst the considered rupture scenarios and site conditions, and thus it should be clear that the use of smaller bounds would excessively restrict the number of available motions for these cases.

Table 7: Available ground motions in the database after applying bounds

	$V_{s30} = 200$	$V_{s30} = 400$	$V_{s30} = 600$
$M_w = 7.5,\ R_{rup} = 10$	78	150	86
$M_w = 7.5,\ R_{rup} = 40$	340	546	267
$M_w = 6.5,\ R_{rup} = 10$	162	234	95
$M_w = 6.5,\ R_{rup} = 40$	874	1368	592

In order to investigate the characteristics of the selected motions when bounds on the causal parameters of the prospective ground motions are applied, Figure 22a-b presents the median, 16th, and 84th percentiles of SA ordinates and cumulative distribution of amplitude scale factors of the selected motions for the M6.5R10V400 scenario using weight vector case 1 (i.e., SA only). As seen in this figure, the selected motions have an appropriate representation for the distribution of SA ordinates, and also the majority of the applied amplitude scale factors are in 0.3-3.0 range, in comparison to the results presented in Figure 2c for the case where no implicit causal parameter bounds were applied. This is due to the fact that by restricting the prospective ground motions to those motions with causal parameters close to characteristics of the considered scenario, only a small change in amplitude of the as-recorded motions is required in order to represent the IMs of the given scenario rupture. This holds true for all of the considered scenario ruptures and the weight vectors.

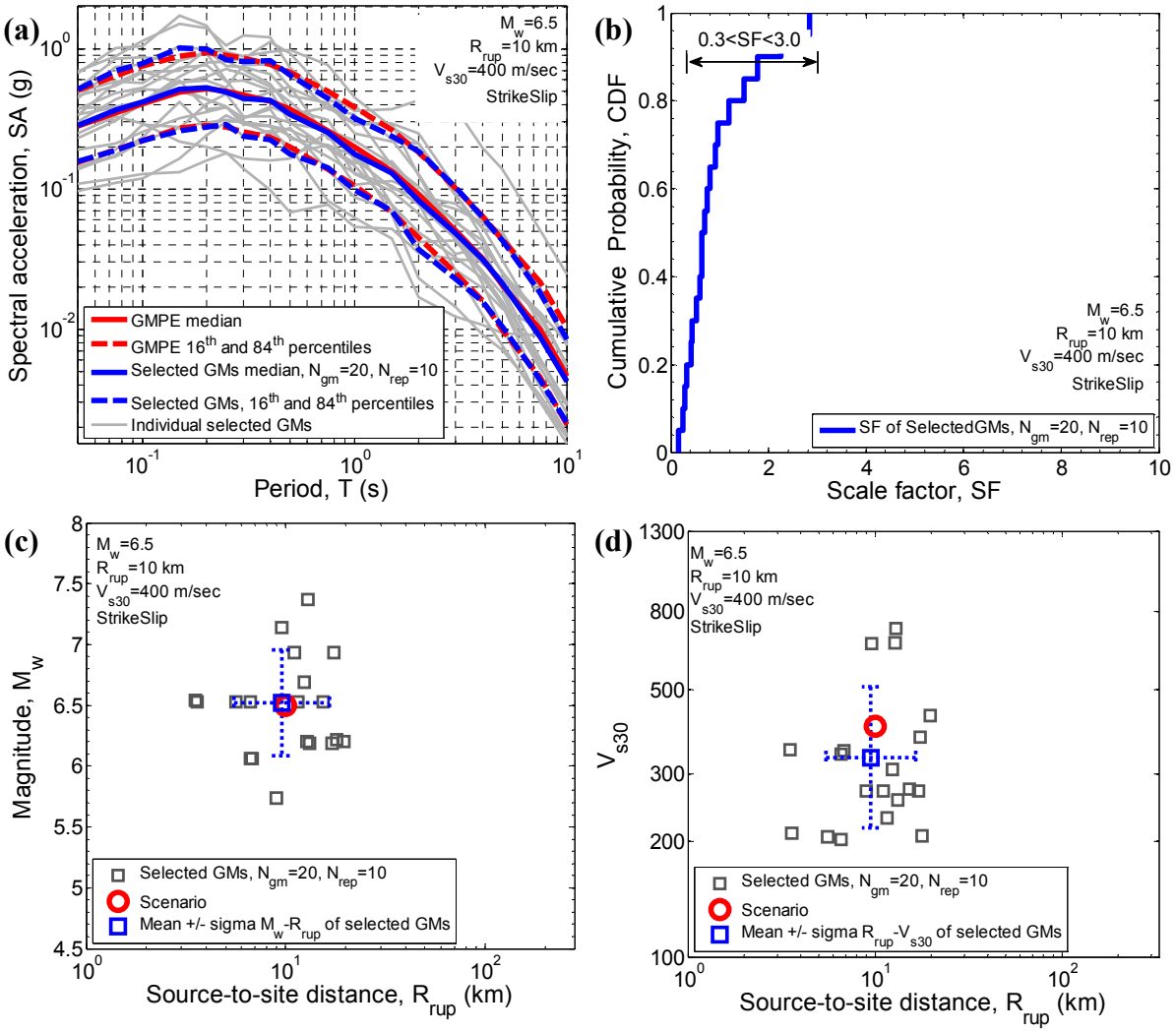

Figure 22: Properties of selected motions with bounds on the implicit causal parameters using weight vector case 1 (i.e., SA only) for the M6.5R10V400 rupture scenario: (a) SA ordinates; (b) cumulative distribution of the amplitude scale factors; (c) $M_w - R_{rup}$; and (d) $V_{s30} - R_{rup}$ distributions

Figure 22c-d compares the $M_w - R_{rup}$ and $V_{s30} - R_{rup}$ distributions of the selected motions using weight vector case 1 (i.e., SA only) with respect to the characteristics of the M6.5R10V400 rupture scenario. As seen in this figure, mean M_w and R_{rup} parameters of the selected suite of motions have a very close match with scenario magnitude and source-to-site distance. Also, the V_{s30} values of the selected motions properly corresponds to the site condition.

It is also worthwhile investigating the effect of using causal parameter bounds on characteristics of IMs that are not considered in the weight vector. Figure 23a-b presents the cumulative distribution of D_{s595} for the M6.5R10V400 rupture scenario using weight vector case 1 (i.e., SA only), respectively before and after applying bounds on the implicit causal parameters. As seen in these figure, applying bounds results in motion with a better

representation of D_{s595}. However, this does not hold true in general as presented in Figure 23c-d for the M7.5R10V400 rupture scenario, illustrating that the unbiased distribution of D_{s595} is biased after applying bounds. Based on the obtained results for other IMs (e.g., CAV), although not presented here for brevity, it is observed that effect of the bounds on characteristics of the IMs that are not considered explicitly in the weight vector are sensitive to characteristics of the considered scenario rupture and the implemented weight vector. This indicates that limiting the prospective motions to those with implicit causal parameters similar to the scenario characteristics does not guarantee selecting a suite with an appropriate representation for the IMs that are not explicitly considered in the selection process via the implemented weight vector.

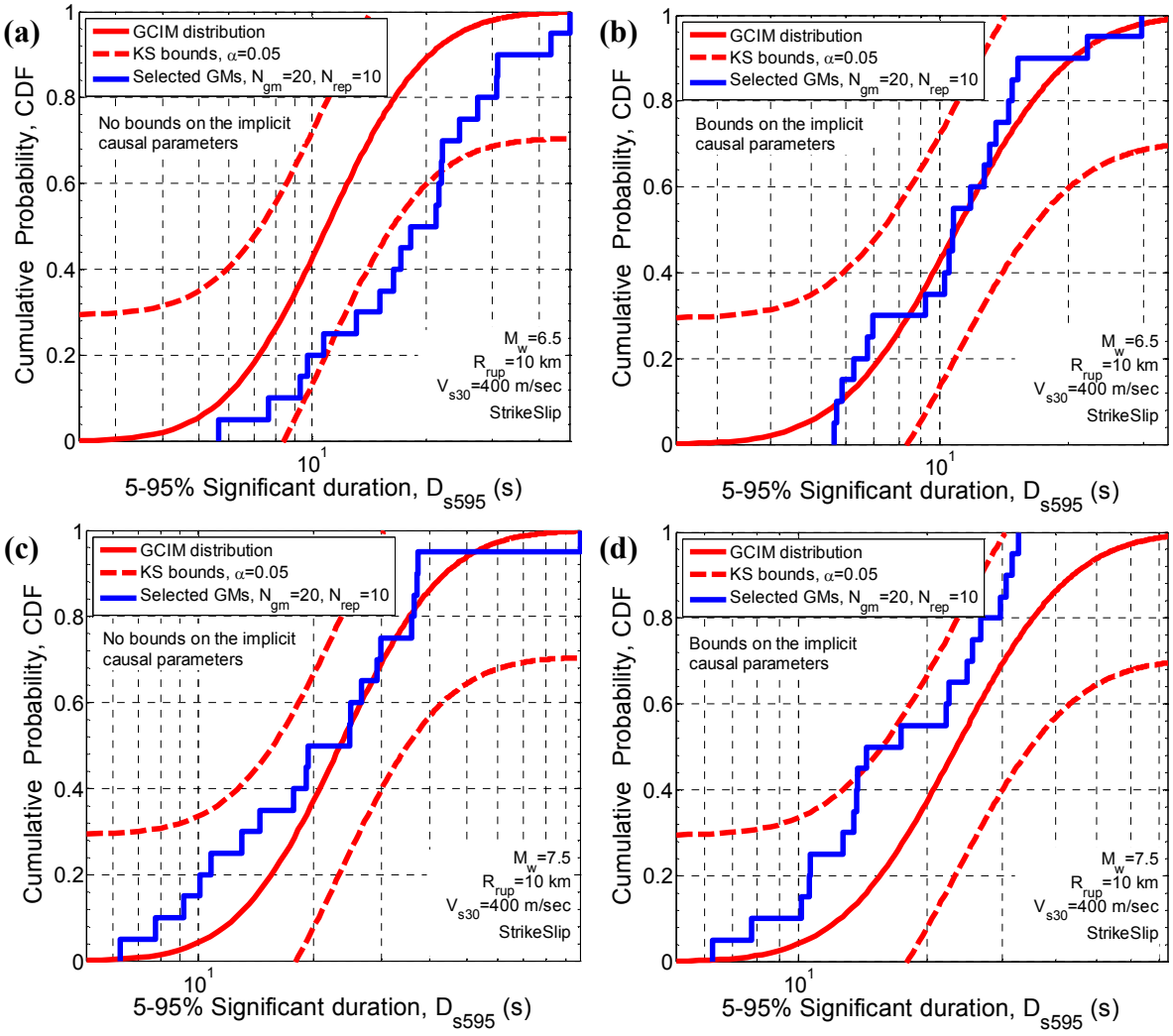

Figure 23: Cumulative distribution of D_{s595} using weight vector case 1 (i.e., SA only) for the M6.5R10V400 and M7.5R10V400 scenario ruptures: (a) and (c) before applying bounds; (b) and (d) after applying bounds

Figure 24 presents the characteristics of the selected motions when weight vector case 6 (i.e., SA, AI, CAV, D_{s575}, and D_{s595}) is used for the selection after applying bounds on the

causal parameters of the prospective motions. As seen in this figure, the distribution of SA ordinates conforms to the target distribution. Although not biased, the distribution of D_{s595}, AI, and CAV slightly deviates from the target distribution, compared to their distribution when no bounds are applied on the implicit causal parameters (see Figure 11c-d). This indicates a trade-off between selecting motions with a high representation for the explicit IMs of the rupture scenario and having bounds on the implicit causal parameters of ground motions. This trade-off is caused by excluding those motions from the database of prospective ground motions that have a better representation for the explicit IMs of the scenario rupture, but have out-of-bounds implicit causal parameters. This trade-off is also reflected in the overall residual (i.e., *R* value) of the selected ensemble of motions after applying bounds on the implicit causal parameters, as discussed in the next paragraph.

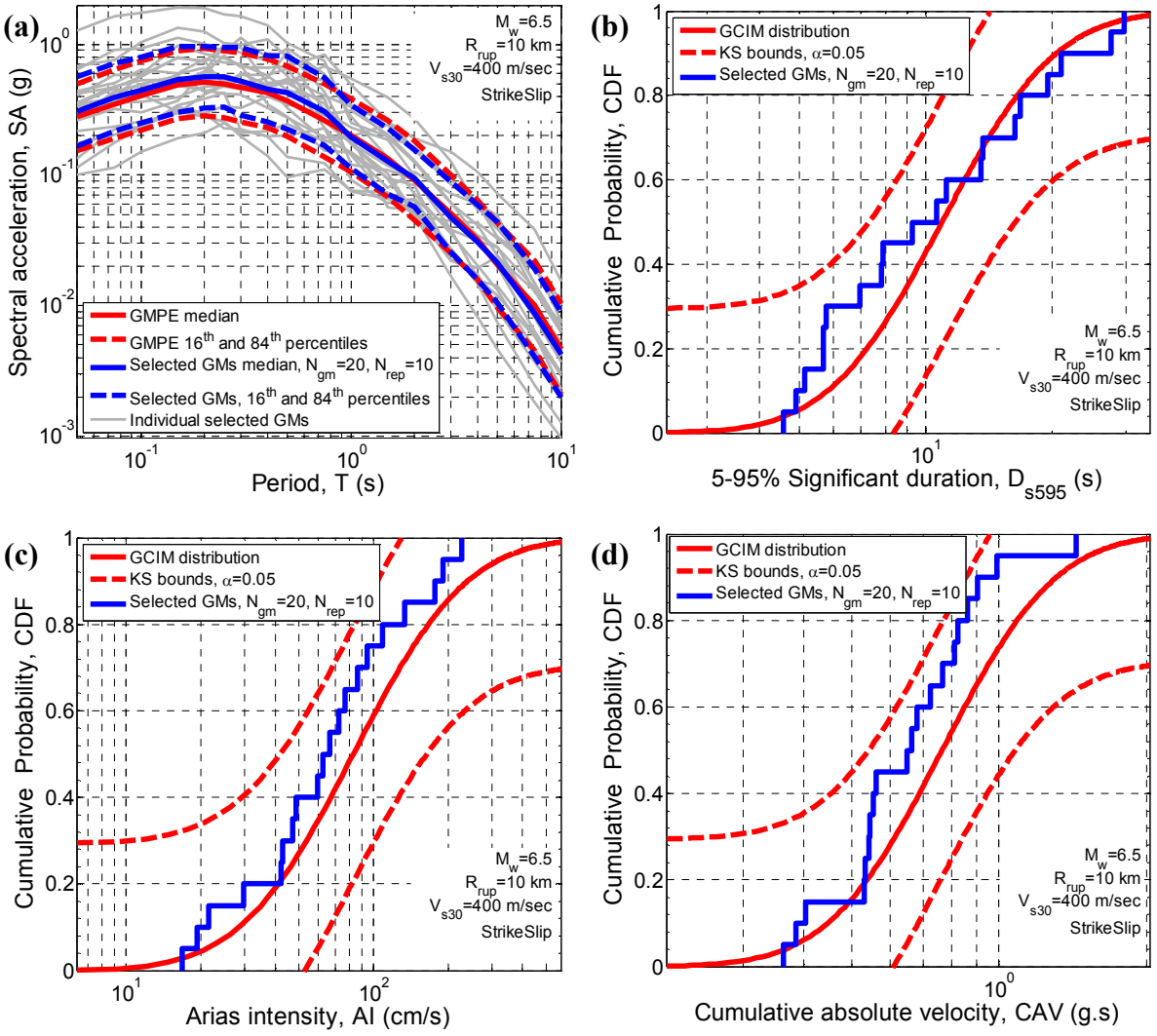

Figure 24: Properties of selected motions after applying bounds on causal parameters using weight vector case 6 (i.e., SA, AI, CAV, D_{s595}, and D_{s575}) for the M6.5R10V400 rupture scenario: (a) SA ordinates; cumulative distribution of (b) D_{s595}; (c) AI; and (d) CAV

In order to examine the changes in the overall representativeness of selected motions when bounds are applied on the implicit causal parameters, Figure 25 presents the overall residual (i.e., R value) of the best ensemble of motions selected for the considered 4 scenario ruptures with a V_{s30}=400 site condition (i.e., stiff soil), using weight vector case 1 (i.e., SA only) and case 6 (i.e., non-zero weight for SA, AI, CAV, D_{s575}, and D_{s595}). As presented in this figure; as an example among the considered rupture scenarios, site conditions, and weigh vectors; applying bounds on the causal parameters generally results in a higher value of overall residual for most of the scenarios and weight vectors, due to exclusion of some ground motions with a better representation for the explicit IMs of motion for the considered scenario. Due to the random nature of the selection and also the fluctuation in the R value with respect to replicate selections (as presented in Figure 14), selected motions from the database of motions with the bounded implicit causal parameters may have a lower R value (e.g., for the M6.5R40V400 scenario with weight vector case 6, Figure 25b). However, the general trend is that the R value of the selected motions from a bounded database of motions is higher compared to the unbounded database. It is also noted that the overall residual, R, increases as more non-zero weights are considered in the weight vector (i.e., weight vector case 6 contains more IMs than weight vector case1).

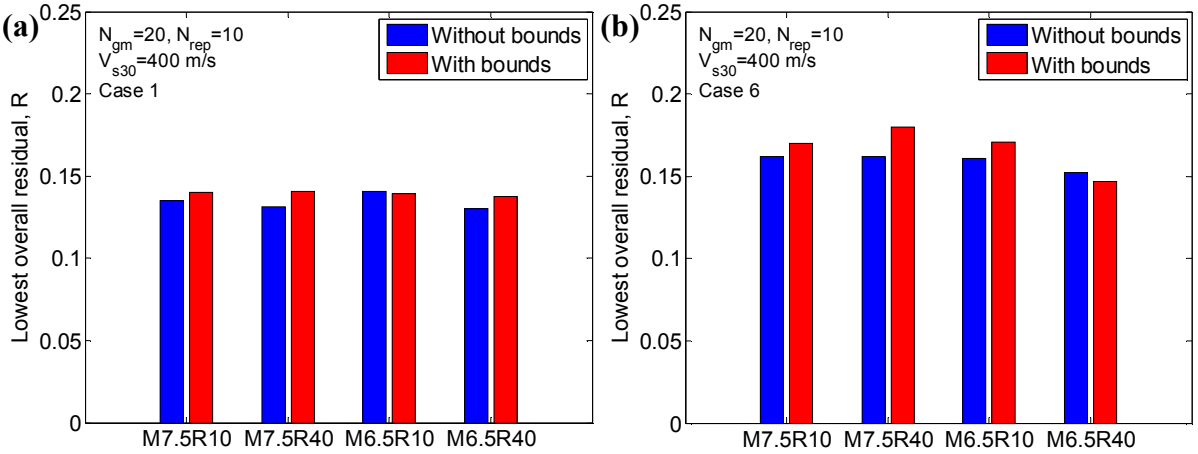

Figure 25: Overall residual (i.e., *R* value) of selected ensemble of 20 motions with and without bounds on the implicit causal parameters for all the rupture scenarios with V_{s30}=400 m/s soil condition, using weight vector: (a) case 1 (i.e., SA only); (b) case 6 (i.e., SA, AI, CAV, D_{s595}, and D_{s575})

In order to investigate the distribution of implicit causal parameters of the selected motions with respect to the scenario characteristics before and after applying bounds, Figure 26 presents the $M_w - R_{rup}$ and $V_{s30} - R_{rup}$ distributions of the selected motions using weight vector case 6 (i.e., SA, AI, CAV, D_{s595}, and D_{s575}) for the M7.5R40V200 scenario. Comparing the distribution of the causal parameters in Figure 26a-b (before using bounds)

with those in Figure 26b-d (after using bounds) indicates that by applying bounds on the causal parameters of the prospective motions, the selected motions will have causal parameters similar to the scenario characteristics. For example, when no bounds were used, many motions with magnitudes close to 6.0 were selected for the M_w7.5 rupture scenario (see Figure 26a), whereas the selected motions from the bounded database have closer magnitudes to the scenario magnitude with a minimum magnitude of 6.5 (see Figure 26c). The same trend can be observed for V_{s30} where motions with V_{s30} over 1000 m/s are selected for the site condition with $V_{s30} = 200$ when no bounds were applied on the causal parameters (see Figure 26b). However, the maximum V_{s30} of the selected motions for the considered site condition when the bounds are used is close to 400 m/s, keeping the characteristics of the selected motions compatible with the considered site condition (see Figure 26d).

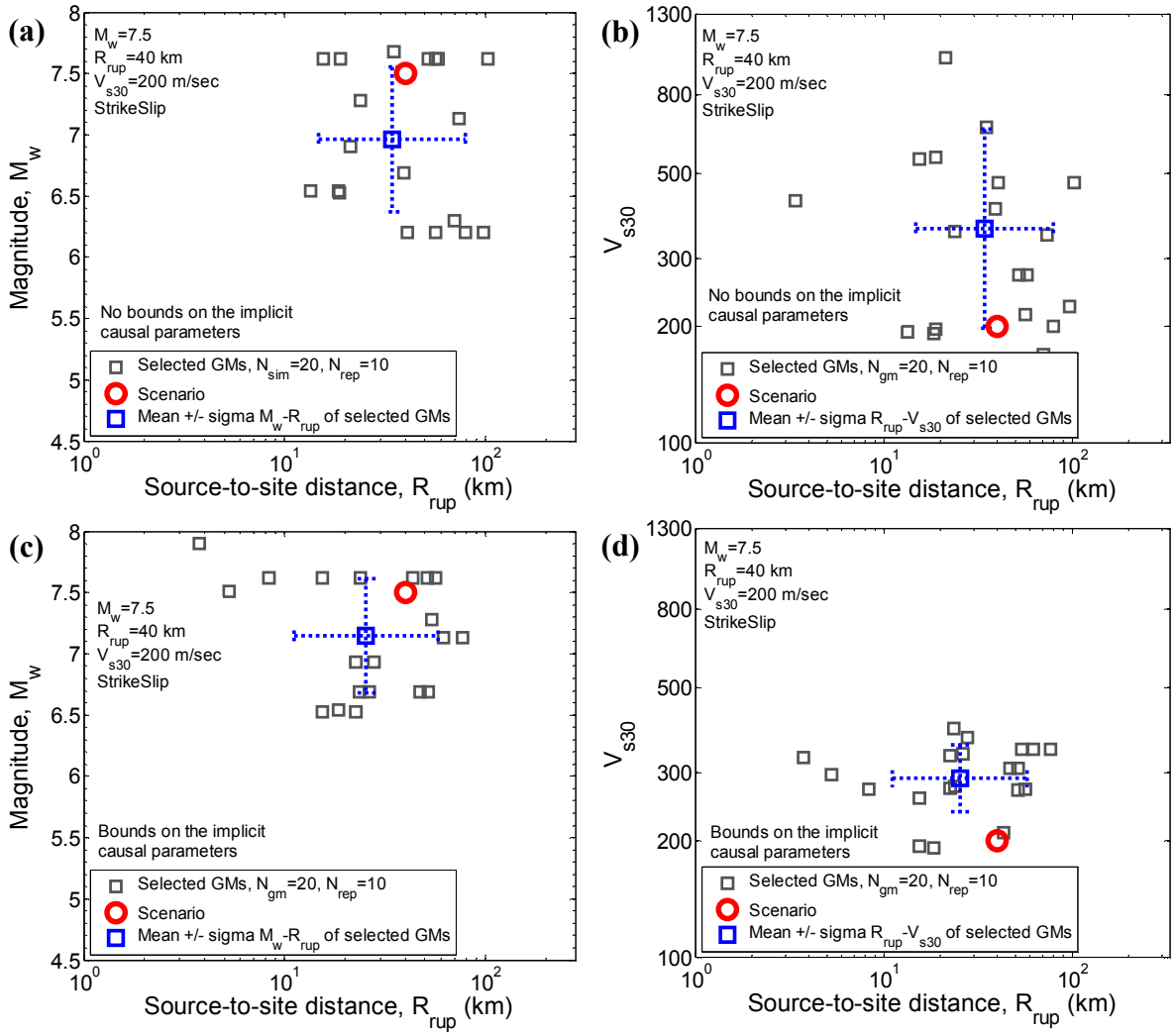

Figure 26: $M_w - R_{rup}$ and $V_{s30} - R_{rup}$ distributions of selected motions for the M7.5R40V200 rupture scenario using weight vector case 6 (i.e., SA, AI, CAV, D_{s595}, and D_{s575}): (a)-(b) before using bounds; and (c)-(d) after using bounds on the implicit causal parameters

Also, as presented in Figure 26, the selected motions encompass the R_{rup} value of the scenario rupture within one standard deviation range before and after applying the bounds on the causal parameters, however, the selected motions after applying bounds have a mean R_{rup} larger than those before. Unlike the case presented in Figure 22c-d for the M6.5R10V400 scenario, depending on the characteristics of the scenario rupture, applying bounds on the causal parameters may not necessarily result in an improved representation for all of the considered causal parameters for any given scenario. It is important to note that similar to the trade-off between selecting motions with appropriate explicit IMs and implicit causal parameters, a trade-off also exist within the implicit causal parameters, as presented in Figure 26.

As mentioned before, the purpose of applying bounds on causal parameters of the prospective ground motions is to avoid selecting motions with drastically different causal parameters with respect to a given scenario rupture and site condition. As illustrated in Figure 22 and Figure 26, this technique can successfully serve this purpose and in some cases, depending on the characteristics of the scenario, result in motions with a very close match to the causal parameters of the given scenario (e.g., see Figure 22c-d). It is important to note that the relatively weak representation of the causal parameters for the M7.5R40V200 scenario (presented in Figure 26c-d) in comparison to the results for the M6.5R10V400 scenario (presented in Figure 22c-d) is seen to be caused by the paucity of motions recorded with causal parameters similar to the M7.5R40V200 scenario that also have an appropriate representation to the explicit IMs of the scenario ground motion.

Based on the results obtained by selecting different number of motions for all of the considered scenarios and site conditions using different weight vectors, it can be summarized that imposing bounds on causal parameters of the prospective ground motions results in motions with an improved representation for the causal parameters of the scenario without a considerable detrimental effects on representativeness of those explicit IMs considered in the weight vector. Also, the amplitude scale factors used to scale the motions with the bounded implicit causal parameters are mostly smaller than those applied on motions with no bounds on the causal parameters. The implications regarding the effect of weight vector on representativeness of the selected motions and number of the replicate selections to achieve a stable result hold true when bounds are applied on the implicit causal parameters of the prospective ground motions.

5 Conclusion

In this chapter, the generalized conditional intensity measure (GCIM) approach was extended to scenario-based ground motion selection. The selection algorithm is based on generating random realizations of the considered intensity measures (IMs) distributions for a specific rupture scenario and then finding the prospective ground motions which best fit the realizations based on an optimal amplitude scale factor and weight vector. Different aspects of the GCIM methodology to select ground motions for different rupture scenarios and site conditions have been scrutinized and the pertinent implications are presented.

It has been shown that considering only spectral acceleration (SA) ordinates, as it is common in many conventional selection procedures, will result in misrepresentation of the cumulative and duration effects of ground motions. Importantly, considering IMs other than SA ordinates does not have a detrimental effect on representativeness of selected motions to distribution of SA ordinates, while ignoring important intensity measures can cause a bias or imprecision in capturing the distribution of the neglected IMs and subsequently cause a bias in the obtained seismic responses. Although not a requirement for the GCIM-based ground motion selection, in order to select ground motions with an improved representation for the implicit causal parameters (e.g., magnitude, source-to-site distance, site condition) of the considered scenario, bounds on the causal parameters of the prospective ground motions can be applied prior to the selection. This results in motions with an appropriate representation for both explicit IMs and the implicit causal parameters. The considered bounds should aim to exclude those motions that have drastically different characteristics compared to the considered scenario rather than limiting the database of available ground motions to a small number of motions. It has been demonstrated that conducting several replicate selections instead of one selection has a positive effect on obtaining a set of motions with a smaller overall residual (i.e., misfit) and an improved representation for distribution of the considered IMs. A minimum number of replicate selections, in order to reach to a stable result, are also presented for different number of desired motions.

Chapter 2: Representative Ground-motion Ensembles for Several Major Earthquake Scenarios in New Zealand

1 Abstract:

In this chapter, representative ground motion ensembles for several major earthquake scenarios in New Zealand are developed. Cases considered include representative ground motions for the occurrence of Alpine, Hope, and Porters Pass earthquakes in Christchurch city, and the occurrence of Wellington, Wairarapa, and Ohariu fault ruptures in Wellington city. Challenges in the development of ground motion ensembles for subduction zone earthquakes are also highlighted. For each considered scenario rupture, ensembles of 20 and 7 ground motions are selected using the generalized conditional intensity measure (GCIM) approach, ensuring that the ground motion ensembles represent both the mean, and distribution of ground motion intensity which such scenarios could impose. These scenario-based ground motion sets can be used to complement ground motions which are often selected in conjunction with probabilistic seismic hazard analysis, in order to understand the performance of structures for the question "what if this fault ruptures?"

2 Introduction

Conducting nonlinear response history analysis of structures for the purpose of seismic performance assessment requires selecting appropriate ground-motion time series which provide an appropriate representation of the seismic hazard at the site. Although it is common to conduct seismic performance assessment based on the results from probabilistic seismic hazard analysis (PSHA), scenario-based assessments can also be highly informative and provide complementary insights (Bommer 2002).

Many methods have been proposed to select ground motions based on matching the (pseudo) acceleration response spectrum of the selected motions to a target spectrum and considering implicit causal earthquake parameters (e.g. magnitude, source-to-site distance, site conditions) (see Katsanos et al. (2010) for a detailed review). Typically such approaches have been considered in the context of a response spectrum obtained from the results of probabilistic seismic hazard analysis (PSHA). Such approaches generally have several shortcomings (Bradley 2010a), namely: (1) ground motion severity is a function of the amplitude, frequency content, and duration of the motion, which is not embodied simply in spectral acceleration ordinates; (2) ground motion ensembles should represent the full distribution of ground motion intensity and not just the mean; and (3) the ground motion ensemble should be a representative of all the seismic sources which contribute to the hazard at the site. These shortcomings have been addressed through the generalized conditional intensity measure (GCIM) approach developed by Bradley (2010a, 2012a), which provides a theoretically consistent approach to obtain ground motions based on PSHA. In addition, the GCIM-based ground motion selection method has been recently extended to select ground motions based on the results from scenario seismic hazard analysis (scenario SHA), as presented in the previous chapter and Tarbali and Bradley (2014).

In the present chapter, the GCIM method is utilized to select representative ground motion ensembles for several major earthquake scenarios in New Zealand. The earthquake rupture forecast (ERF) model developed by Stirling et al. (2012) is used to obtain the characteristics of seismic sources, and the New Zealand-specific ground motion prediction equation (GMPE) developed by Bradley (2013b) is used to predict spectral accelerations, peak ground acceleration, and peak ground velocity for the purposes of scenario-based seismic hazard analysis and ground-motion selection. Other ground motion intensity measures of importance in seismic hazard analysis and ground motion selection are obtained using foreign (i.e., non-NZ-specific) GMPEs developed for active shallow crustal events.

Results are first presented for rupture scenarios impacting Christchurch city then Wellington city, and finally the present issues with ground motion selection for subduction zone ruptures are discussed.

3 Ground motion selection for scenario ruptures in Christchurch

3.1 Dominant seismic sources

In order to identify the scenario ruptures with significant contributions to the seismic hazard at a generic location in central Christchurch city (Latitude −43:5300°; Longitude 172.6203°), PSHA was conducted using the open-source seismic-hazard-analysis software, OpenSHA (Field et al. 2003). The soil condition at the site is assumed to be site class D according to NZS1170.5 (2004), with an inferred time-averaged 30m shear wave velocity of V_{s30}=250 m/s. Figure 27 presents the deaggregation of the seismic hazard at this site for both peak ground acceleration (PGA) and T=2s period spectral acceleration (SA(2.0s)) for a 10% probability of exceedance in 50 years. As seen in this figure, PGA seismic hazard at this generic site is mostly dominated by events with small magnitudes and small source-to-site distances associated with distributed seismicity, with similar results for SA ordinates at small vibration periods. However, as shown for the deaggregation of the SA(2.0s) hazard, events with large magnitudes and moderate-to-large source-to-site distances dominate at long vibration periods (specifically T >1s).

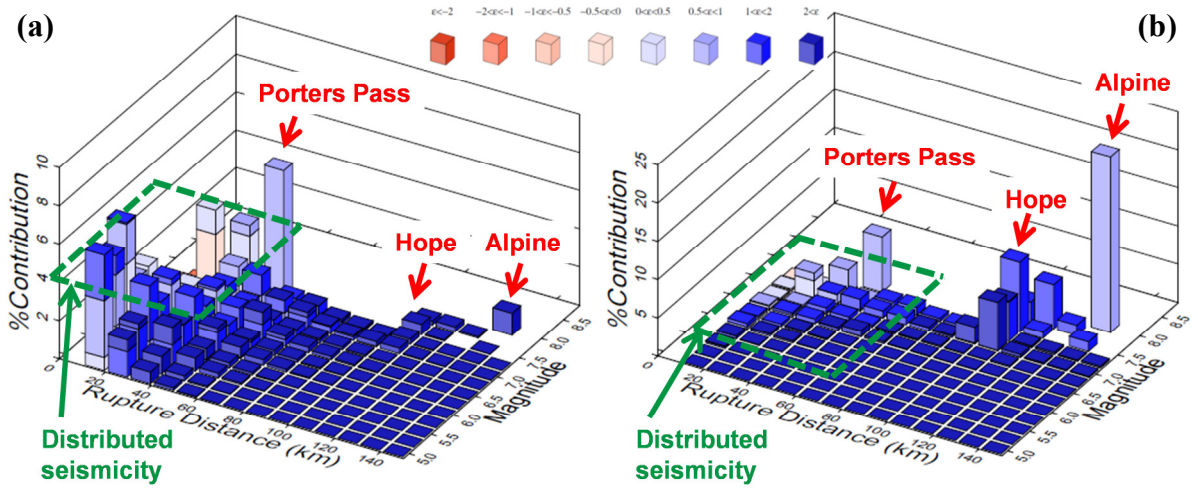

Figure 27: Deaggregation of seismic hazard in Christchurch city for: (a) PGA; and (b) SA(2.0s) for a 10% probability of exceedance in 50 years

Based on the scenarios with a large contribution to the seismic hazard for different periods of vibration, ground shaking produced in Christchurch city due to ruptures of the

Alpine, Hope, and Porters Pass faults are considered in this study for scenario ground-motion selection. The characteristics of these scenario ruptures are presented in Table 8.

Table 8: Characteristics of the considered scenario ruptures for Christchurch city[1]

Fault	Magnitude, M_w	Source-to-site distance, R_{rup} (km)	Rupture mechanism
Alpine (Fiord-Kelly segment)	8.1	133	Strike-slip
Hope (Conway segment)	7.45	106	Strike-slip
Porters Pass	7.45	44	Strike-slip

[1]Based on the ERF of Stirling et al. (2012).

3.2 Intensity measures of the considered scenario ruptures

Table 2 presents median predicted values of several intensity measures for the rupture scenarios considered for Christchurch city. As shown, the spectral acceleration ordinates (and PGA) of the Porters Pass scenario are greater than those for scenarios with larger source-to-site distances (i.e. Alpine and Hope), especially for periods of vibration smaller than T=2 s. Similarly, the Porter Pass rupture is predicted to produce a greater PGV compared to Alpine and Hope fault ruptures. In contrast, the Alpine fault rupture has a median predicted 5-95% significant duration of D_{s595}=56.2s, which is double the significant duration from the Porter Pass rupture (due to a smaller magnitude and source-to-site distance in comparison to the Alpine fault rupture).

Table 9: Median intensity measures of the considered scenario ruptures for Christchurch city

Fault	PGA (g)	SA(0.5s) (g)	SA(1.0s) (g)	SA(2.0s) (g)	PGV (cm/s)	CAV[1] (g.s)	D_{s595}[2] (s)
Alpine (Fiord-Kelly segment)	0.07	0.13	0.11	0.07	12.1	0.9	56.2
Hope (Conway segment)	0.05	0.10	0.07	0.04	7.9	0.5	36.6
Porters Pass	0.15	0.23	0.15	0.08	18.0	0.7	27.5

[1]CAV=cumulative absolute velocity (Campbell and Bozorgnia 2010); [2]D_{s595}= 5-95% significant duration (Bommer et al. 2009);

Prior to selecting ground motions, it is important to identify the type of engineering system considered for seismic performance assessment, so that the selection process can aim to place emphasis on those intensity measures that are important to determine the

characteristic response of the system. For instance, empirical evidence suggests that the peak inter-story drift of a building structure is strongly affected by spectral acceleration ordinates of the applied motion for periods near the first several vibration modes of the structure (e.g., Shome et al. 1998, Tothong and Cornell 2007). In contrast, for example, the response of geotechnical structures with liquefaction-susceptible soils and the collapse capacity of building structures can be considerably affected by duration and cumulative effects of ground motions (Bradley 2010a, Bradley et al. 2013, Villaverde 2007). This problem-specific issue has been addressed in the GCIM-based ground-motion selection method by using a weight vector in the selection algorithm (Bradley 2012a), to weight these different ground motion aspects in record selection. In order to consider different aspects of a ground motion, including the intensity, frequency content, duration, and cumulative effects, the selection process is based on appropriateness of multiple intensity measures for the considered rupture scenarios.

The considered intensity measures for the purpose of this chapter are: spectral acceleration for 18 vibration periods (T=0.05, 0.075, 0.1, 0.15, 0.2, 0.25, 0.3, 0.4, 0.5, 0.75, 1.0, 1.5, 2.0, 3.0, 4.0, 5.0, 7.5, and 10.0 s), cumulative absolute velocity (CAV) (Campbell and Bozorgnia 2010), and significant durations (D_{s595} and D_{s575}) (Bommer et al. 2009). The relative importance of these intensity measures is applied by using a weight vector presented in Table 3, in which the total weight of 70% is evenly distributed across the 18 SA ordinates, and 10% weight is allocated to each of CAV, D_{s595}, and D_{s575} intensity measures. Additional intensity measures such as peak ground acceleration (PGA); peak ground velocity (PGV); acceleration spectrum intensity (ASI) (Bradley 2010b); spectrum intensity (SI) (Bradley et al. 2009); and displacement spectrum intensity (DSI) (Bradley 2011a) were also considered. Although considering various intensity measures can result in motions with a proper representation for different aspects of ground motions (i.e., amplitude, frequency content, duration, and cumulative effects) for a given scenario rupture, based on the results presented in the previous chapter, considering SA ordinates, CAV, and significant duration intensity measures (i.e., D_{s595} and D_{s575}) can fairly represent these aspects. Therefore, only these intensity measures are given non-zero weights in the implemented weight vector (Table 10).

Table 10: Weight vector considered for ground-motion selection

SA	CAV	D_{s575}	D_{s595}
0.7[1]	0.1	0.1	0.1

[1]Evenly distributed to 18 SA ordinates between T=0-10s, i.e., each SA ordinate has a weight of 0.7/18.

3.3 Selected 20 ground motions for scenario ruptures in Christchurch

For each of the considered scenarios, 20 ground-motion time series are selected from the NGA database of strong ground motions from active shallow crustal earthquakes (Chiou et al. 2008). As discussed in the previous chapter, limiting the available database of ground motions to those motions with implicit causal parameters (e.g., magnitude, source-to-site distance, site condition) similar to the characteristics of the considered scenario rupture can result in motions with an appropriate representation for the causal parameters of the scenario, along with the explicit intensity measures of motion. In this regard, for each scenario considered, the NGA database is limited based on the bounds presented in Table 11. As seen in this table, the prospective ground motions are limited to those motions one unit of magnitude greater and smaller than the corresponding rupture scenario magnitude, and the source-to-site distances of the motions (R_{rup}) are bounded to 0.5 to 1.5 times the scenario R_{rup}. Site condition of the prospective motions is limited to site class D (deep or soft soils) and E (very soft soils) (NZS1170.5 2004), using V_{s30} values less than 400 m/s.

Table 11: Bounds on the implicit causal parameters of the prospective ground motions for the considered scenario ruptures for Christchurch city

Causal parameters	Magnitude, M_w	Source-to-site distance, R_{rup} (km)	Site condition, V_{s30} (m/s)
Alpine (Fiord-Kelly segment)	$7.1 < M_w < 9.1$	$66 < R_{rup} < 198$	$V_{s30} < 400$
Hope (Conway segment)	$6.45 < M_w < 8.45$	$53 < R_{rup} < 159$	$V_{s30} < 400$
Porters Pass	$6.45 < M_w < 8.45$	$22 < R_{rup} < 66$	$V_{s30} < 400$

It should also be noted that the motions in the NGA database have been processed to be directly used in seismic response analyses and are accessible at http://peer.berkeley.edu/nga/. The ground motions selected in this study are presented in Appendix A and B of this chapter and can also be downloaded from https://sites.google.com/site/brendonabradley/research/ground-motion-selection.

In order to illustrate the properties of selected motions, Figure 28 presents the median, 16th and 84th percentiles, and the individual acceleration response spectrum of the selected motions (which have been amplitude scaled), along with the predicted median target spectrum and the target 16th and 84th percentile spectra for the considered rupture scenarios.

In addition, Figure 28d presents cumulative distribution of 5-95% significant duration, D_{s595}, for the considered rupture scenarios and the corresponding target distribution.

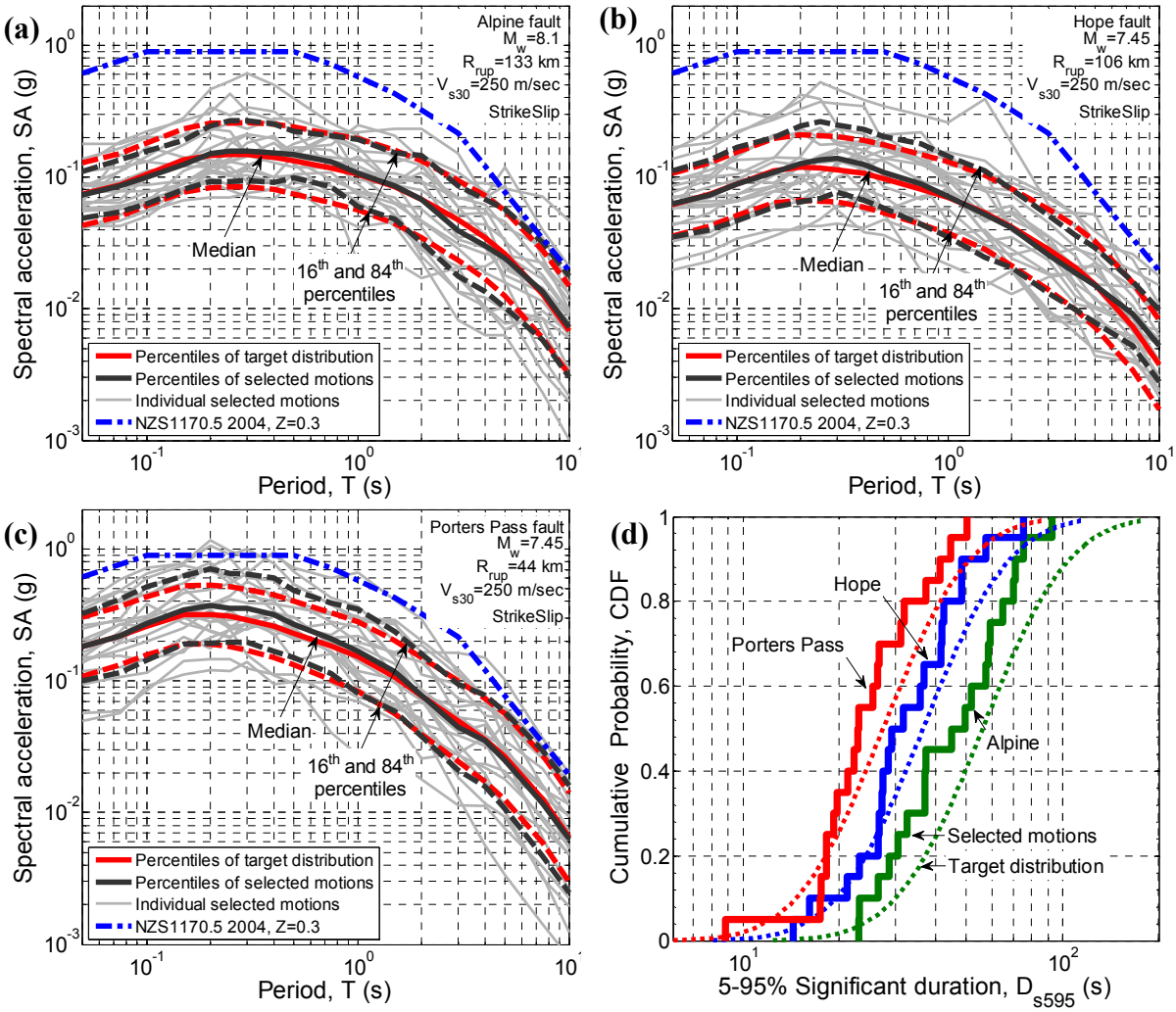

Figure 28: SA ordinates of the selected motions and the corresponding median, 16th, and 84th percentile spectra representing: (a) Alpine; (b) Hope; (c) Porters Pass scenario ruptures; and (d) cumulative distribution of 5-95% significant duration and the corresponding target distribution for the considered scenario rupture

Based on the presented results, it can be seen that the distribution of SA ordinates of the selected motions appropriately represents the predicted target distribution. Also, the distribution of the D_{s595} (Figure 28d), along with CAV and 5-75% significant duration, D_{s575}, (although not presented here for brevity) of the selected motions corresponds well to the target distribution of the scenario ruptures.

As seen in Figure 28, the predicted median scenario spectrum, the median spectrum of the selected motions, and the individual acceleration response spectrum of majority of the selected motions for the corresponding scenario ruptures are below the elastic site spectra

presented in NZS1170.5 (2004) for Christchurch (Z=0.3; shown here for reference only). In addition, as presented in Figure 28d, the M_w8.1 rupture of the Alpine fault and M_w7.45 rupture of the Hope fault (both with large source-to-site distances) will produce motions with long significant durations, whereas the M_w7.45 rupture of the Porter Pass fault (with a smaller source-to-site distance) will result in motions with shorter significant durations. The large differences in significant duration of the considered rupture scenarios and the considerable effect of duration on seismic response of engineering systems illustrates the importance of considering this intensity measure when selecting ground motions for seismic response analysis.

Considering the fact that the implicit causal parameters of ground motion, such as magnitude, source-to-site distance, and site condition are not explicitly considered in the GCIM-based ground-motion selection methodology (Bradley 2012a), it is worthwhile examining the distribution of these parameters for the selected motions with respect to each scenario rupture. As illustrated in Figure 29, the selected motions for the Hope fault rupture are well distributed with respect to the scenario magnitude (i.e. the 16th to 84th percentile range of M_w encompass the scenario). This is also generally the case for the Porters Pass fault rupture as well. In contrast, the selected motions for the Alpine fault rupture have a lower magnitude distribution than the scenario itself. This is caused by the paucity of recorded ground motions with magnitudes larger than M_w7.5-8, in contrast to a relative abundance in the recorded motions from events with smaller magnitudes. This is illustrated in Figure 29d, which depicts the $M_w - R_{rup}$ distribution of the motions in the NGA database (Chiou et al. 2008) and the motions that are available for the considered rupture scenarios for Christchurch city based on the bounds presented in Table 11. As seen in this figure, a small portion of the total database of motions is available for the Alpine fault rupture relative to the other two scenarios. Figure 29a-c illustrates that the selected motion can properly represent the scenario source-to-site distance for all three of the considered scenario ruptures, with the mean R_{rup} very close to the target scenario R_{rup}.

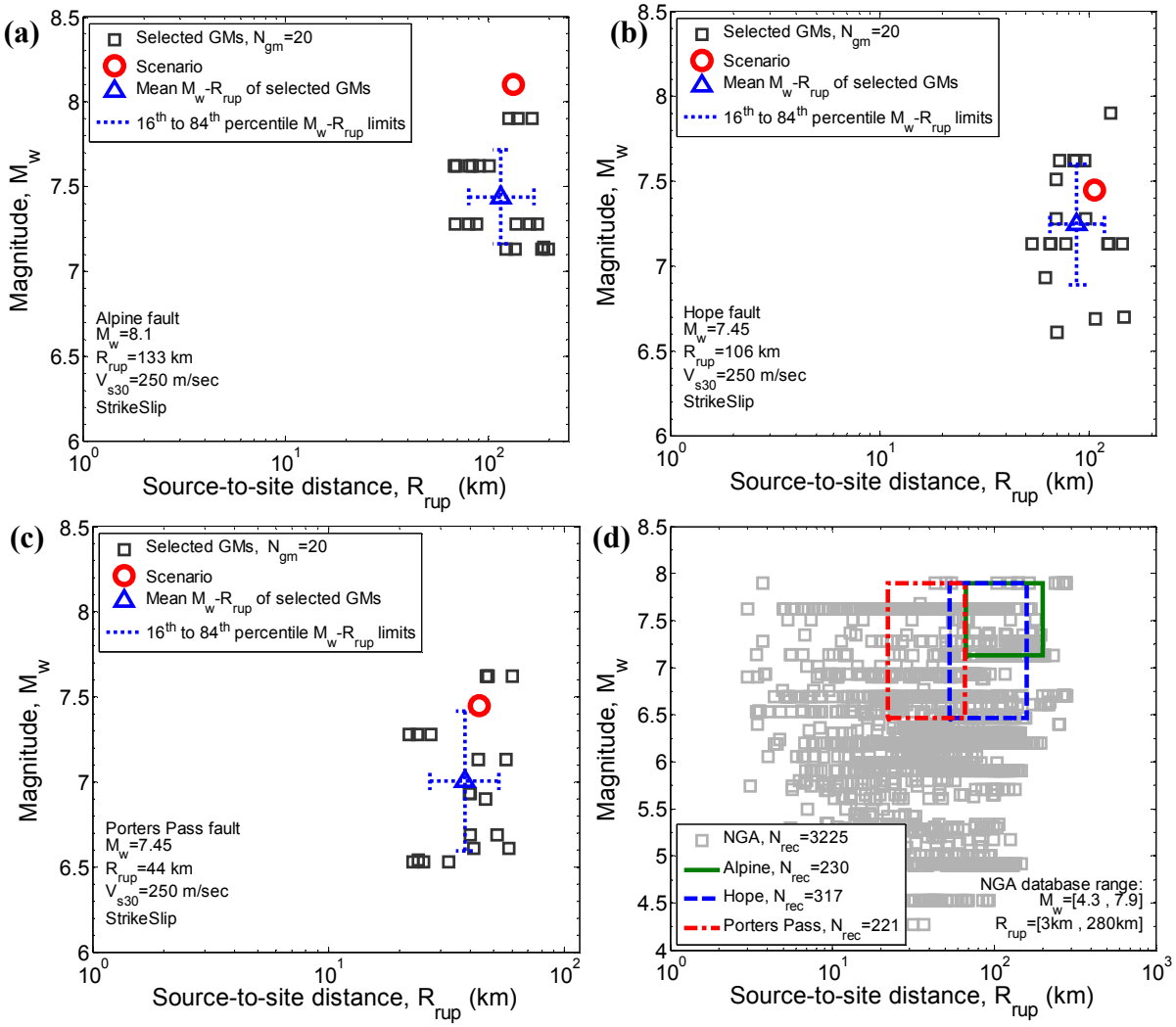

Figure 29: Magnitude-distance distribution of the selected motions representing: (a) Alpine; (b) Hope; (c) Porters Pass scenario ruptures

Figure 30a-c presents $V_{s30} - R_{rup}$ distribution of the selected motions representing the considered scenarios for Christchurch city. As seen in this figure, the selected motions can encompass the scenario within the 16th to 84th percentile bound. Also, the median V_{s30} of the selected motions is appropriately close to V_{s30} of the considered generic site. As discussed in the previous chapter, it can be seen that imposing bounds on magnitude, source-to-site distance, and site condition results in motions with a proper representation for these causal parameters of the considered scenarios.

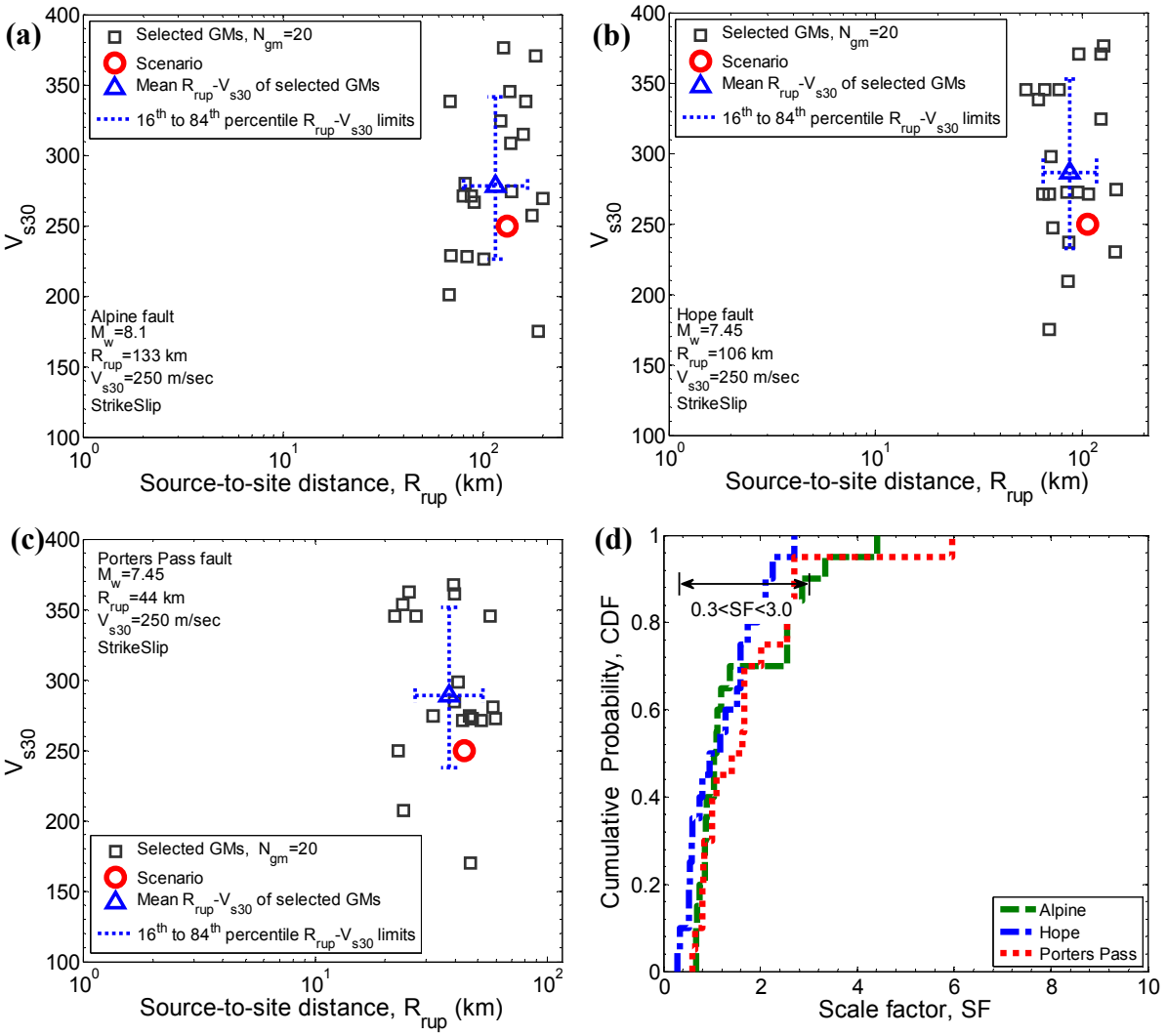

Figure 30: $V_{s30} - R_{rup}$ distribution of the selected ground motions, representing: (a) Alpine; (b) Hope; and (c) Porters Pass scenario ruptures, and (d) cumulative distribution of the amplitude scale factor of the selected motions

In addition to the distributions of the causal parameters (M_w, R_{rup}, V_{s30}), the applied amplitude scale factor, *SF*, required for the selected motions can be used to check the quality of the obtained ensemble of ground motions. Figure 30d presents the amplitude scale factor of the selected motions for the considered rupture scenarios for Christchurch city. As seen in this figure, all of the amplitude scale factors for the Hope fault rupture and 90% of the amplitude scale factors for the rupture of Alpine and Porter Pass faults are in the range of 0.3 to 3.0. Similar ranges are often recommended as scaling limits in seismic design standards (e.g., ASCE/SEI7-10 2010, NZS1170.5 2004). It should be noted that, as discussed in the previous chapter, having bounds on the implicit causal parameters of ground motions results in selecting motions with smaller amplitude scaling factors. This is due to the fact that by limiting the available motions to those with causal parameters similar to the scenario

characteristics, small changes in the amplitude of the motions are required to represent the distribution of the explicit intensity measures of motion.

It is important to note that there is a trade-off when selecting motions with an appropriate representation for the predicted intensity measures (SA, D_{s595} etc.); magnitude-distance distribution (or other implicit causal parameters); and amplitude scale factors. While ideally the selected motions would have the appropriate representation of implicit causal parameters and amplitude scale factors near 1.0, an emphasis in ground motion selection should be placed on the appropriateness of the explicit intensity measures of the ground motion (SA, D_{s595} etc.) rather than the implicit causal parameters, as elaborated on by Bradley (2012) and also in the previous chapter.

3.4 A subset of 7 ground motions from the selected 20 motions

A subset of 7 ground motions from the selected 20 motions are also tabulated in Appendix B, which can be used in code-based analyses to assess the design or retrofit of the system against the occurrence of the considered rupture scenarios. Figure 31, as an example, illustrates the SA ordinates, cumulative distribution of 5-95% significant duration, $M_w - R_{rup}$ and $V_{s30} - R_{rup}$ distributions of the subset of 7 motions representing the Alpine fault scenario rupture.

As seen in Figure 31, the selected 7 motions appropriately represent the predicted intensity measures of the motions due to the scenario rupture. Considering the distribution of the causal parameters of the 20 motions, the V_{s30} and R_{rup} of the subset of 7 motions have an appropriate representation of the scenario characteristics. It is important to note that the individual amplitude scale factors applied on these 7 motions, in order to collectively represent the predicted distribution of the considered intensity measures, are slightly different than those applied on the same motions when they were selected in a set with 20 motions. As presented in Appendix B, all of the amplitude scale factors applied on the subset of 7 motions are within the range of 0.3 to 3.0.

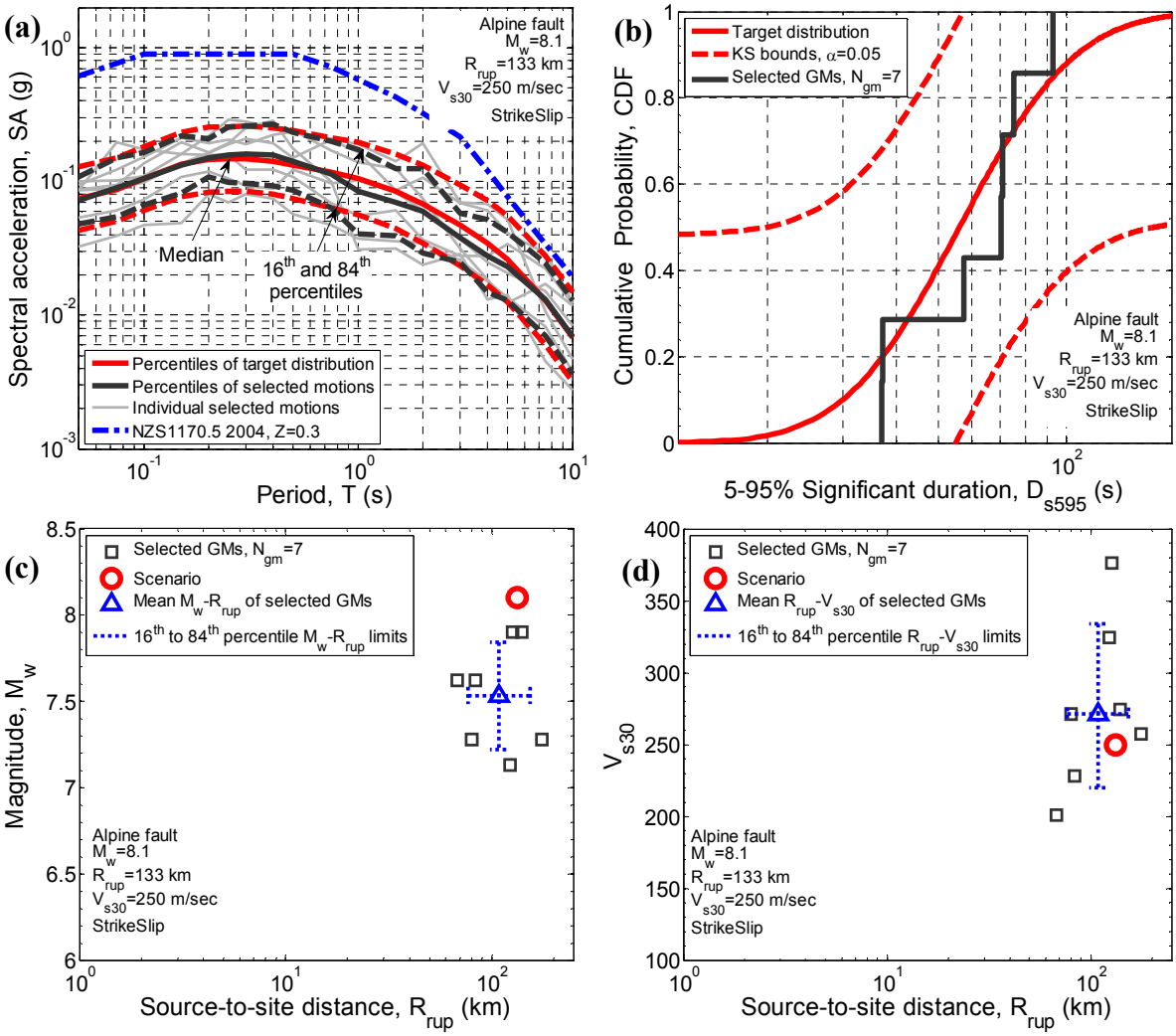

Figure 31: Distribution of the subset of 7 motions representing the Alpine fault scenario rupture: (a) SA ordinates; (b) cumulative distribution of 5-95% significant duration; (c) $M_w - R_{rup}$ distribution; and (d) $V_{s30} - R_{rup}$ distribution

4 Ground motion selection for scenario ruptures in Wellington

4.1 Dominant seismic sources

PSHA has been conducted for a generic location in central Wellington city (Latitude −41:2889° and Longitude 174.7772°) for a site class D soil (NZS1170.5 2004) with V_{s30}= 250 m/s. Figure 32 illustrates the seismic hazard deaggregation for PGA and SA(2.0s) for a 10% probability of exceedance in 50 years. Based on the obtained results for deaggregation of the seismic hazard, it is observed that the seismic hazard at this generic location in Wellington city is mostly dominated by events with large magnitudes and very small source-to-site distances. By identifying the scenarios with large contributions to the seismic hazard, ruptures of the Wellington, Wairarapa, and Ohariu faults are considered in this study for

scenario ground-motion selection. Characteristics of these scenario ruptures are presented in Table 4.

It is important to note that the presented deaggregation results illustrate the contribution of a M_w8.64 rupture of the Hikurangi subduction zone (Wellington Max segment) within 18 km distance from Wellington city. The current issues related to robustly selecting ground motions to represent subduction zone earthquakes are discussed later in this chapter, and therefore attention here has been limited to selecting ground motions to represent active shallow-crustal ruptures.

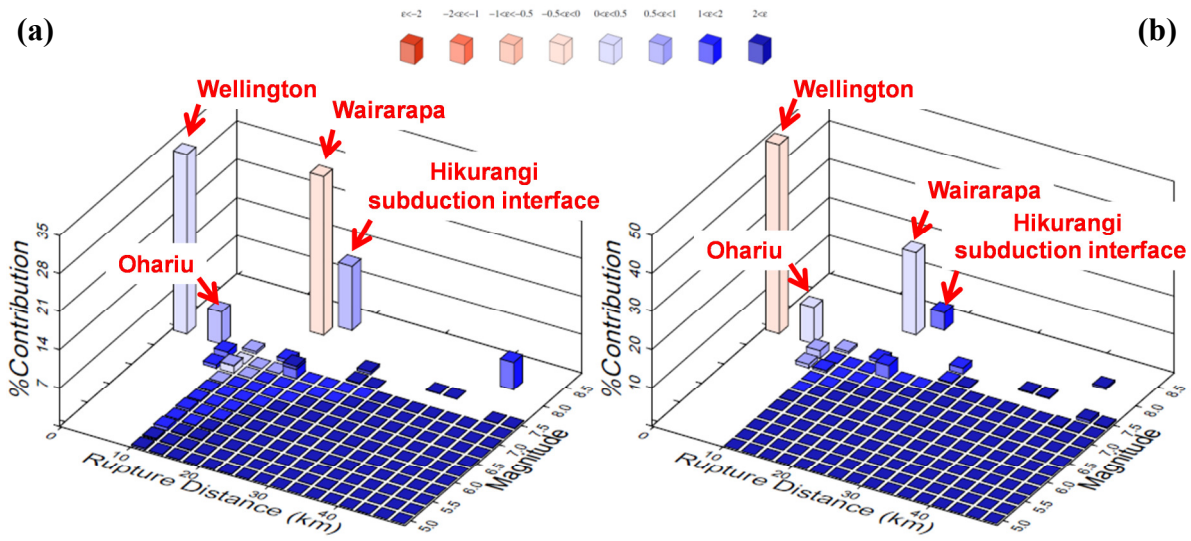

Figure 32: Deaggregation of seismic hazard in Wellington city for: (a) PGA; and (b) SA(2.0s) for a 10% probability of exceedance in 50 years

Table 12: Characteristics of the considered scenario ruptures for Wellington city[1]

Fault	Magnitude, M_w	Source-to-site distance, R_{rup} (km)	Rupture mechanism
Wellington (Well-Hutt Valley segment)	7.53	1.0	Strike-slip
Wairarapa (Nicholson segment)	8.17	17.0	Strike-slip
Ohariu (South segment)	7.36	6.0	Strike-slip

[1]Based on the ERF of Stirling et al. (2012).

4.2 Intensity measures of the considered scenario ruptures

Table 13 presents the median intensity measures for the scenario ruptures considered for Wellington city. As presented, the Wellington fault with a large magnitude and very small source-to-site distance, and the Wairarapa fault with a very large magnitude and small

source-to-site distance have close median SA ordinates. In addition, the Wellington rupture results in a greater PGV compared to the Wairarapa and Ohariu ruptures, because of the very small source-to-site distance from this fault to the site. Finally, because of the large magnitude of the rupture in the Wairarapa fault (i.e. M_w8.17), the median predicted ground motion significant duration (i.e., median D_{s595}) is considerably greater than that for the other two ruptures.

Table 13. Median intensity measures of the considered scenario ruptures for Wellington city

Fault	PGA (g)	SA(0.5s) (g)	SA(1.0s) (g)	SA(2.0s) (g)	PGV (cm/s)	CAV (g.s)	Ds595 (s)
Wellington (Well-Hutt Valley segment)	0.6	1.0	0.9	0.6	104.7	2.0	24.0
Wairarap (Nicholsonsegment)	0.7	1.1	0.8	0.4	74.7	2.0	41.5
Ohariu (South segment)	0.5	0.7	0.6	0.4	70.0	2.1	21.0

4.3 Selected 20 ground motions for scenario ruptures in Wellington

Similar to the Christchurch scenarios previously discussed, ensembles of 20 ground motions were selected for each of the three considered ruptures for Wellington city, using the GCIM-based ground motion selection method. Table 14 presents the bounds applied on the implicit causal parameters of the prospective ground motions for the three considered scenario ruptures. Due to the short source-site distance of the three considered scenarios, R_{rup} of the prospective ground motions are bounded to values less than 30km. The weight vector presented in Table 10 is also implemented here for the Wellington city cases.

Table 14: Bounds on the implicit causal parameters of the prospective ground motions for the considered scenario ruptures for Wellington city

Causal parameters	Magnitude, M_w	Source-to-site distance, R_{rup}(km)	Site condition, V_{s30} (m/s)
Wellington (Well-Hutt Valley segment)	$6.53 < M_w < 8.53$	$R_{rup} < 30$	$V_{s30} < 400$
Wairarapa (Nicholson segment)	$7.17 < M_w < 9.17$	$R_{rup} < 30$	$V_{s30} < 400$
Ohariu (South segment)	$6.36 < M_w < 8.36$	$R_{rup} < 30$	$V_{s30} < 400$

Figure 33a-c presents the median, 16th, and 84th percentiles and the individual (amplitude scaled) acceleration response spectrum of the selected motions, along with the predicted median, 16th, and 84th percentile target spectra for the considered scenario ruptures for Wellington city. As shown in Figure 33a-b, the predicted median scenario spectrum, and the median spectrum of the selected motions for rupture of the Wellington fault (which has the highest contribution to the seismic hazard at the site) and Wairarapa fault are very close to the Z=0.4 elastic code spectra of NZS1170.5 (2004) at medium to long periods of vibration (provided here for comparison only). It should be noted that the near-fault effect has been considered in calculating the code elastic site spectra for Wellington (NZS1170.5 2004).

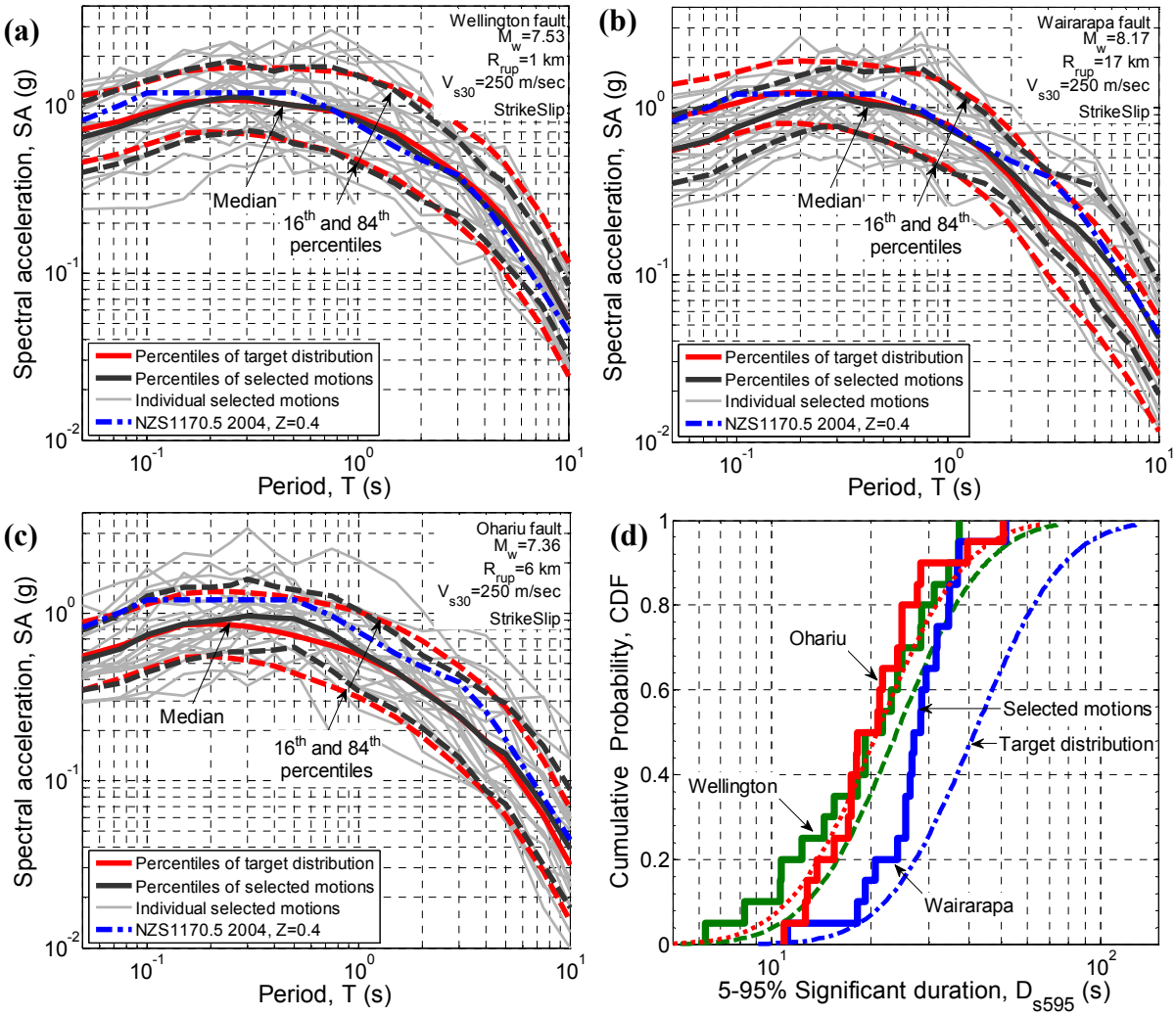

Figure 33: SA ordinates of the selected motions and the corresponding median, 16th, and 84th percentile spectra representing: (a) Wellington; (b) Wairarapa; (c) Ohariu scenario ruptures; and (d) cumulative distribution of 5-95% significant duration and the corresponding target distribution for the considered scenario ruptures

As presented in Figure 33a-c, the selected ground motions can appropriately represent the SA ordinates for Wellington and Ohariu fault ruptures, for the whole range of vibration periods (i.e., T=0.05s-10.0s). However for the Wairarapa fault rupture, the selected motions deviate from the target distribution for short (i.e., T<0.2) and long (i.e., T>4.0) vibration period ranges. Also, based on the presented cumulative distribution of the 5-95% significant duration of the selected ground motions and the corresponding target distribution in Figure 33d, it can be seen that the selected motions can properly represent the 5-95% significant duration for the Wellington and Ohariu fault ruptures. However, there is a deviation from the target distribution for 5-95% significant duration of the Wairarapa fault rupture. When considering the resulting ground motions selected for the Wairarapa rupture scenario (Figure 33b and Figure 33d), it is important to note that in comparing the selected motions with the 'target' we are implicitly assuming that the target is itself correct. While this is generally a reasonable assumption, in the case of rupture scenarios with very large magnitudes, (i.e., M_w 8.17 for Wairarapa), the GMPE utilized to calculate the target distribution can be weakly constrained for such large events. Therefore, the 'target' may itself be inherently biased and therefore the deviation observed is considered acceptable.

Figure 34 provides a comparison of the magnitude-distance distribution of the selected motions with respect to magnitude-distance pair of the corresponding scenarios for Wellington city. In the case of the Wellington and Ohariu fault ruptures, it can be seen that the magnitude distribution of the selected motions fairly corresponds to the rupture magnitude, while the magnitudes of the selected motions for the Wairarapa rupture fall below that expected for that event. In terms of source-to-site distances it can be seen that the ground motions selected for the Wairarapa fault rupture corresponds well to the scenario source-to-site distance, with a mean R_{rup} very close to the scenario R_{rup}. However, source-to-site distances of the selected motions for the Wellington and Ohariu fault ruptures are notably larger than those representative of these scenarios. Clearly, these biases are related to the paucity of the motions recorded from large magnitude events with short source-to-site distances. Figure 34d illustrates the $M_w - R_{rup}$ distribution of the motions in the NGA database (Chiou et al. 2008) and the ones that are available for each rupture scenario for Wellington city based on the bounds presented in Table 14. As seen in this figure, there are few motions with implicit causal parameters close to the characteristics of the Wellington fault rupture relative to the other two scenarios.

As already noted, it is important to remember that ground-motion selection requires a trade-off between the intensity measure values of the ground motions themselves, and implicit causal parameters such as M_w, R_{rup}, V_{s30}, etc. Because it is known that there is little variation of ground motion properties in the immediate near-field (i.e. R_{rup}=0-10km) region, then the distance biases shown in Figure 34 for the Wellington and Ohariu fault ruptures (with R_{rup} values of 1.0 and 6.0 km, respectively) are not considered significant.

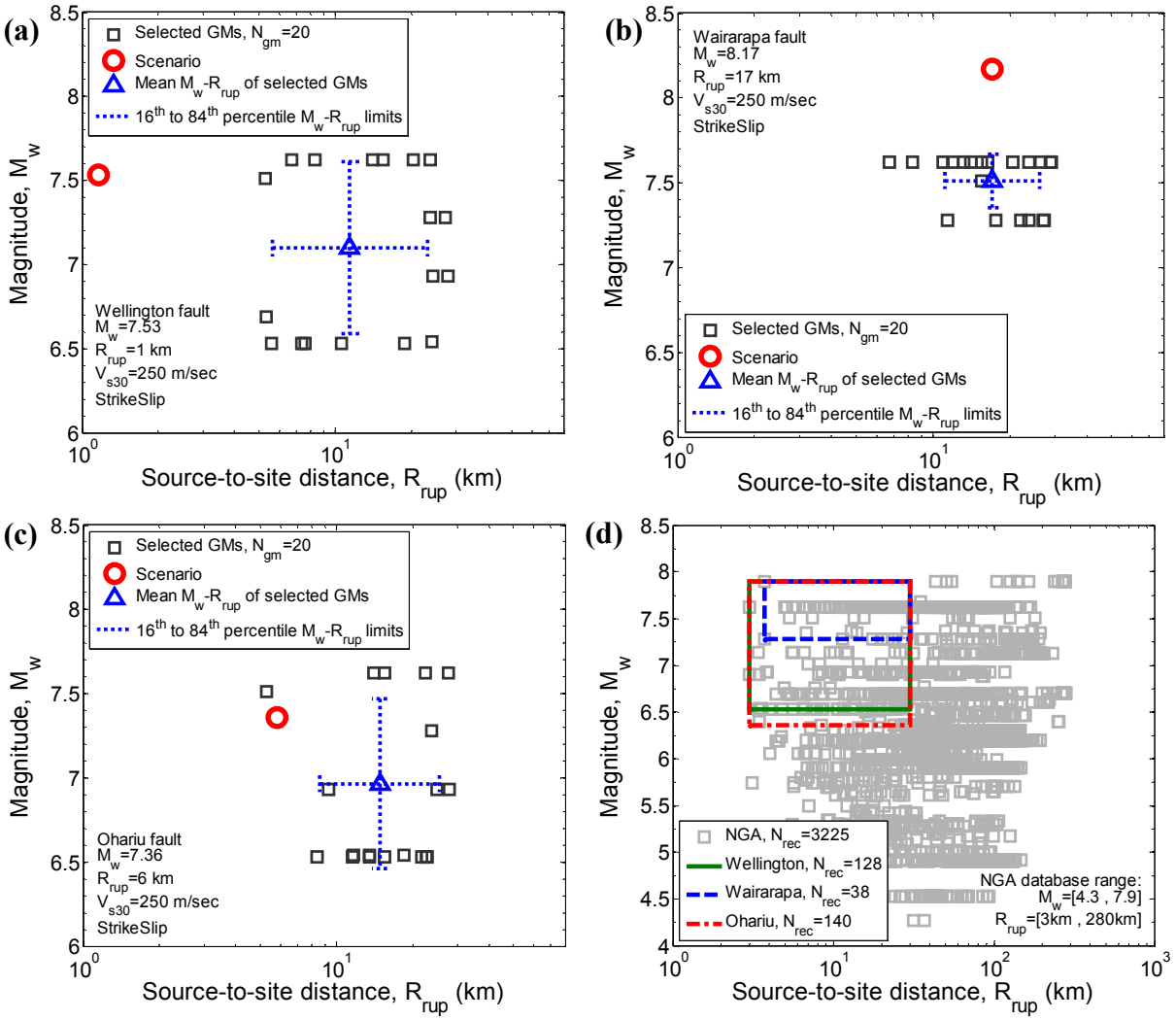

Figure 34: Magnitude-distance distribution of the selected motions representing: (a) Wellington; (b) Wairarapa; (c) Ohariu scenario ruptures

Figure 35a-c presents $V_{s30} - R_{rup}$ distribution of the selected ground motions representing the considered scenarios for Wellington city. As seen in this figure, the V_{s30} values of the selected motions for the Wellington and Ohariu fault ruptures correspond well to the considered site condition. Also, most of the selected motions for the Wairarapa fault

rupture have V_{s30} values which are mostly similar to characteristics of a site class D soil (NZS1170.5 2004).

As presented in Figure 35d, the amplitude scale factor of the selected motions are mostly large values, compared to the results presented in Figure 30d for Christchurch city, with approximately 80% of them for Wellington and Wairarapa fault ruptures and 70% of them for Ohariu fault rupture in the *SF*=0.3-3.0 range. As discussed in the previous chapter, selecting ground motions for scenarios like those encountered in Wellington city (with short source-to-site distances and large magnitudes) often requires scaling the existing motions using larger scale factors, as there is a shortage of motions recorded during such events in the existing strong ground motion database (Chiou et al. 2008) with adequate intensity measure properties and recorded at appropriate site classes.

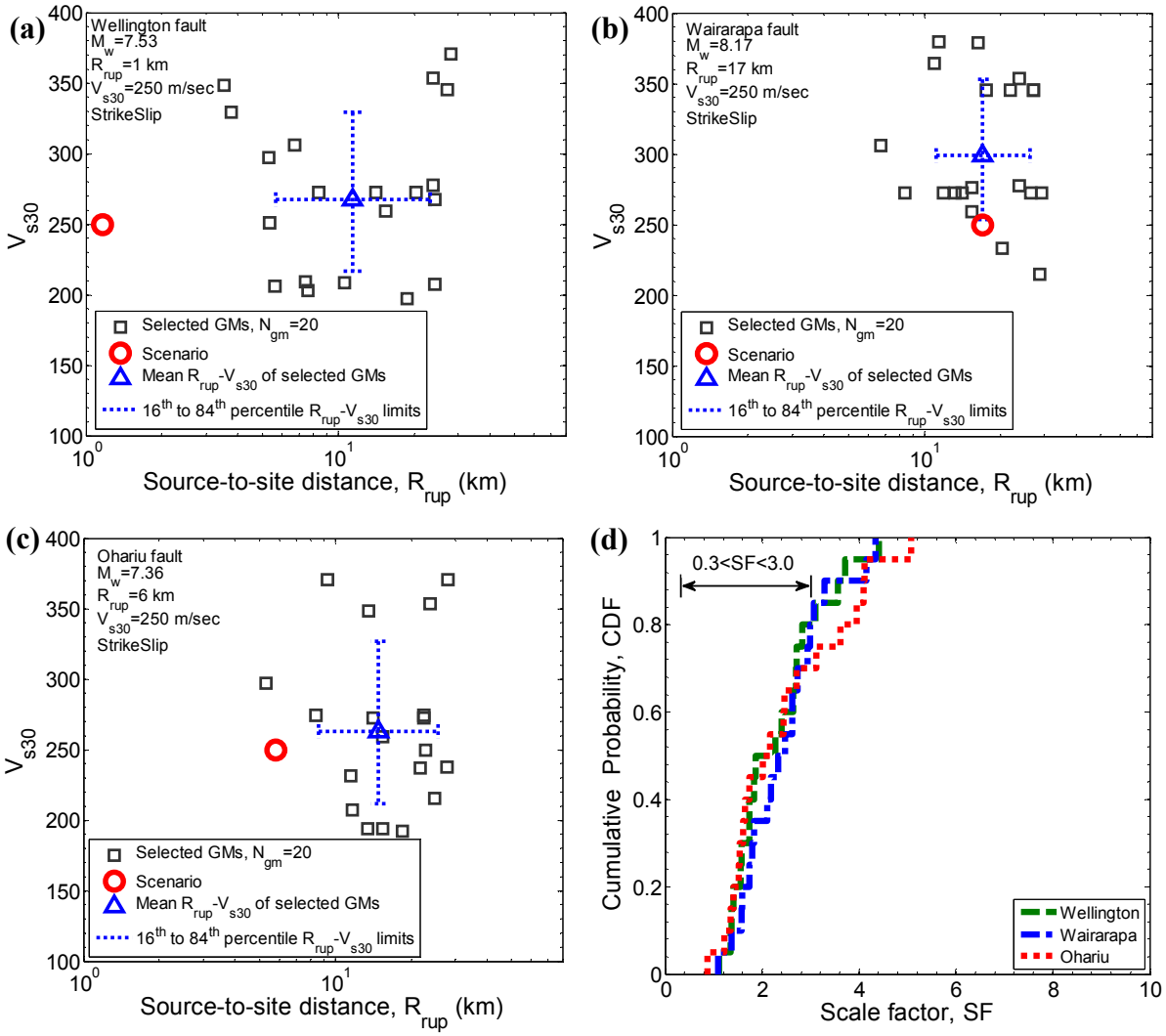

Figure 35: $V_{s30} - R_{rup}$ distribution of the selected ground motions, representing: (a) Wellington; (b) Wairarapa; and (c) Ohariu scenario ruptures, and (d) cumulative distribution of the amplitude scale factor of the selected motions

4.4 A subset of 7 ground motions from the selected 20 motions

A subset of 7 ground motions from the selected 20 motions are also tabulated in Appendix B to represent the considered scenario ruptures in Wellington city. Figure 36 illustrates the SA ordinates, cumulative distribution of 5-95% significant duration, $M_w - R_{rup}$ and $V_{s30} - R_{rup}$ distributions of the subset of 7 motions representing the Wellington fault scenario rupture. As seen in this figure, the selected 7 motions appropriately represent the predicted distribution of the considered intensity measures. However, the issues associated with representativeness of the causal parameters of the 20 motion elaborated earlier are present in the subset of 7 motions.

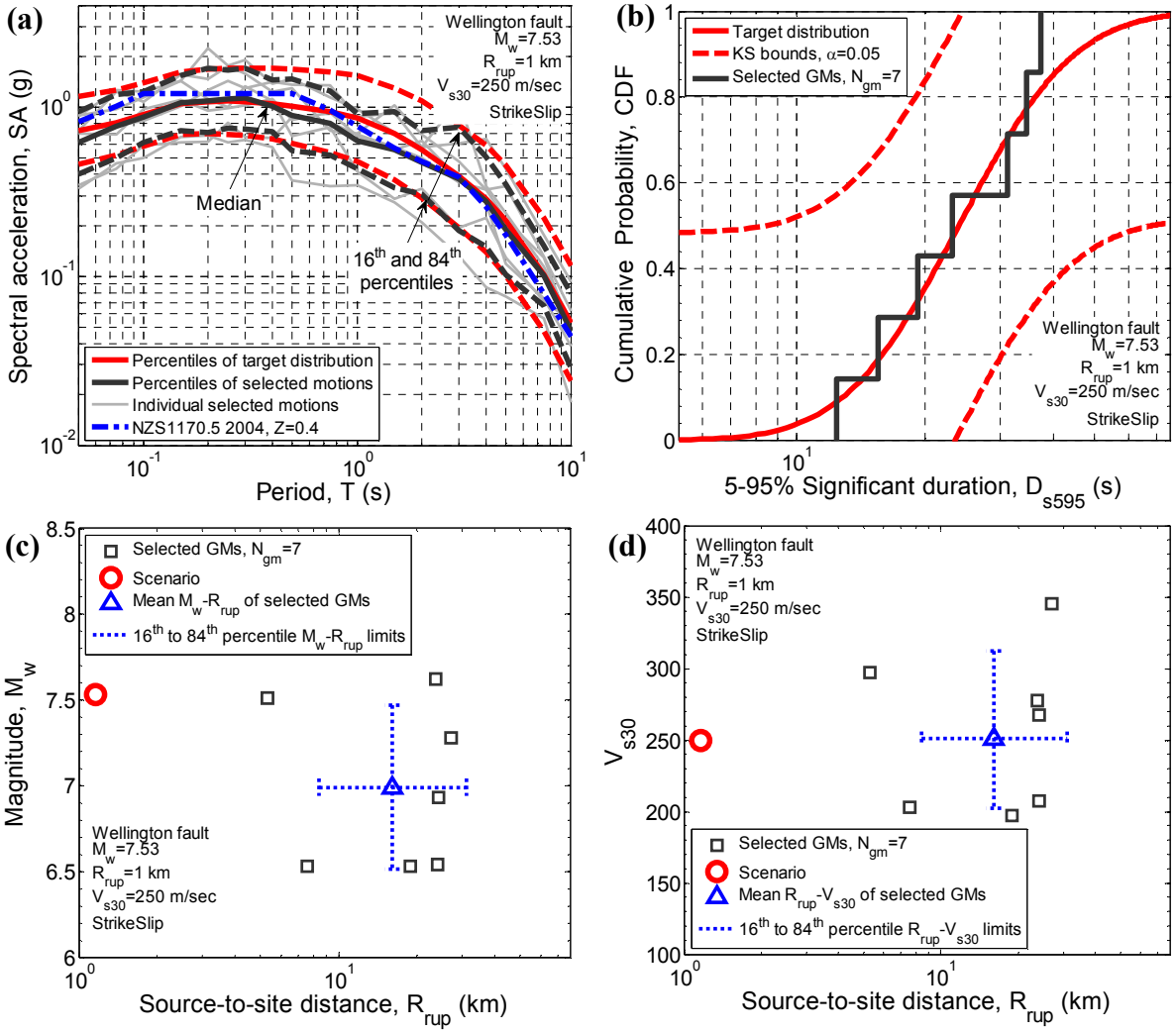

Figure 36: Distribution of the subset of 7 motions representing the Wellington fault scenario rupture: (a) SA ordinates; (b) cumulative distribution of 5-95% significant duration; (c) $M_w - R_{rup}$ distribution; and (d) $V_{s30} - R_{rup}$ distribution

5 Selecting representative ground motions for subduction zone events

The ground motions selected in this study are aimed to represent major active shallow crustal rupture scenarios in Christchurch and Wellington cities. However, the occurrence of major subduction zone earthquakes (both interface and slab) should also be considered in ground-motion selection for regions prone to this type of earthquakes, such as Wellington. As noted, in the presented deaggregation results for Wellington, the occurrence of a M_w8.64 rupture of the Hikurangi subduction interface (Wellington Max segment) within 18 km distance of Wellington contributes significantly to the seismic hazard. At present, routine ground motion selection for subduction zone events is hindered by a lack of: (1) a comprehensive database of strong ground motions recorded from subduction zone events; and (2) appropriate subduction zone GMPEs and correlation equations for various ground-motions intensity measures. Such efforts are topics of on-going research among the authors as well as many others in the research community.

6 Conclusion

This paper demonstrates selecting ground motions to represent several major earthquake scenarios in New Zealand, using the generalized conditional intensity measure (GCIM) approach. Six different rupture scenarios were considered that pose a significant seismic hazard in Christchurch city (Alpine, Hope and Porters Pass ruptures) and Wellington city (Wellington, Ohariu, and Wairarapa ruptures). For each rupture scenario considered, sets of 20 ground motions were selected to appropriately represent the predicted distribution of various intensity measures (spectral accelerations, significant duration etc.). Subsets of 7 motions from these 20 ground motions were also tabulated and can be utilized for standard code-based seismic response analyses. A paucity of recorded motions from events with large magnitudes and short source-to-site distances in existing strong ground motion databases impedes selecting motions for large magnitude small source-to-site distance rupture scenarios and also consequently requires the use of large amplitude scale factors to scale available motions. However, it should be remembered that implicit causal parameters, such as magnitude and source-to-site distance, are of secondary importance when compared to explicit measures of intensity of ground motion (spectral accelerations, significant duration etc.).

Appendix A: Tabulated ground motion details (20 ground motions)

Presented in this appendix is the NGA ID number (Chiou et al. 2008) of the 20 ground motions and their corresponding amplitude scale factor, selected for the scenario rupture of the Alpine, Hope, and Porters Pass faults for Christchurch city (Table A1-A3), and Wellington, Wairarapa, and Ohariu faults for Wellington city (Table A4-A6). Also, subsets of 7 ground motions from these 20 motions are presented in Appendix B.

It is important to note that the ground-motion selection has been conducted based on the geometric mean of the intensity measures of motion. Presented ground-motion time series are the as-recorded motions in two horizontal directions and the vertical direction (which have file names with suffix "_1", "_2", and "_3" for the two horizontal and vertical components; accessible at https://sites.google.com/site/brendonabradley/research/ground-motion-selection). Geometric mean of peak ground acceleration (PGA) and peak ground velocity (PGV) of the two as-recorded horizontal motions are presented in the tables below. These motions are also accessible at http://peer.berkeley.edu/nga/, using the NGA ID number.

Table A1. Selected ground motions representing the Alpine fault scenario rupture for Christchurch city

NGA#	Event	Year	Station	*Mw*	Mechanism	R_{rup} (km)	V_{s30} (m/s)	PGA (g)	PGV (cm/s)	Scale factor
836	Landers	1992	Baker Fire Station	7.28	Strike-Slip	87.9	271.4	0.1069	9.8487	1.1827
842	Landers	1992	Brea - S Flower Av	7.28	Strike-Slip	137.4	308.6	0.0424	10.498	2.7397
860	Landers	1992	Hemet Fire Station	7.28	Strike-Slip	68.7	338.5	0.0898	5.6042	0.7402
869	Landers	1992	LA - N Westmoreland	7.28	Strike-Slip	159.1	315.1	0.0377	3.5485	4.4053
888	Landers	1992	San Bernardino - E & Hospitality	7.28	Strike-Slip	79.8	271.4	0.0827	17.1588	0.6816
895	Landers	1992	Tarzana - Cedar Hill	7.28	Strike-Slip	175.7	257.2	0.0489	7.0652	1.1025
1188	Chi-Chi- Taiwan	1999	CHY016	7.62	Reverse-Oblique	66.7	200.9	0.1019	16.1417	0.8841
1192	Chi-Chi- Taiwan	1999	CHY023	7.62	Reverse-Oblique	81.3	279.8	0.0493	9.0844	1.0436
1217	Chi-Chi- Taiwan	1999	CHY060	7.62	Reverse-Oblique	68.9	228.9	0.0461	14.8224	0.8833
1223	Chi-Chi- Taiwan	1999	CHY067	7.62	Reverse-Oblique	83.6	228	0.0605	10.3253	0.6646
1342	Chi-Chi- Taiwan	1999	ILA055	7.62	Reverse-Oblique	90.3	266.8	0.0749	24.9999	0.8506
1415	Chi-Chi- Taiwan	1999	TAP010	7.62	Reverse-Oblique	101.3	226.4	0.1039	22.798	0.8478
1599	Duzce- Turkey	1999	Ambarli	7.14	Strike-Slip	188.7	175	0.0275	5.5939	2.5517
1790	Hector Mine	1999	Huntington Beach - Lake St	7.13	Strike-Slip	184	370.8	0.0224	10.0151	3.3447
1814	Hector Mine	1999	Newhall - Fire Sta	7.13	Strike-Slip	198.1	269.1	0.018	4.6309	2.8727
1823	Hector Mine	1999	Salton City	7.13	Strike-Slip	123.2	324.5	0.0512	7.9271	2.5562
1837	Hector Mine	1999	Valyermo Forest Fire Station	7.13	Strike-Slip	135.8	345.4	0.0602	6.3605	1.3702
2109	Denali- Alaska	2002	Fairbanks - Ester Fire Station	7.9	Strike-Slip	139.8	274.5	0.0497	4.0012	1.1225
2115	Denali- Alaska	2002	TAPS Pump Station #11	7.9	Strike-Slip	126.4	376.1	0.0761	11.5231	0.6744
2116	Denali- Alaska	2002	TAPS Pump Station #12	7.9	Strike-Slip	164.7	338.6	0.0379	4.3939	1.0491

Table A2. Selected ground motions representing the Hope fault scenario rupture for Christchurch city

NGA#	Event	Year	Station	*Mw*	Mechanism	R_{rup} (km)	V_{s30} (m/s)	PGA (g)	PGV (cm/s)	Scale factor
82	San Fernando	1971	Port Hueneme	6.61	Reverse	68.8	297.9	0.0275	5.4297	1.175
742	Loma Prieta	1989	Bear Valley #1- Fire Station	6.93	Reverse-Oblique	61.7	338.5	0.074	5.8732	1.52
832	Landers	1992	Amboy	7.28	Strike-Slip	69.2	271.4	0.1279	18.9953	0.5485
887	Landers	1992	Riverside Airport	7.28	Strike-Slip	96	370.8	0.0417	3.0494	2.6995
1068	Northridge-01	1994	San Bernardino - Co Service Bldg - Freefield	6.69	Reverse	107.7	271.4	0.0409	4.654	2.2529
1147	Kocaeli- Turkey	1999	Ambarli	7.51	Strike-Slip	69.6	175	0.2129	36.671	0.2814
1220	Chi-Chi- Taiwan	1999	CHY063	7.62	Reverse-Oblique	72.2	246.9	0.0635	8.5603	0.9396
1332	Chi-Chi- Taiwan	1999	ILA042	7.62	Reverse-Oblique	85.7	209.4	0.0768	16.666	0.7539
1344	Chi-Chi- Taiwan	1999	ILA059	7.62	Reverse-Oblique	86.3	236.8	0.0653	15.3931	0.3323
1433	Chi-Chi- Taiwan	1999	TAP047	7.62	Reverse-Oblique	84.5	400.3	0.0568	15.1991	1.2757
1559	Chi-Chi- Taiwan	1999	TTN003	7.62	Reverse-Oblique	95	262.6	0.0196	3.1005	2.1116
1766	Hector Mine	1999	Baker Fire Station	7.13	Strike-Slip	64.8	271.4	0.1097	8.4377	0.5181
1773	Hector Mine	1999	Cabazon	7.13	Strike-Slip	76.9	345.4	0.041	7.3971	0.8003
1783	Hector Mine	1999	Fort Irwin	7.13	Strike-Slip	65.9	345.4	0.1251	10.0637	0.5307
1813	Hector Mine	1999	Morongo Valley	7.13	Strike-Slip	53.2	345.4	0.0846	16.5223	1.9402
1821	Hector Mine	1999	Pomona - 4th & Locust FF	7.13	Strike-Slip	143.4	229.8	0.0368	6.4202	0.5988
1822	Hector Mine	1999	Riverside Airport	7.13	Strike-Slip	123.8	370.8	0.0238	2.9607	1.5853
1823	Hector Mine	1999	Salton City	7.13	Strike-Slip	123.2	324.5	0.0512	7.9271	1.7395
2089	Nenana Mountain- Alaska	2002	Fairbanks - Ester Fire Station	6.7	Strike-Slip	146.3	274.5	0.0176	1.6938	1.5851
2115	Denali- Alaska	2002	TAPS Pump Station #11	7.9	Strike-Slip	126.4	376.1	0.0761	11.5231	0.5851

Table A3. Selected ground motions representing the Porters Pass fault scenario rupture for Christchurch city

NGA#	Event	Year	Station	*Mw*	Mechanism	R_{rup} (km)	V_{s30} (m/s)	PGA (g)	PGV (cm/s)	Scale factor
51	San Fernando	1971	2516 Via Tejon PV	6.61	Reverse	55.2	280.6	0.0292	3.4345	1.6707
93	San Fernando	1971	Whittier Narrows Dam	6.61	Reverse	39.5	298.7	0.1153	9.3048	2.019
176	Imperial Valley-06	1979	El Centro Array #13	6.53	Strike-Slip	22	249.9	0.1271	14.231	2.7055
190	Imperial Valley-06	1979	Superstition Mtn Camera	6.53	Strike-Slip	24.6	362.4	0.1401	6.7852	0.8189
191	Imperial Valley-06	1979	Victoria	6.53	Strike-Slip	31.9	274.5	0.1301	7.7914	1.6648
287	Irpinia- Italy-01	1980	Bovino	6.9	Normal	46.2	274.5	0.0443	2.6882	5.9594
729	Superstition Hills-02	1987	Wildlife Liquef. Array	6.54	Strike-Slip	23.9	207.5	0.1958	27.821	0.6572
761	Loma Prieta	1989	Fremont - Emerson Court	6.93	Reverse-Oblique	39.9	284.8	0.1581	13.5695	0.7948
762	Loma Prieta	1989	Fremont - Mission San Jose	6.93	Reverse-Oblique	39.5	367.6	0.1401	11.3569	1.0067
850	Landers	1992	Desert Hot Springs	7.28	Strike-Slip	21.8	345.4	0.1607	20.4204	2.5506
880	Landers	1992	Mission Creek Fault	7.28	Strike-Slip	27	345.4	0.1243	12.6347	0.9963
900	Landers	1992	Yermo Fire Station	7.28	Strike-Slip	23.6	353.6	0.2222	36.4046	0.8346
1026	Northridge-01	1994	Lawndale - Osage Ave	6.69	Reverse	39.9	361.2	0.1157	8.253	1.0889
1059	Northridge-01	1994	Port Hueneme - Naval Lab.	6.69	Reverse	51.8	271.4	0.0926	8.0926	2.6953
1215	Chi-Chi- Taiwan	1999	CHY058	7.62	Reverse-Oblique	59.8	237.6	0.057	12.1121	1.6721
1228	Chi-Chi- Taiwan	1999	CHY076	7.62	Reverse-Oblique	42.2	169.8	0.0754	19.5592	0.6019
1258	Chi-Chi- Taiwan	1999	HWA005	7.62	Reverse-Oblique	47.6	489.2	0.1425	14.3445	0.8057
1279	Chi-Chi- Taiwan	1999	HWA030	7.62	Reverse-Oblique	47	487.4	0.0711	12.2492	1.6258
1762	Hector Mine	1999	Amboy	7.13	Strike-Slip	43	271.4	0.1986	23.8956	1.4158
1776	Hector Mine	1999	Desert Hot Springs	7.13	Strike-Slip	56.4	345.4	0.0716	8.8339	2.5616

Table A4. Selected ground motions representing the Wellington fault scenario rupture for Wellington city

NGA#	Event	Year	Station	*Mw*	Mechanism	R_{rup} (km)	V_{s30} (m/s)	PGA (g)	PGV (cm/s)	Scale factor
161	Imperial Valley-06	1979	Brawley Airport	6.53	Strike-Slip	10.4	208.7	0.1822	35.9744	3.7038
173	Imperial Valley-06	1979	El Centro Array #10	6.53	Strike-Slip	6.2	202.8	0.2001	42.9521	4.4048
175	Imperial Valley-06	1979	El Centro Array #12	6.53	Strike-Slip	17.9	196.9	0.1258	19.6423	3.0942
179	Imperial Valley-06	1979	El Centro Array #4	6.53	Strike-Slip	7	208.9	0.4118	55.8948	1.7413
183	Imperial Valley-06	1979	El Centro Array #8	6.53	Strike-Slip	3.9	206.1	0.5256	50.2289	1.3476
723	Superstition Hills-02	1987	Parachute Test Site	6.54	Strike-Slip	0.9	348.7	0.3792	72.7429	2.6372
729	Superstition Hills-02	1987	Wildlife Liquef. Array	6.54	Strike-Slip	23.9	207.5	0.1958	27.821	1.5489
776	Loma Prieta	1989	Hollister - South & Pine	6.93	Reverse-Oblique	27.9	370.8	0.2855	48.3396	2.707
806	Loma Prieta	1989	Sunnyvale - Colton Ave.	6.93	Reverse-Oblique	24.2	267.7	0.2008	34.4243	1.863
880	Landers	1992	Mission Creek Fault	7.28	Strike-Slip	27	345.4	0.1243	12.6347	2.7252
900	Landers	1992	Yermo Fire Station	7.28	Strike-Slip	23.6	353.6	0.2222	36.4046	2.8196
1084	Northridge-01	1994	Sylmar - Converter Sta	6.69	Reverse	5.3	251.2	0.6875	110.2475	1.7328
1176	Kocaeli- Turkey	1999	Yarimca	7.51	Strike-Slip	4.8	297	0.2949	59.2684	2.3979
1194	Chi-Chi- Taiwan	1999	CHY025	7.62	Reverse-Oblique	19.1	277.5	0.1563	42.5934	3.569
1244	Chi-Chi- Taiwan	1999	CHY101	7.62	Reverse-Oblique	10	258.9	0.4136	96.3896	1.3801
1499	Chi-Chi- Taiwan	1999	TCU060	7.62	Reverse-Oblique	8.5	495.8	0.1515	39.863	2.2787
1503	Chi-Chi- Taiwan	1999	TCU065	7.62	Reverse-Oblique	0.6	305.9	0.6928	101.3717	1.8327
1528	Chi-Chi- Taiwan	1999	TCU101	7.62	Reverse-Oblique	2.1	504.4	0.2275	60.1778	1.117
1547	Chi-Chi- Taiwan	1999	TCU123	7.62	Reverse-Oblique	14.9	241.7	0.1483	39.0104	1.5831
2114	Denali- Alaska	2002	TAPS Pump Station #10	7.9	Strike-Slip	2.7	329.4	0.2993	107.6261	1.4119

Table A5. Selected ground motions representing the Wairarapa fault scenario rupture for Wellington city

NGA#	Event	Year	Station	*Mw*	Mechanism	R_{rup} (km)	V_{s30} (m/s)	PGA (g)	PGV (cm/s)	Scale factor
850	Landers	1992	Desert Hot Springs	7.28	Strike-Slip	21.8	345.4	0.1607	20.4204	1.8414
864	Landers	1992	Joshua Tree	7.28	Strike-Slip	11	379.3	0.2779	34.1526	3.2833
880	Landers	1992	Mission Creek Fault	7.28	Strike-Slip	27	345.4	0.1243	12.6347	3.0705
881	Landers	1992	Morongo Valley	7.28	Strike-Slip	17.3	345.4	0.1636	18.1469	4.3373
882	Landers	1992	North Palm Springs	7.28	Strike-Slip	26.8	345.4	0.133	12.7627	4.1549
900	Landers	1992	Yermo Fire Station	7.28	Strike-Slip	23.6	353.6	0.2222	36.4046	2.6164
1158	Kocaeli- Turkey	1999	Duzce	7.51	Strike-Slip	15.4	276	0.3255	52.6049	1.0927
1194	Chi-Chi- Taiwan	1999	CHY025	7.62	Reverse-Oblique	19.1	277.5	0.1563	42.5934	2.4859
1201	Chi-Chi- Taiwan	1999	CHY034	7.62	Reverse-Oblique	14.8	378.8	0.312	38.369	2.938
1203	Chi-Chi- Taiwan	1999	CHY036	7.62	Reverse-Oblique	16.1	233.1	0.2561	38.0662	2.7295
1209	Chi-Chi- Taiwan	1999	CHY047	7.62	Reverse-Oblique	24.1	291.9	0.1777	21.2703	1.5903
1244	Chi-Chi- Taiwan	1999	CHY101	7.62	Reverse-Oblique	10	258.9	0.4136	96.3896	2.177
1484	Chi-Chi- Taiwan	1999	TCU042	7.62	Reverse-Oblique	26.3	424	0.1999	43.6773	2.33
1491	Chi-Chi- Taiwan	1999	TCU051	7.62	Reverse-Oblique	7.7	467.5	0.1894	43.6514	1.7379
1495	Chi-Chi- Taiwan	1999	TCU055	7.62	Reverse-Oblique	6.4	447.8	0.2212	39.0252	1.3758
1499	Chi-Chi- Taiwan	1999	TCU060	7.62	Reverse-Oblique	8.5	495.8	0.1515	39.863	2.9895
1503	Chi-Chi- Taiwan	1999	TCU065	7.62	Reverse-Oblique	0.6	305.9	0.6928	101.3717	1.5759
1513	Chi-Chi- Taiwan	1999	TCU079	7.62	Reverse-Oblique	11	364	0.5371	54.5024	1.8037
1528	Chi-Chi- Taiwan	1999	TCU101	7.62	Reverse-Oblique	2.1	504.4	0.2275	60.1778	2.102
1553	Chi-Chi- Taiwan	1999	TCU141	7.62	Reverse-Oblique	24.2	209.2	0.0934	35.3613	2.6225

Table A6. Selected ground motions representing the Ohariu fault scenario rupture for Wellington city

NGA#	Event	Year	Station	*Mw*	Mechanism	R_{rup} (km)	V_{s30} (m/s)	PGA (g)	PGV (cm/s)	Scale factor
162	Imperial Valley-06	1979	Calexico Fire Station	6.53	Strike-Slip	10.4	231.2	0.2377	18.4746	2.1624
165	Imperial Valley-06	1979	Chihuahua	6.53	Strike-Slip	7.3	274.5	0.2748	28.6534	1.7312
169	Imperial Valley-06	1979	Delta	6.53	Strike-Slip	22	274.5	0.2791	27.0066	1.2178
172	Imperial Valley-06	1979	El Centro Array #1	6.53	Strike-Slip	21.7	237.3	0.1377	12.9672	3.6154
176	Imperial Valley-06	1979	El Centro Array #13	6.53	Strike-Slip	22	249.9	0.1271	14.231	5.0745
187	Imperial Valley-06	1979	Parachute Test Site	6.53	Strike-Slip	12.7	348.7	0.1603	16.057	1.6109
192	Imperial Valley-06	1979	Westmorland Fire Sta	6.53	Strike-Slip	15.2	193.7	0.0867	15.5389	4.0908
721	Superstition Hills-02	1987	El Centro Imp. Co. Cent	6.54	Strike-Slip	18.2	192.1	0.2624	43.2971	1.4148
725	Superstition Hills-02	1987	Poe Road (temp)	6.54	Strike-Slip	11.2	207.5	0.3411	29.4641	2.0134
728	Superstition Hills-02	1987	Westmorland Fire Sta	6.54	Strike-Slip	13	193.7	0.2221	28.6237	3.1168
776	Loma Prieta	1989	Hollister - South & Pine	6.93	Reverse-Oblique	27.9	370.8	0.2855	48.3396	1.5117
778	Loma Prieta	1989	Hollister Diff. Array	6.93	Reverse-Oblique	24.8	215.5	0.2866	42.5642	1.532
803	Loma Prieta	1989	Saratoga - W Valley Coll.	6.93	Reverse-Oblique	9.3	370.8	0.3215	65.4306	3.9497
900	Landers	1992	Yermo Fire Station	7.28	Strike-Slip	23.6	353.6	0.2222	36.4046	2.4335
1176	Kocaeli- Turkey	1999	Yarimca	7.51	Strike-Slip	4.8	297	0.2949	59.2684	1.3453
1244	Chi-Chi- Taiwan	1999	CHY101	7.62	Reverse-Oblique	10	258.9	0.4136	96.3896	1.6535
1499	Chi-Chi- Taiwan	1999	TCU060	7.62	Reverse-Oblique	8.5	495.8	0.1515	39.863	2.7249
1502	Chi-Chi- Taiwan	1999	TCU064	7.62	Reverse-Oblique	16.6	357.5	0.1144	43.9444	2.4549
1537	Chi-Chi- Taiwan	1999	TCU111	7.62	Reverse-Oblique	22.1	237.5	0.1163	45.3199	4.1217
2114	Denali- Alaska	2002	TAPS Pump Station #10	7.9	Strike-Slip	2.7	329.4	0.2993	107.6261	0.8762

Appendix B: Tabulated ground motion details (7 ground motions)

A subset of 7 ground motions from the selected 20 motions representing the scenario rupture of the Alpine, Hope, and Porters Pass faults for Christchurch city (Table B1-B3) and Wellington, Wairarapa, and Ohariu faults for Wellington city (Table B4-B6).

Table B1. Selected ground motions representing the Alpine fault scenario rupture for Christchurch city

NGA#	Event	Year	Station	*Mw*	Mechanism	R_{rup} (km)	V_{s30} (m/s)	PGA (g)	PGV (cm/s)	Scale factor
888	Landers	1992	San Bernardino - E & Hospitality	7.28	Strike-Slip	79.8	271.4	0.0827	17.1588	1.0657
895	Landers	1992	Tarzana - Cedar Hill	7.28	Strike-Slip	175.7	257.2	0.0489	7.0652	1.9705
1188	Chi-Chi- Taiwan	1999	CHY016	7.62	Reverse-Oblique	66.7	200.9	0.1019	16.1417	0.871
1223	Chi-Chi- Taiwan	1999	CHY067	7.62	Reverse-Oblique	83.6	228	0.0605	10.3253	0.8763
1823	Hector Mine	1999	Salton City	7.13	Strike-Slip	123.2	324.5	0.0512	7.9271	0.6053
2109	Denali- Alaska	2002	Fairbanks - Ester Fire Station	7.9	Strike-Slip	139.8	274.5	0.0497	4.0012	1.5551
2115	Denali- Alaska	2002	TAPS Pump Station #11	7.9	Strike-Slip	126.4	376.1	0.0761	11.5231	0.8952

Table B2. Selected ground motions representing the Hope fault scenario rupture for Christchurch city

NGA#	Event	Year	Station	*Mw*	Mechanism	R_{rup} (km)	V_{s30} (m/s)	PGA (g)	PGV (cm/s)	Scale factor
887	Landers	1992	Riverside Airport	7.28	Strike-Slip	96	370.8	0.0417	3.0494	1.3989
1147	Kocaeli- Turkey	1999	Ambarli	7.51	Strike-Slip	69.6	175	0.2129	36.671	0.29
1332	Chi-Chi- Taiwan	1999	ILA042	7.62	Reverse-Oblique	85.7	209.4	0.0768	16.666	0.9539
1344	Chi-Chi- Taiwan	1999	ILA059	7.62	Reverse-Oblique	86.3	236.8	0.0653	15.3931	0.4258
1766	Hector Mine	1999	Baker Fire Station	7.13	Strike-Slip	64.8	271.4	0.1097	8.4377	0.8238
1813	Hector Mine	1999	Morongo Valley	7.13	Strike-Slip	53.2	345.4	0.0846	16.5223	0.5477
1823	Hector Mine	1999	Salton City	7.13	Strike-Slip	123.2	324.5	0.0512	7.9271	1.5911

Table B3. Selected ground motions representing the Porters Pass fault scenario rupture for Christchurch city

NGA#	Event	Year	Station	*Mw*	Mechanism	R_{rup} (km)	V_{s30} (m/s)	PGA (g)	PGV (cm/s)	Scale factor
93	San Fernando	1971	Whittier Narrows Dam	6.61	Reverse	39.5	298.7	0.1153	9.3048	0.9415
729	Superstition Hills-02	1987	Wildlife Liquef. Array	6.54	Strike-Slip	23.9	207.5	0.1958	27.821	0.4585
761	Loma Prieta	1989	Fremont - Emerson Court	6.93	Reverse-Oblique	39.9	284.8	0.1581	13.5695	1.3095
762	Loma Prieta	1989	Fremont - Mission San Jose	6.93	Reverse-Oblique	39.5	367.6	0.1401	11.3569	2.3683
880	Landers	1992	Mission Creek Fault	7.28	Strike-Slip	27	345.4	0.1243	12.6347	1.5013
1026	Northridge-01	1994	Lawndale - Osage Ave	6.69	Reverse	39.9	361.2	0.1157	8.253	0.5715
1228	Chi-Chi- Taiwan	1999	CHY076	7.62	Reverse-Oblique	42.2	169.8	0.0754	19.5592	0.7355

Table B4. Selected ground motions representing the Wellington fault scenario rupture for Wellington city

NGA#	Event	Year	Station	*Mw*	Mechanism	R_{rup} (km)	V_{s30} (m/s)	PGA (g)	PGV (cm/s)	Scale factor
173	Imperial Valley-06	1979	El Centro Array #10	6.53	Strike-Slip	6.2	202.8	0.2001	42.9521	3.1727
175	Imperial Valley-06	1979	El Centro Array #12	6.53	Strike-Slip	17.9	196.9	0.1258	19.6423	1.9574
729	Superstition Hills-02	1987	Wildlife Liquef. Array	6.54	Strike-Slip	23.9	207.5	0.1958	27.821	2.2384
806	Loma Prieta	1989	Sunnyvale - Colton Ave.	6.93	Reverse-Oblique	24.2	267.7	0.2008	34.4243	3.6175
880	Landers	1992	Mission Creek Fault	7.28	Strike-Slip	27	345.4	0.1243	12.6347	4.7101
1176	Kocaeli- Turkey	1999	Yarimca	7.51	Strike-Slip	4.8	297	0.2949	59.2684	2.3268
1194	Chi-Chi- Taiwan	1999	CHY025	7.62	Reverse-Oblique	19.1	277.5	0.1563	42.5934	2.1339

Table B5. Selected ground motions representing the Wairarapa fault scenario rupture for Wellington city

NGA#	Event	Year	Station	*Mw*	Mechanism	R_{rup} (km)	V_{s30} (m/s)	PGA (g)	PGV (cm/s)	Scale factor
850	Landers	1992	Desert Hot Springs	7.28	Strike-Slip	21.8	345.4	0.1607	20.4204	4.686
880	Landers	1992	Mission Creek Fault	7.28	Strike-Slip	27	345.4	0.1243	12.6347	5.4119
882	Landers	1992	North Palm Springs	7.28	Strike-Slip	26.8	345.4	0.133	12.7627	3.207
900	Landers	1992	Yermo Fire Station	7.28	Strike-Slip	23.6	353.6	0.2222	36.4046	3.9688
1495	Chi-Chi- Taiwan	1999	TCU055	7.62	Reverse-Oblique	6.4	447.8	0.2212	39.0252	1.2495
1503	Chi-Chi- Taiwan	1999	TCU065	7.62	Reverse-Oblique	0.6	305.9	0.6928	101.3717	0.5771
1513	Chi-Chi- Taiwan	1999	TCU079	7.62	Reverse-Oblique	11	364	0.5371	54.5024	0.769

Table B6. Selected ground motions representing the Ohariu fault scenario rupture for Wellington city

NGA#	Event	Year	Station	*Mw*	Mechanism	R_{rup} (km)	V_{s30} (m/s)	PGA (g)	PGV (cm/s)	Scale factor
172	Imperial Valley-06	1979	El Centro Array #1	6.53	Strike-Slip	21.7	237.3	0.1377	12.9672	2.155
176	Imperial Valley-06	1979	El Centro Array #13	6.53	Strike-Slip	22	249.9	0.1271	14.231	3.4927
187	Imperial Valley-06	1979	Parachute Test Site	6.53	Strike-Slip	12.7	348.7	0.1603	16.057	5.0066
776	Loma Prieta	1989	Hollister - South & Pine	6.93	Reverse-Oblique	27.9	370.8	0.2855	48.3396	3.2506
778	Loma Prieta	1989	Hollister Diff. Array	6.93	Reverse-Oblique	24.8	215.5	0.2866	42.5642	1.6283
1244	Chi-Chi- Taiwan	1999	CHY101	7.62	Reverse-Oblique	10	258.9	0.4136	96.3896	1.1842
1537	Chi-Chi- Taiwan	1999	TCU111	7.62	Reverse-Oblique	22.1	237.5	0.1163	45.3199	2.3622

Acknowledgement

Financial support of the University of Canterbury and New Zealand Earthquake Commission (EQC) are greatly appreciated.

References

Bommer, J. J. (2002). Deterministic vs. probabilistic seismic hazard assessment: an exaggerated and obstructive dichotomy. *Journal of Earthquake Engineering* **6**(spec01): 43-73.

McGuire, R. K. (1995). Probabilistic seismic hazard analysis and design earthquakes: closing the loop. *Bulletin of the Seismological Society of America* **85**(5): 1275-1284.

Shome, N., C. A. Cornell, P. Bazzurro & J. E. Carballo (1998). Earthquakes, records, and nonlinear responses. *Earthquake Spectra* **14**(3): 469-500.

Bommer, J. J. & A. B. Acevedo (2004). The use of real earthquake accelerograms as input to dynamic analysis. *Journal of Earthquake Engineering* **8**(spec01): 43-91.

Kottke, A. & E. M. Rathje (2008). A semi-automated procedure for selecting and scaling recorded earthquake motions for dynamic analysis. *Earthquake Spectra* **24**(4): 911-932.

Baker, J. W. (2010). Conditional mean spectrum: Tool for ground-motion selection. *Journal of Structural Engineering* **137**(3): 322-331.

Jayaram, N., T. Lin & J. W. Baker (2011). A computationally efficient ground-motion selection algorithm for matching a target response spectrum mean and variance. *Earthquake Spectra* **27**(3): 797-815.

Wang, G. (2011). A ground motion selection and modification method capturing response spectrum characteristics and variability of scenario earthquakes. *Soil Dynamics and Earthquake Engineering* **31**(4): 611-625.

Katsanos, E. I., A. G. Sextos & G. D. Manolis (2010). Selection of earthquake ground motion records: A state-of-the-art review from a structural engineering perspective. *Soil Dynamics and Earthquake Engineering* **30**(4): 157-169.

Bradley, B. A. (2010a). A generalized conditional intensity measure approach and holistic ground-motion selection. *Earthquake Engineering & Structural Dynamics* **39**(12): 1321-1342.

Bradley, B. A. (2012a). A ground motion selection algorithm based on the generalized conditional intensity measure approach. *Soil Dynamics and Earthquake Engineering* **40**: 48-61.

Baker, J. W. & N. Jayaram (2008). Correlation of spectral acceleration values from NGA ground motion models. *Earthquake Spectra* **24**(1): 299-317.

Bradley, B. A. (2011a). Empirical equations for the prediction of displacement spectrum intensity and its correlation with other intensity measures. *Soil Dynamics and Earthquake Engineering* **31**(8): 1182-1191.

Bradley, B. A. (2011b). Empirical correlation of PGA, spectral accelerations and spectrum intensities from active shallow crustal earthquakes. *Earthquake Engineering & Structural Dynamics* **40**(15): 1707-1721.

Bradley, B. A. (2011c). Correlation of significant duration with amplitude and cumulative intensity measures and its use in ground motion selection. *Journal of Earthquake Engineering* **15**(6): 809-832.

Bradley, B. A. (2012b). Empirical correlations between peak ground velocity and spectrum-based intensity measures. *Earthquake Spectra* **28**(1): 17-35.

Bradley, B. A. (2012c). Empirical correlations between cumulative absolute velocity and amplitude-based ground motion intensity measures. *Earthquake Spectra* **28**(1): 37-54.

Bradley, B. A. (2014). Correlation of arias intensity with amplitude, duration and cumulative intensity measures. *Soil Dynamics and Earthquake Engineering* **(under-review)**.

Boore, D. M. & G. M. Atkinson (2008). Ground-motion prediction equations for the average horizontal component of PGA, PGV, and 5%-damped PSA at spectral periods between 0.01 s and 10.0 s. *Earthquake Spectra* **24**(1): 99-138.

Chiou, B., R. Darragh, N. Gregor & W. Silva (2008). NGA project strong-motion database. *Earthquake Spectra* **24**(1): 23-44.

Bradley, B. A. (2013a). Ground motion selection for seismic risk analysis of civil infrastructures. Handbook of seismic risk analysis and management of civil infrastructure systems. S. Tasfamariam and K. Goda*, Woodhead Publishing Ltd.*

Bradley, B. A. (2010b). Site-specific and spatially distributed ground-motion prediction of acceleration spectrum intensity. *Bulletin of the Seismological Society of America* **100**(2): 792-801.

Bradley, B. A., M. Cubrinovski, G. A. MacRae & R. P. Dhakal (2009). Ground-motion prediction equation for SI based on spectral acceleration equations. *Bulletin of the Seismological Society of America* **99**(1): 277-285.

Campbell, K. W. & Y. Bozorgnia (2010). A ground motion prediction equation for the horizontal component of cumulative absolute velocity (CAV) based on the PEER-NGA strong motion database. *Earthquake Spectra* **26**(3): 635-650.

Campbell, K. W. & Y. Bozorgnia (2012). A comparison of ground motion prediction equations for Arias intensity and cumulative absolute velocity developed using a consistent database and functional form. *Earthquake Spectra* **28**(3): 931-941.

Bommer, J. J., P. J. Stafford & J. E. Alarcón (2009). Empirical equations for the prediction of the significant, bracketed, and uniform duration of earthquake ground motion. *Bulletin of the Seismological Society of America* **99**(6): 3217-3233.

Bradley, B. A., R. P. Dhakal, G. A. MacRae & M. Cubrinovski (2010). Prediction of spatially distributed seismic demands in specific structures: Ground motion and structural response. *Earthquake Engineering & Structural Dynamics* **39**(5): 501-520.

Tothong, P. & C. A. Cornell (2007). Probabilistic seismic demand analysis using advanced ground motion intensity measures, attenuation relationships and near-fault effects. John A. Blume Earthquake Engineering Center, Department of Civil and Environmental Engineering, Stanford University, Stanford, CA.

Bradley, B. A., K. Araki, T. Ishii & K. Saitoh (2013). Effect of lattice-shaped ground improvement geometry on seismic response of liquefiable soil deposits via 3-D seismic effective stress analysis. *Soil Dynamics and Earthquake Engineering* **48**: 35-47.

Villaverde, R. (2007). Methods to assess the seismic collapse capacity of building structures: State of the art. *Journal of Structural Engineering* **133**(1): 57-66.

ASCE/SEI7-10 (2010). Minimum Design Loads for Buildings and Other Structures, ASCE/SEI 7-10. American Society of Civil Engineers, Reston, Virginia.

NIST (2011). Selecting and Scaling Earthquake Ground Motions for Performing Response History Analysis, *NIST/GCR 11-917-15,* NEHRP Consultants Joint Venture for the National Institute of Standards and Technology, Gaithersburg, Maryland.

NZS1170.5 (2004). NZS1170.5:2004, Structural design actions. Part 5: Earthquake actions - New Zealand. *Wellington, NZ, Standards New Zealand*.

Ang, A. H. & W. H. Tang (1975). Probability concepts in engineering planning and design, *John Wiley & Sons, Inc.*

Bommer, J. J. & A. Martinez-Pereira (1999). The effective duration of earthquake strong motion. *Journal of Earthquake Engineering* **3**(2): 127-172.

Bommer, J. J., J. Hancock & J. E. Alarcón (2006). Correlations between duration and number of effective cycles of earthquake ground motion. *Soil Dynamics and Earthquake Engineering* **26**(1): 1-13.

Bradley, B. A. (2012d). The seismic demand hazard and importance of the conditioning intensity measure. *Earthquake Engineering & Structural Dynamics* **41**(11): 1417-1437.

NEHRP (2003). Building Seismic Safety Council, NEHRP Recommended Provisions for seismic Regulations for New buildings and other Structures, Part1: Provisions, FEMA 368, Federal Emergency Management Agency, Washington, D.C.

Tarbali, K. & B. A. Bradley (2014). Scenario-based ground-motion selection using the generalized conditional intensity measure (GCIM) approach. *Proceedings of the 10th National Conference in Earthquake Engineering*, *Anchorage, AK*, Earthquake Engineering Research Institute.

Stirling, M., G. McVerry, M. Gerstenberger, N. Litchfield, R. Van Dissen, K. Berryman, P. Barnes, L. Wallace, P. Villamor & R. Langridge (2012). National seismic hazard model for New Zealand: 2010 update. *Bulletin of the Seismological Society of America* **102**(4): 1514-1542.

Bradley, B. A. (2013b). A New Zealand-Specific Pseudospectral Acceleration Ground-Motion Prediction Equation for Active Shallow Crustal Earthquakes Based on Foreign Models. *Bulletin of the Seismological Society of America* **103**(3): 1801-1822.

Field, E. H., T. H. Jordan & C. A. Cornell (2003). OpenSHA: A developing community-modeling environment for seismic hazard analysis. *Seismological Research Letters* **74**(4): 406-419.